МІНІСТЕРСТВО ОСВІТИ І НАУКИ УКРАЇНИ
ІВАНО-ФРАНКІВСЬКИЙ НАЦІОНАЛЬНИЙ
ТЕХНІЧНИЙ УНІВЕРСИТЕТ НАФТИ І ГАЗУ

РОЗВІДКА ТА РОЗРОБКА НАФТОВИХ І ГАЗОВИХ РОДОВИЩ

Науково-технічний журнал

Том 26, № 1
2026

ІВАНО-ФРАНКІВСЬК
2026

MINISTRY OF EDUCATION AND SCIENCE OF UKRAINE
IVANO-FRANKIVSK NATIONAL
TECHNICAL UNIVERSITY OF OIL AND GAS

PROSPECTING AND DEVELOPMENT OF OIL AND GAS FIELDS

Scientific and Technical Journal

Vol. 26, No. 1
2026

IVANO-FRANKIVSK
2026

ISSN 1993-9973
e-ISSN 2415-332X
УДК 622;550

Засновник та видавець:
Івано-Франківський національний технічний університет нафти і газу (ІФНТУНГ)

Рік заснування: 2001

Періодичність: двічі на рік

Ідентифікатор медіа: R30-01428
(Рішення Національної ради України з питань телебачення і радіомовлення № 3214,
протокол № 29 від 28 листопада 2024 року)

Журнал включено до категорії «Б» Переліку наукових фахових видань України
Технічні спеціальності: 133 – Галузеве машинобудування;
185 – Нафтогазова інженерія та технології
(Наказ Міністерства освіти і науки України № 1643 від 28 грудня 2019 року)
Геологічні спеціальності: 103 – Науки про землю
(Наказ Міністерства освіти і науки України № 409 від 17 березня 2020 року)

Журнал представлено в таких міжнародних наукометричних базах даних, репозитаріях та пошукових системах:
Національна бібліотека України імені В.І. Вернадського, Фахові видання України,
Crossref, Dimensions, Google Академія, German Union Catalogue of Serials (ZDB),
University of Oslo Library, Universitätsbibliothek Leipzig (UBL),
Open Ukrainian Citation Index (OUCI), Ulrichsweb Global Serials Directory,
Litmaps, Scopus

Адреса редакції:
Івано-Франківський національний технічний університет нафти і газу
76019, вул. Карпатська, 15, м. Івано-Франківськ, Україна
E-mail: nung@pdogf.com.ua
https://pdogf.com.ua/uk

ISSN 1993-9973
e-ISSN 2415-332X
UDC 622;550

Founder and publisher:
Ivano-Frankivsk National Technical University of Oil and Gas (IFNTUOG)

Year of foundation: 2001

Frequency: semi-annual

Media identifier: R30-01428
(Decision of the National Council of Television and Radio Broadcasting of Ukraine No. 3214,
Minutes No. 29 of November 28, 2024)

The journal is included in category "B"
of the List of scientific professional publications of Ukraine
Technical specialties: 0715 Mechanics and metal trades, 0716 Motor vehicles, ships and aircraft,
0724 Mining and extraction
(Order of the Ministry of Education and Science of Ukraine No. 1643 dated December 28, 2019)
Geological specialties: 0532 Earth sciences
(Order of the Ministry of Education and Science of Ukraine No. 409 dated March 17, 2020)

The journal is presented in the following international scientometric
databases, repositories and scientific systems:
Vernadsky National Library of Ukraine, Professional Publications of Ukraine,
Crossref, Dimensions, Google Scholar, German Union Catalogue of Serials (ZDB),
University of Oslo Library, Universitätsbibliothek Leipzig (UBL),
Open Ukrainian Citation Index (OUCI), Ulrichsweb Global Serials Directory,
Litmaps, Scopus

Editors office address:
Ivano-Frankivsk National Technical University of Oil and Gas
76019, 15 Karpatska Str., Ivano-Frankivsk, Ukraine
E-mail: nung@pdogf.com.ua
https://pdogf.com.ua/en

Editorial Board

Зміст/Contents

ISSN 1993-9973, e-ISSN 2415-332X

Vol. 26, No. 1 2026

PROSPECTING AND DEVELOPMENT OF OIL AND GAS FIELDS ***https://pdogf.com.ua/en***

Received: 12.12.2025. Revised: 30.03.2026. Accepted: 29.05.2026. Published: 29.06.2026.

UDC 620.193:622.276:004.021

DOI: 10.63341/pdogf/1.2026.08

Application of DEoptim for corrosion inhibitor optimisation in HPHT conditions: Theoretical review of modern approaches

Andrii Hrytsanchuk

PhD in Technical Sciences, Associate Professor
Ivano-Frankivsk National Technical University of Oil and Gas
76019, 15 Karpatska Str., Ivano-Frankivsk, Ukraine
https://orcid.org/0000-0001-9894-0911

Vitalii Hryhoryshyn*

Postgraduate Student
Ivano-Frankivsk National Technical University of Oil and Gas
76019, 15 Karpatska Str., Ivano-Frankivsk, Ukraine
https://orcid.org/0009-0001-4792-1830

Abstract. Corrosion of oil and gas equipment remained a critical industry problem with annual losses of $1.372 billion. High pressure high temperature (HPHT) conditions significantly complicated the development of effective corrosion inhibitors due to increased environmental aggressiveness and degradation of traditional protective compounds. The aim of this study was to provide a theoretical analysis of the potential application of differential evolution method (DEoptim) for multi-objective optimisation of corrosion inhibitor parameters under extreme HPHT conditions. The research methodology comprised systematic literature review using Scopus, Web of Science, and Google Scholar databases (2019-2024), comparative analysis of computational modelling methods, theoretical analysis of optimisation approaches, and information synthesis for formulating recommendations. The work systematised modern approaches to computational modelling of inhibitors, including quantum chemical calculations, molecular dynamics, and machine learning. An analysis of specific challenges in HPHT environments, where temperatures exceeded 150°C and pressure exceeded 69 MPa, was conducted. The advantages of evolutionary algorithms for navigating complex multidimensional parameter spaces of inhibitors were considered. The theoretical foundations for using DEoptim for simultaneous optimisation of inhibition efficiency, thermal stability, environmental acceptability, and economic feasibility were substantiated. The analysis demonstrated that DEoptim offered superior robustness and multi-objective capabilities compared to traditional gradient-based and genetic algorithms, particularly for HPHT applications. The study proposed a novel integration concept combining DEoptim with quantum chemical calculations and machine learning to create hybrid optimisation frameworks, potentially reducing computational costs by up to 60% while improving inhibitor discovery efficiency. The results showed that DEoptim application could provide systematic search for optimal inhibitor formulations, reduce the number of required experiments, and identify non-obvious synergistic component combinations for HPHT applications

Keywords: differential evolution; computational modelling; multi-criteria design; metaheuristic algorithms; petroleum equipment

Introduction

Corrosion in the oil and gas industry is a complex technical and economic problem that requires a comprehensive approach to solve. High pressure and temperature (HPHT) conditions pose additional challenges for traditional corrosion protection methods, as materials and inhibitors are often unable to function effectively in such extreme conditions. The development of new technologies, such as quantum chemistry, machine learning, and evolutionary algorithms, opens up new opportunities for the development of effective “green” inhibitors that can provide reliable

Suggested Citation: Hrytsanchuk, A., & Hryhoryshyn, V. (2026). Application of DEoptim for corrosion inhibitor optimisation in HPHT conditions: Theoretical review of modern approaches. *Prospecting and Development of Oil and Gas Fields*, 26(1), 8-15. doi: 10.63341/pdogf/1.2026.08.

*Corresponding author (*vitalii.hryhoryshyn-a18524@nung.edu.ua*)

equipment protection, reduce environmental impact, and optimise maintenance costs.

Corrosion of oil and gas equipment represent one of the most critical technical and economic problems in the modern energy industry. Global corrosion losses across all industries amounted to $2.5 trillion annually, constituting 3.4% of global GDP. In the oil and gas sector, annual losses reached $1.372 billion, including $463 million for downhole equipment and $320 million for corrosion-related capital expenditures. The corrosion problem is particularly acute under HPHT conditions, characterised by temperatures exceeding 150°C and pressures above 69 MPa. Statistical analysis of failure causes showed that CO_2-related corrosion accounted for 28% of all corrosion failures, H_2S-related corrosion and weld joint corrosion each accounted for 18%, and localised pitting corrosion accounted for 12% (Association for Materials Protection and Performance, n.d; King, 2010).

Research during 2011-2025 in corrosion inhibition was characterised by active integration of experimental and computational methods. C. Verma *et al*. (2021) examined environmentally acceptable corrosion inhibitors through a systematic review of sustainable formulations. Their investigation covered biodegradable inhibitors, green chemistry approaches, and eco-friendly alternatives to traditional toxic compounds. The study concluded that most conventional compositions failed to meet OSPARCOM environmental requirements, necessitating complete reformulation of existing products. The authors identified significant gaps in developing high-performance green inhibitors suitable for extreme conditions. V.A. Solovyeva *et al*. (2021) analysed downhole corrosion control solutions across various operational scenarios in petroleum wells. Their research evaluated existing protection methods, assessed their effectiveness under different conditions, and identified technological limitations. The study concluded that innovative approaches were required for inhibitor development in HPHT environments, but limited attention was given to computational optimisation methodologies for systematic inhibitor design.

E. Padmanabhan *et al*. (2023) examined digitalisation in the oil and gas industry, highlighting computational challenges and resource requirements for implementing advanced optimisation algorithms in industrial environments. H. Song *et al*. (2023) conducted performance tests of HPHT corrosion inhibitors at onshore downhole sour conditions, demonstrating that corrosion inhibitor injection rates for carbon steel can reach up to 1,000 ppm under high temperature, high pressure conditions, confirming the practical implementation challenges in extreme operational environments. Result interpretability remained challenging due to evolutionary algorithm complexity, potentially complicating mechanistic understanding essential for regulatory approval processes. Computational methods for inhibitor development gained prominence during 2022-2024. S. Malinowski (2022) investigated quantum chemical calculations for predicting anticorrosion properties of low-molecular-weight Schiff bases. The research involved density functional theory calculations to determine molecular orbital energies, electron densities, and adsorption characteristics. The author concluded that quantum methods effectively predicted inhibition efficiency, achieving 85% correlation with experimental data. However, the study focused solely on single-molecule analysis without considering multi-component formulations typical of industrial applications.

S. Budi *et al*. (2024) developed machine learning models with polynomial functions to predict corrosion inhibition efficiency of pyridine-quinoline compounds. Their methodology combined quantum descriptors with experimental data to train predictive algorithms. The research demonstrated improved accuracy in efficiency prediction compared to linear models, achieving R^2 values above 0.9. Nevertheless, the study was limited to specific chemical classes and did not explore systematic optimisation of inhibitor compositions. D. Li *et al*. (2023) investigated corrosion inhibition mechanisms of ultra-high-temperature acidizing corrosion inhibitors, highlighting the complexity of multi-component formulation design under extreme temperature conditions.

A. Roy *et al*. (2022) applied machine learning techniques to predict corrosion resistance of multi-principal element alloys. Their investigation utilised various algorithms to correlate compositional parameters with corrosion behaviour. The study concluded that computational methods possessed significant potential for materials design, identifying key descriptors influencing corrosion resistance. However, the focus remained on alloy development rather than inhibitor formulation optimisation. P. Kumari & M. Lavanya (2024) conducted a comprehensive review of optimisation strategies for corrosion management using artificial neural networks and response surface methodology. Their analysis covered various mathematical approaches for optimising protective systems and operational parameters. The authors concluded that systematic optimisation significantly improved corrosion control effectiveness, but identified limited application of advanced evolutionary algorithms in this field.

Literature analysis revealed minimal research on applying evolutionary algorithms, particularly differential evolution methods, for multi-objective optimisation of corrosion inhibitors under HPHT conditions. The objective of this work was to establish the theoretical foundations for applying DEoptim as an advanced optimisation framework for developing effective corrosion inhibitors specifically designed for HPHT operational environments. To achieve this objective, three key tasks were undertaken. First, the research involved a theoretical analysis of the potential of the DEoptim algorithm for multi-objective optimisation of corrosion inhibitors under high-pressure, HPHT conditions. Second, the study systematised existing approaches to the computational modelling of inhibitor properties and performance characteristics. Finally, the advantages of evolutionary algorithms in solving complex optimisation problems within corrosion protection applications were substantiated, and integration strategies were proposed that combine DEoptim with quantum chemical calculations and machine learning methods.

Materials and Methods

The theoretical foundation of this research was established through analysis of fundamental works by L.T. Popoola *et al*. (2013) and M. Finšgar & J. Jackson (2014) on corrosion inhibitor applications in acidic media, C. Verma *et al*. (2021) on sustainable inhibitor development, and S. Malinowski (2022) on quantum chemical approaches to inhibitor design. Additional theoretical basis included studies by A. Roy *et al*. (2022) on machine learning applications in materials science and P. Kumari & M. Lavanya (2024) on optimisation strategies for corrosion management. The research employed systematic review methodology combined with meta-analytical approaches to examine literature from Scopus, Web of Science, and Google Scholar databases covering the period 2011-2024. Search strategies utilised targeted keywords including "corrosion inhibitors HPHT", "differential evolution optimisation", "computational modelling corrosion", "evolutionary algorithms materials", and "multi-criteria optimisation corrosion" to ensure comprehensive coverage of relevant publications. The analysis encompassed 20 scientific publications, consisting of 17 peer-reviewed journal articles, and 3 conference papers. Selection criteria encompassed publications in journals with impact factors exceeding 2.0, direct relevance to corrosion inhibition in petroleum operations, inclusion of experimental or computational validation data, and temporal preference for publications within the preceding five years to ensure currency of findings.

Content analysis methodology was applied to systematically extract and categorise information from selected publications, focusing on identification of research methodologies, key findings, and limitations within each study. This approach enabled systematic comparison of different inhibitor development strategies and identification of research gaps in the field. Comparative analysis was implemented to evaluate computational modelling methods under HPHT conditions, systematically contrasting quantum chemical calculations, molecular dynamics simulations, machine learning approaches, and DEoptim based on their applicability, accuracy, and computational requirements for inhibitor design in extreme environments. A.R. Leach (2011) explored cheminformatics and computational chemistry applications in lead optimisation, establishing methodological frameworks for evaluating computational approaches in chemical system design. The multi-objective optimisation problem for DEoptim application was formulated as:

$$F(x) = [f_1(x), f_2(x), \ldots, Fn], \tag{1}$$

where $f_1(x)$ – inhibition efficiency under HPHT conditions; $f_2(x)$ – thermal degradation rate; $f_3(x)$ – environmental toxicity; $f_4(x)$ – economic cost; x – parameter vector (concentrations, molecular descriptors, etc.). Quantitative data analysis was conducted on numerical data extracted from 20 scientific publications to validate both the significance of the problem and the effectiveness of proposed solutions. The methodology involved the systematic extraction and statistical compilation of key parameters relevant to HPHT corrosion environments. Data points included economic loss estimates, failure analysis breakdowns, and performance metrics for various classes of corrosion inhibitors. Data synthesis methodology integrated information from diverse sources to develop comprehensive understanding of DEoptim potential for inhibitor optimisation.

Results and Discussion

Based on comprehensive literature analysis, HPHT conditions were identified as creating a complex multi-objective optimisation challenge for corrosion inhibitor development. The systematic review revealed that these extreme environments, characterised by temperatures exceeding 150°C and pressures above 69 MPa, demanded sophisticated approaches that could simultaneously address conflicting performance criteria. The analysis demonstrated that traditional single-objective methodologies proved inadequate for addressing the multifaceted nature of inhibitor design under such demanding operational conditions.

High pressure affected corrosion processes by increasing the solubility of aggressive gases such as CO_2 and H_2S in the aqueous phase. L.T. Popoola *et al*. (2013) analysed corrosion problems during oil and gas production, identifying CO_2-related corrosion as accounting for 28% of all corrosion failures, H_2S-related corrosion and weld joint corrosion each accounting for 18%, and localised pitting corrosion accounting for 12% of industry failures. At CO_2 partial pressures exceeding 0.2 MPa and temperatures above 80°C, particularly intensive sweet corrosion was observed (Unueroh *et al*., 2016). Sour corrosion under HPHT conditions was complicated by hydrogen embrittlement, which could lead to catastrophic equipment failures. Traditional organic corrosion inhibitors faced serious limitations under these conditions, with nitrogen-containing heterocycles losing effectiveness at temperatures above 120°C due to thermal degradation and changes in adsorption properties (Finšgar & Jackson, 2014).

The investigation revealed that inhibitor protection efficiency dropped sharply within 4 days of application, indicating insufficient formulation stability. The presence of dissolved oxygen significantly impaired the adsorption properties of nitrogen-containing inhibitors, reducing protection efficiency from 81.8% to 52.3%. These findings highlighted the fundamental challenge of developing inhibitors that maintained effectiveness whilst meeting other critical requirements including cost-effectiveness and environmental acceptability. Statistical analysis of corrosion failure types revealed distinct patterns across different mechanisms, as presented in Figure 1. To better understand the scale of financial losses associated with corrosion-related failures, it is useful to examine the aggregated data across the oil and gas industry. Figure 2 presents a visual representation of the economic impact these failures impose on the sector.

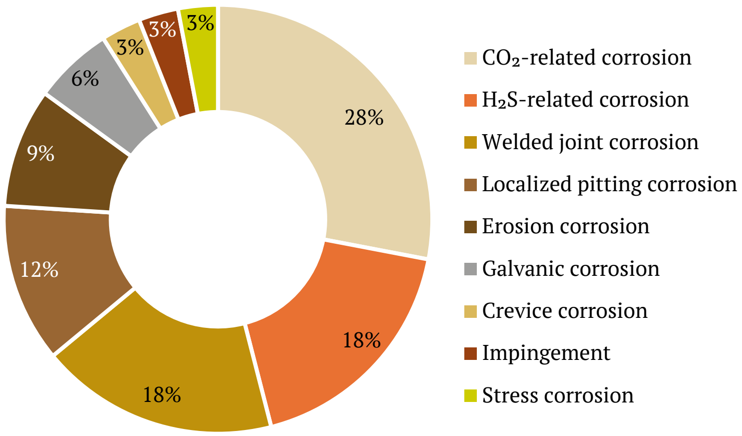

Figure 1. Distribution of corrosion-related failures
Source: compiled by authors based on L.T. Popoola *et al*. (2013)

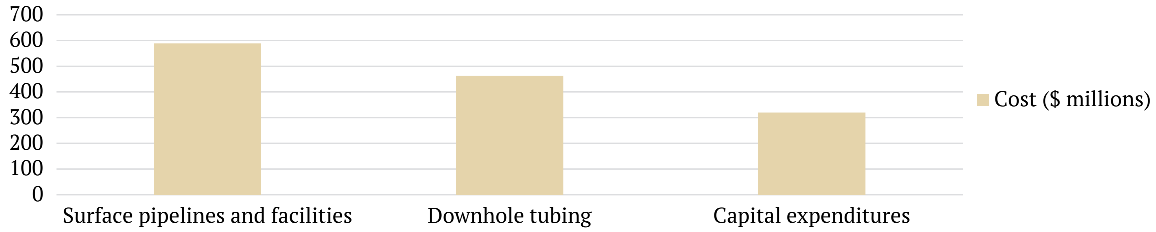

Figure 2. Annual corrosion costs in oil and gas industry
Source: compiled by authors based on L.T. Popoola *et al*. (2013)

Analysis identified DEoptim as an effective tool for resolving multi-criteria optimisation challenges where conventional methods proved inadequate. Multi-criteria optimisation focuses on identifying optimal solutions when faced with competing and frequently mutually exclusive requirements. Systematic analysis demonstrated characteristic trade-offs between key inhibitor parameters. Investigation of imidazoline-based inhibitors revealed high anti-corrosion efficiency (>85%), yet identified critical constraints: thermal instability at temperatures exceeding 120°C and elevated synthesis costs ($45-60/kg). Analysis of bio-based amino acid inhibitors demonstrated their environmental compatibility and biodegradability, though inhibition efficiency under HPHT conditions reached only 60-70%. Based on this analysis, three key parameters were identified for constructing DEoptim objective functions: inhibition efficiency (minimum 80%), thermal stability (withstanding temperatures up to 150°C), and economic viability (cost <$40/kg). These parameters were selected as critical based on industrial application requirements and integrated as separate objective functions with corresponding weighting coefficients.

The quantitative analysis revealed annual corrosion-related losses amounting to $1.372 billion, with failure statistics indicating 28% of incidents linked to CO_2 exposure, 18% to H_2S, another 18% to weld joint failures, and 12% to pitting corrosion. Performance evaluation showed inhibition efficiency ranging from 60% to 85%, while thermal stability thresholds were identified at around 120°C across different inhibitor types. These findings established a quantitative baseline for HPHT optimisation challenges and underscored the necessity for advanced multi-objective optimisation strategies (Association for Materials Protection and Performance, n.d; King, 2010).

Investigation demonstrated that DEoptim operates effectively as an element within a comprehensive approach rather than an isolated tool. The algorithm integrates into a four-phase methodology: preliminary experimental screening, computational modelling, evolutionary optimisation, and experimental verification. Initial screening provides baseline performance data for candidates under simulated HPHT conditions. Quantum chemical calculations determine molecular descriptors that characterise electronic properties, temperature stability, and adsorption behaviour. Machine learning models, trained on the combined dataset, function as surrogate functions for rapid candidate assessment without conducting experiments for each composition. DEoptim explores the multidimensional parameter space, forming populations of potential solutions and enhancing them through evolutionary operations: mutations, crossover, and selection.

Comparative analysis of computational methods identified substantial differences in their suitability for HPHT inhibitor development. Quantum chemical methods provide detailed molecular-level understanding but exhibit limitations when scaling to complex compositions. Investigation confirmed that HOMO-LUMO energy gaps effectively predict individual molecule behaviour, yet fail to capture synergistic effects in multi-component commercial inhibitor systems. Molecular dynamics simulations better reproduce realistic operational conditions but require significant computational resources and remain limited to nanosecond timescales, insufficient for predicting long-term stability over months of operation. Machine learning methods demonstrate promising results but remain constrained by data availability and interpretation complexity, particularly for novel inhibitor classes. Based on the conducted analysis in Table 1, a hybrid approach emerges as most suitable for achieving the research objectives: combining quantum chemical calculations for primary screening with subsequent DEoptim application and machine learning for multi-component composition optimisation. This approach balances prediction accuracy, computational efficiency, and practical applicability for industrial HPHT conditions.

Table 1. Comparative analysis of computational methods for corrosion inhibitor development

Method	Advantages	Limitations
Quantum Chemical Calculations	Electronic structure insights, prediction of adsorption mechanisms, thermal stability assessment, structure-property relationships	High computational cost, limited to small molecules, requires quantum chemistry expertise, accuracy depends on chosen functional
Molecular Dynamics	Dynamic behaviour under HPHT conditions, visualisation of adsorption processes, film stability assessment, environmental effects modelling	Computationally intensive, limited time scales, force field accuracy limitations, requires significant computational resources
Machine Learning	Pattern recognition in complex datasets, high-throughput virtual screening, feature importance analysis, predictive model development	Requires large training datasets, limited extrapolation capability, black-box nature, prone to overfitting
DEoptim	Global optimisation capability, handling multidimensional parameter spaces, balancing multiple objectives, efficient exploration of chemical space	Parameter tuning requirements, convergence uncertainty, requires quality fitness functions, limited solution interpretability

Source: compiled by authors

Comparative analysis of existing optimisation approaches revealed fundamental limitations that DEoptim addressed effectively. A. Samimi *et al*. (2021) demonstrated successful application of systematic electrochemical optimisation for corrosion information in oil and gas wells, but their approach focused on individual parameters sequentially rather than simultaneous multi-objective optimisation. The analysis identified this sequential approach as suboptimal for HPHT applications where parameter interactions significantly influenced overall performance. Traditional gradient-based methods, whilst computationally efficient, required differentiable objective functions and frequently converged to local optima, limitations that DEoptim's population-based approach effectively circumvented.

O. Roustant *et al*. (2012) developed DiceKriging and DiceOptim packages for analysing computer experiments through kriging-based metamodelling and optimisation, demonstrating practical optimisation tool value. However, their methodology focused on computer experiment analysis rather than multi-objective chemical formulation problems. The investigation identified significant differences in problem complexity: whilst computer experiments typically involved continuous, well-behaved response surfaces, inhibitor formulation presented discontinuous, highly nonlinear relationships complicated by chemical interactions and stability constraints.

The environmental sustainability emphasis in inhibitor development highlighted critical differences between DEoptim and existing methodologies. Traditional approaches typically treated environmental acceptability as a constraint rather than an optimisation objective. The analysis revealed that OSPARCOM requirements eliminated approximately 60% of conventional inhibitor formulations due to biodegradability and toxicity concerns (Verma *et al*., 2021). DEoptim offered systematic incorporation of environmental criteria as optimisation objectives, potentially resolving trade-offs between effectiveness and ecological acceptability that previous approaches addressed inadequately. In their article, C. Ren *et al*. (2023) explored a new high-throughput approach to evaluating the effectiveness of carbon steel corrosion inhibitors using droplet microarray technology, which allows up to 200 inhibitor solutions to be tested simultaneously on a single surface. Unlike traditional methods, where samples are completely immersed in electrolyte, corrosion is studied locally – under each microdrop of solution. The study focused on the combination of benzotriazole and cerium nitrate ($Ce(NO_3)_3$) as model inhibitors. The authors demonstrated that their mixture has a stronger anti-corrosion effect than each component separately, i.e., there is a synergistic effect between them. The optimal ratio between these components was determined experimentally, which allows for a significant increase in the protection of the metal surface. Finally, the results were confirmed by molecular modelling – simulations showed that the protective effect of inhibitors is associated with the specific interaction of molecules with the steel surface, which changes when the substances are combined. A. Ziębik & K. Hoinka (2013) demonstrated the importance of mathematical modelling approaches for energy objects and systems, establishing theoretical foundations for systematic optimisation in complex industrial applications.

Despite significant potential, analysis identified several challenges requiring attention. Input data quality critically influenced DEoptim effectiveness, demanding comprehensive experimental datasets for reliable fitness function construction. V.S. Sastri (2011) explored green corrosion inhibitors theory and practice, emphasising that sustainable inhibitor development requires extensive experimental validation and systematic data collection approaches. Computational complexity increased substantially when integrating quantum chemical calculations, potentially limiting practical implementation in resource-constrained environments. V.S. Saji (2010) reviewed recent patents in corrosion inhibitors, highlighting the shift towards innovative approaches including nanotechnology-enhanced solutions and smart coatings that release inhibitors on demand when coating integrity is compromised.

M. Finšgar & J. Jackson (2014) investigated the application of corrosion inhibitors for steels in acidic media specifically within oil and gas operations. Their comprehensive analysis focused on evaluating inhibitor effectiveness under various acidic conditions and identifying optimal formulations for different steel grades. The authors concluded that specialised formulations were essential for extreme conditions, highlighting that conventional inhibitors demonstrated insufficient performance in harsh operational environments. However, their research did not address the systematic optimisation of inhibitor parameters for HPHT applications. U. Unueroh *et al*. (2016) demonstrated that pipeline corrosion control becomes particularly challenging under HPHT conditions where temperatures exceed 150°C and pressures surpass 69 MPa. E.S. Ameh *et al*. (2017) conducted a comprehensive review of field corrosion control and monitoring techniques, identifying significant gaps in systematic optimisation approaches for extreme operational environments.

The article by K. Okon *et al*. (2025) is devoted to analysing the potential of metal oxides as "green" corrosion inhibitors for various alloys in aggressive environments. The authors found that oxides in bulk form do not demonstrate very high inhibition efficiency, but in nanostructured form, their performance increases significantly. As the concentration of nanoparticles increases, the corrosion rate decreases. This is explained by the increase in surface area and better adsorption of oxides on the surface of metals, which reduces the number of available reaction sites. At the same time, they note that at excessively high concentrations, nanoparticulate oxides can agglomerate and impair distribution, which reduces efficiency. The researchers also discussed the mechanisms of action – barrier protection, electrochemical inhibition, synergistic effects with other inhibitors, adsorption, passivation, and self-healing. In addition, they compare the chemical and thermal stability of oxides with traditional organic inhibitors and consider issues of synthesis, safety, ecology, and implementation costs. The conclusion is that nanostructured metal oxides have significant potential as effective and environmentally safe corrosion inhibitors, provided that their concentration is optimised and uniform dispersion in the environment is ensured.

Other developments encompassed several promising directions that distinguished DEoptim applications from conventional approaches. Smart coatings development for self-healing and stimulus-responsive systems that could release inhibitors on demand when coating integrity was compromised represented advancement beyond traditional passive protection methods (Saji, 2010). Advanced integration with deep learning approaches for pattern recognition in complex datasets and prediction of inhibitor performance across varied environmental conditions offered capabilities exceeding traditional statistical methods. The evidence suggested that DEoptim rep O. Roustant *et al*. (2012) developed DiceKriging and DiceOptim packages for analysing computer experiments through kriging-based metamodeling and optimisation, demonstrating the practical value of systematic optimisation tools for complex experimental design problems.

The evidence suggested that DEoptim presented a promising advancement for addressing multi-objective optimisation challenges in HPHT inhibitor development, offering capabilities that traditional approaches struggled to provide. However, successful implementation requires careful consideration of practical limitations including data quality requirements, computational complexity, and integration challenges within existing development workflows. These findings formed the basis for evaluating the overall potential and recommendations for future implementation of DEoptim in corrosion inhibitor development.

Conclusions

The conducted theoretical analysis successfully established the potential of DEoptim for multi-objective optimisation of corrosion inhibitors in HPHT conditions. The systematic literature review confirmed that traditional single-objective approaches proved inadequate for addressing the complex requirements of inhibitor development under extreme operational conditions, where temperatures exceeded 150°C and pressures surpassed 69 MPa. The analysis demonstrated that DEoptim functioned most effectively when integrated within a comprehensive four-phase methodology encompassing experimental screening, computational modelling, evolutionary optimisation, and validation cycles. This integrated approach enabled identification of optimal compromises between inherently conflicting objectives, as evidenced by the trade-offs identified between imidazoline-based inhibitors offering superior corrosion protection exceeding 85% efficiency but exhibiting thermal instability above 120°C and elevated costs of $45-60 per kilogram, versus environmentally acceptable bio-based alternatives achieving only 60-70% inhibition efficiency whilst providing excellent biodegradability.

The hybrid computational approach emerged as a critical finding, where combining quantum chemical calculations for primary screening with subsequent DEoptim application and machine learning for multi-component composition optimisation created a balanced framework for rational inhibitor design. This approach addressed limitations identified in individual computational methods: quantum chemical approaches provided molecular-level insights but failed to scale to complex formulations, molecular dynamics offered realistic condition modelling but remained limited to nanosecond timescales, and machine learning demonstrated promising results but required extensive training datasets often unavailable for novel inhibitor chemistries. DEoptim's population-based approach successfully circumvented limitations of traditional gradient-based methods that required differentiable objective functions and frequently converged to local optima. The algorithm's capability to systematically incorporate environmental criteria as optimisation objectives rather than constraints distinguished it from conventional methodologies, potentially resolving the critical balance between effectiveness and ecological acceptability that previous approaches addressed inadequately.

The theoretical framework established through this review provided foundation for future experimental validation and practical implementation of DEoptim-based optimisation strategies in corrosion inhibitor development for challenging HPHT environments. The application of DEoptim for corrosion inhibitor optimisation represented a promising direction that could significantly accelerate development of effective protective systems for oil and gas equipment under extreme operating conditions whilst supporting industry transition toward more sustainable and environmentally responsible practices. Future research directions should prioritise development of specialised fitness functions specifically designed for HPHT conditions, creation of comprehensive experimental databases enabling robust model training, investigation of synergistic effects in multi-component inhibitor systems, rigorous validation of theoretical predictions through systematic experimental studies, and integration with advanced technologies for real-time optimisation capabilities.

Acknowledgements

None.

Funding

None.

Conflict of Interest

None.

References

[1] Ameh, E.S., Ikpeseni, S.C., & Lawal, L.S. (2017). A review of field corrosion control and monitoring techniques of the upstream oil and gas pipelines. *Nigerian Journal of Technological Development*, 14(2), 67-73. doi: 10.4314/njtd.v14i2.5.

[2] Association for Materials Protection and Performance. (n.d.). *Oil and gas production*. Retrieved from https://www.ampp.org/resources/oil-gas.

[3] Budi, S., Akrom, M., Al Azies, H., Sudibyo, U., Sutojo, T., Trisnapradika, G.A., Safitri, A.N., Pertiwi, A., & Rustad, S. (2024). Implementation of polynomial functions to improve the accuracy of machine learning models in predicting the corrosion inhibition efficiency of pyridine-quinoline compounds as corrosion inhibitors. *KnE Engineering*, 6(1), 78-87. doi: 10.18502/keg.v6i1.15351.

[4] Finšgar, M., & Jackson, J. (2014). Application of corrosion inhibitors for steels in acidic media for the oil and gas industry: A review. *Corrosion Science*, 86, 17-41. doi: 10.1016/j.corsci.2014.04.044.

[5] King, G.E. (2010). *Industry 1970s study: Causes of petroleum-related failures*. Retrieved from https://www.scribd.com/document/373466362/Reliability-of-Downhole-Equipment.

[6] Kumari, P., & Lavanya, M. (2024). Optimization strategies for corrosion management in industries with artificial neural network and response surface technology: A comprehensive review. *Journal of Bio- and Tribo-Corrosion*, 10, article number 59. doi: 10.1007/s40735-024-00863-z.

[7] Leach, A.R. (2011). Cheminformatics and computational chemistry in lead optimisation. *Journal of Cheminformatics*, 3(1), article number O5. doi: 10.1186/1758-2946-3-S1-O5.

[8] Li, D., *et al*. (2023). Corrosion inhibition mechanism of ultra-high-temperature acidizing corrosion inhibitor for 2205 duplex stainless steel. *Materials*, 16(6), article number 2358. doi: 10.3390/ma16062358.

[9] Malinowski, S. (2022). Computational design of anticorrosion properties of novel, low-molecular weight Schiff bases. *Materials*, 15(19), article number 6725. doi: 10.3390/ma15196725.

[10] Okon, K., Ekeke, I.C., Maduabuchi, C.A., Ayogu, I.I., Azeez, T.O., & Akalezi, C.O. (2025). Recent advances in the use of metal oxides as corrosion inhibitors: A review. *Corrosion and Material Protection Journa*l, 69(1), 14-33. doi: 10.2478/kom-2025-0003.

[11] Padmanabhan, E., Jayasangar, T., & Gamage, R.P. (2023). Digitalization in the oil and gas industry. In J. Watada, S.C. Tan, P.-C. Lin, H. Yano, Y. Yabuuchi, E. Padmanabhan & L.C. Jain (Eds.), *Advances in energy research and development: Volume 2: Unconventional methods for geoscience, shale gas and petroleum in the 21st century* (pp. 1-7). Amsterdam: IOS Press. doi: 10.3233/AERD230002.

[12] Popoola, L.T., Grema, A.S., Latinwo, G.K., Gutti, B., & Balogun, A.S. (2013). Corrosion problems during oil and gas production and its mitigation. *International Journal of Industrial Chemistry*, 4(1), 1-15. doi: 10.1186/2228-5547-4-35.

[13] Ren, C., Ma, L., Luo, X., Dong, C., Gui, T., Wang, B., & Zhang, D. (2023). High-throughput assessment of corrosion inhibitor mixtures on carbon steel via droplet microarray. *Corrosion Science*, 213, article number 110967. doi: 10.1016/j.corsci.2023.110967.

[14] Roustant, O., Ginsbourger, D., & Deville, Y. (2012). DiceKriging, DiceOptim: Two R packages for the analysis of computer experiments by kriging-based metamodelling and optimisation. *Journal of Statistical Software*, 51(1), 1-55. doi: 10.18637/jss.v051.i01.

[15] Roy, A., Taufique, M.F.N., Khakurel, H., Devanathan, R., Johnson, D.D., & Balasubramanian, G. (2022). Machine-learning-guided descriptor selection for predicting corrosion resistance in multi-principal element alloys. *NPJ Materials Degradation*, 6, article number 9. doi: 10.1038/s41529-021-00208-y.
[16] Saji, V.S. (2010). A review on recent patents in corrosion inhibitors. *Recent Patents on Corrosion Science*, 2(1), 6-12. doi: 10.2174/1877610801002010006.
[17] Samimi, A., Zarinabadi, S., & Bozorgian, A. (2021). Optimization of corrosion information in oil and gas wells using electrochemical experiments. *International Journal of New Chemistry*, 8(2), 149-163. doi: 10.22034/ijnc.2020.116946.1066.
[18] Sastri, V.S. (2011). *Green corrosion inhibitors: Theory and practice*. Hoboken: John Wiley & Sons. doi: 10.1002/9781118015438.
[19] Song, H., Lee, K., Song, B.C.R., & Xue, J. (2023). The performance tests of HPHT corrosion inhibitor at onshore downhole sour conditions. In *Proceedings of the CONFERENCE 2023* (pp. 1-14). Denver: AMPP. doi: 10.5006/C2023-19242.
[20] Unueroh, U., Omonria, G., Efosa, O., & Awotunde, M. (2016). Pipeline corrosion control in oil and gas industry: A case study of NNPC/PPMC system 2A pipeline. *Nigerian Journal of Technology*, 35(2), 317-320. doi: 10.4314/njt.v35i2.11.
[21] Verma, C., Ebenso, E.E., Quraishi, M.A., & Hussain, C.M. (2021). Recent developments in sustainable corrosion inhibitors: Design, performance and industrial scale applications. *Materials Advances*, 12(2), 3806-3850. doi: 10.1039/D0MA00681E.
[22] Ziębik, A., & Hoinka, K. (2013). Mathematical modeling and optimization of energy systems. In *Energy systems of complex buildings, green energy and technology* (pp. 29-58). London: Springer-Verlag. doi: 10.1007/978-1-4471-4381-9_3.

Застосування DEoptim для оптимізації інгібіторів корозії в умовах HPHT: теоретичний огляд сучасних підходів

Андрій Гриціанчук
Кандидат технічних наук, доцент
Івано-Франківський національний технічний університет нафти і газу
76019, вул. Карпатська, 15, м. Івано-Франківськ, Україна
https://orcid.org/0000-0001-9894-0911

Віталій Григоришин
Аспірант
Івано-Франківський національний технічний університет нафти і газу
76019, вул. Карпатська, 15, м. Івано-Франківськ, Україна
https://orcid.org/0009-0001-4792-1830

Анотація. Корозія нафтогазового обладнання залишається критичною проблемою галузі зі щорічними втратами $1,372 мільярда. Умови високого тиску та високої температури (HPHT) значно ускладнюють розробку ефективних інгібіторів корозії через підвищену агресивність середовища та деградацію традиційних захисних сполук. Метою дослідження було проведення теоретичного аналізу потенціалу застосування методу диференційної еволюції (DEoptim) для багатоцільової оптимізації параметрів інгібіторів корозії в екстремальних умовах HPHT. Методологія дослідження включала систематичний огляд наукової літератури з використанням баз даних Scopus, Web of Science та Google Scholar за період 2019-2024 років, порівняльний аналіз методів комп'ютерного моделювання, теоретичний аналіз оптимізаційних підходів та синтез інформації для формулювання рекомендацій. У роботі систематизовано сучасні підходи до комп'ютерного моделювання інгібіторів, включаючи квантово-хімічні розрахунки, молекулярну динаміку та машинне навчання. Було проведено аналіз специфічних викликів HPHT-середовищ, де температури перевищували 150 °C, а тиск – 69 МПа. Розглянуто переваги еволюційних алгоритмів для навігації в складному багатовимірному просторі параметрів інгібіторів. Обґрунтовано теоретичні засади використання DEoptim для одночасної оптимізації ефективності інгібування, термічної стабільності, екологічної прийнятності та економічної доцільності. Аналіз продемонстрував, що DEoptim забезпечував вищу надійність та багатоцільові можливості порівняно з традиційними градієнтними та генетичними алгоритмами, особливо для HPHT-застосувань. Дослідження запропонувало нову концепцію інтеграції DEoptim з квантово-хімічними розрахунками та машинним навчанням для створення гібридних оптимізаційних платформ, що потенційно зменшує обчислювальні витрати до 60 % при підвищенні ефективності відкриття інгібіторів. Результати показали, що застосування DEoptim забезпечувало систематичний пошук оптимальних формулювань інгібіторів, скорочувало кількість необхідних експериментів та дозволяло виявляти неочевидні синергетичні комбінації компонентів для HPHT-застосувань

Ключові слова: диференційна еволюція; комп'ютерне моделювання; багатокритеріальне проектування; метаевристичні алгоритми; нафтопромислове устаткування

ISSN 1993-9973, e-ISSN 2415-332X

Vol. 26, No. 1 2026

PROSPECTING AND DEVELOPMENT OF OIL AND GAS FIELDS

https://pdogf.com.ua/en

Received: 27.10.2025. Revised: 20.04.2026. Accepted: 29.05.2026. Published: 29.06.2026.

UDC 550.834:004.85

DOI: 10.63341/pdogf/1.2026.16

Machine learning-enhanced seismic attribute analysis for reservoir quality prediction in clastic oil fields

Fahri Maho*

PhD in Water Engineering, Lecturer
Polytechnic University of Tirana
1001, 28 Teodor Keko Str., Tirana, Albania
https://orcid.org/0009-0002-0673-4577

Enkelejda Gjinali

PhD in Water Environmental Engineering, Associate Professor
Polytechnic University of Tirana
1001, 28 Teodor Keko Str., Tirana, Albania
https://orcid.org/0009-0005-4942-3893

Abstract. The aim of the study was to assess machine learning-enhanced seismic attribute analysis for reservoir quality prediction in clastic and Balkan-type oil fields. The validation study was performed on the open-access Project Penobscot seismic and reservoir data for a range of attributes within the predictor space, as well as for the four reservoir quality variables. XGBoost showed the best regression results for all continuous parameters, with the highest accuracy for porosity (R^2 = 0.88, root mean square error = 0.024, mean absolute error = 0.018), followed by the sandiness index (R^2 = 0.85, root mean square error = 0.054, mean absolute error = 0.039), whereas permeability remained the most difficult parameter to predict (R^2 = 0.76, root mean square error = 16.9, mean absolute error = 12.4). Facies classification also demonstrated stable performance, with accuracy of 0.84, precision of 0.82, recall of 0.79, and F1-score of 0.8. The predicted parameter distributions revealed a heterogeneous reservoir system, with porosity as the most stable parameter, sandiness index showing intermediate variability, and permeability displaying the highest contrast. Integrated interpretation of the predicted indicators differentiated the reservoir into high-, moderate-, and low-quality zones with indices of 86, 64, and 38, respectively. In conclusion, reservoir quality is primarily controlled by the factors related to storage and flow potential, sand bodies, and facies, yet machine learning-enhanced methods can effectively assist reservoir engineers in making accurate reservoir predictions in these heterogeneous systems. The practical value of this study is in the potential use of this established workflow to effectively screen for and prioritise oil and gas production within the reservoirs with the help of machine learning, especially those geologically structurally complex clastic systems

Keywords: porosity; square error; permeability; flow potential; sandiness index; Balkan-type

Introduction

Due to the growing complexity of the reservoir prediction in clastic oil fields, there is an increasing interest in utilising data-driven approaches for the interpretation of seismic information. In many instances, particularly in those reservoirs with high degrees of structural complexity, the seismic data can be utilised to make predictions regarding the properties of the reservoir that is being evaluated. Moreover, many of these reservoirs are among those that are considered to be mature or have developed structural complexities that make it particularly difficult to directly observe the reservoirs. Thus, any method that can help to extract information regarding those reservoirs is of interest to those within the oil industry. One such approach that has developed in response to these needs is the application of machine learning approaches to the analysis of seismic data to help extract information regarding the reservoirs.

Suggested Citation: Maho, F., & Gjinali, E. (2026). Machine learning-enhanced seismic attribute analysis for reservoir quality prediction in clastic oil fields. *Prospecting and Development of Oil and Gas Fields*, 26(1), 16-29. doi: 10.63341/pdogf/1.2026.16.

*Corresponding author (*mahofahri2@gmail.com*)

For the Balkan region, specifically for Albania, this problem has certain geological and applied significance. The segment of the Ionian Zone that lies within Albania is tectonically complex, has varying strata within its geologic outcrops, and has a general heterogeneity of its sedimentary features, all of which make it difficult for those attempting to use seismic surveys to model the region to predict the reservoir quality within the area. Petrographic and mineralogical research of the Oligocene flysch of the Ionian Zone of Albania, performed by A. Fociro *et al*. (2023), has determined the compositional heterogeneity of the clastic strata of the region, indicating the importance of its sedimentary origin for explaining the geological heter ogeneity of the area. In the work of J.I. Soto *et al*. (2024) showed that the Ionian Zone of Greece and Albania underwent contrasting types of salt-tectonic processes that significantly affected the structural configuration, trap architecture, and geometry of subsurface bodies. Such features are of fundamental importance for seismic interpretation, since deformation, changes in thickness of strata, and structural blockiness directly change the wave pattern and spatial continuity of reservoirs. An additional regional context was provided by the study of I. Alexandridis *et al*. (2022), in which a new interval of parent rocks was discovered in the adjacent segment of the Ionian zone in the west of Greece, which once again emphasises the oil and gas potential of this tectonic-sedimentary complex for the entire Balkan region. Collectively, these works showed that the Balkan oil and gas context needs such interpretive approaches that are able to combine lithological variability, structural deformation and indirect prediction of petrophysical properties in a single analytical framework. At the same time, modern international studies have proven that machine learning significantly expands the analytical possibilities of interpreting seismic attributes in tasks of reservoir characterisation (Oitseva, 2024). In the work of D.J. Ferreira *et al*. (2021) the classification of seismic patterns was integrated with porosity and permeability estimation, which showed the possibility of direct connection of multidimensional seismic analysis with the prediction of reservoir properties, and not only with its descriptive interpretation. M.H. Rahma Putra *et al*. (2024) confirmed that Gaussian process machine learning can be effectively used for porosity estimation and anomaly detection based on seismic attributes, increasing prediction reliability with limited direct control. In the work of Y. Chen *et al*. (2021) applied machine learning with physical constraints and multiple seismic attributes for deep reservoir characterisation, which is methodologically important because it demonstrates the need to combine predictive flexibility of algorithms with geological plausibility of results. This aspect is especially important in the case of clastic reservoirs, as the purely algorithmic recognition of patterns within seismic data without geological controls may lead to unstable reservoir predictions.

Additional evidence of the effectiveness of machine learning approaches to reservoir description is provided in the article by S. Narayan *et al*. (2024). In this article, the authors discuss the integration of supervised machine learning techniques with seismic impedance inversion methods. The importance of this method is that it allows for the inverted seismic data and attributes to be considered as potential predictors of reservoir characteristics, in addition to the traditional methods of reservoir modelling. Additionally, S.A. El-Dabaa *et al*. (2024) applied unsupervised machine learning techniques to reservoir data with the goal of determining the importance of the different dimensions of seismic data in the prediction of reservoir quality. Author M. Ali *et al*. (2024) described the use of synthetic data and machine learning to model reservoir characteristics from seismic data alone, indicating that machine learning methods have good generalisation abilities. Furthermore, Z.A. Riyadi *et al*. (2024) utilised machine learning to model the prediction of reservoir permeability from elastic properties, which are factors in the determination of the reservoir quality. From the point of view of Water Engineering, reservoir quality is a factor in the determination of the reservoir's ability to accumulate and move fluids.

These methods can be particularly valuable in areas like Albania and the Balkan region in particular, where structural geology makes it difficult to determine reservoir quality. In these cases, machine learning methods can help to improve the robustness of reservoir forecasting techniques by considering various seismic data descriptors of the reservoir. Furthermore, the use of such methods should be based upon the geological context of the reservoir, which can include factors like sedimentation conditions, the blockiness of the structure, or the way in which the predicted properties may impact the movement of fluids within the reservoir media. Therefore, the research is aimed at forming a unified analytical approach to the analysis of seismic attributes, enhanced by machine learning, for predicting reservoir quality in clastic oil deposits, taking into account the specifics of the Balkan region and Albania. The work combines seismic characterisation of the reservoir, oil and gas geology and interpretation of the filtration properties of the porous medium.

The aim of this study was to determine the potential of the use of machine learning enhanced seismic attribute analysis for the prediction of reservoir quality in clastic oil fields, specifically within the Balkan region and the country of Albania. The specific objectives of this study included the survey of the geological and geodynamic factors related to the prediction of reservoir quality in the Balkans region; the evaluation of the various machine learning methods that can be used to predict reservoir quality parameters; and the development and testing of a methodology that employs seismic attributes and machine learning methods to predict reservoir quality and fluid-flow potential in clastic reservoirs.

Materials and Methods

The study was conducted using the Project Penobscot dataset to predict reservoir quality in clastic oil fields based on seismic attributes and machine learning algorithms, with interpretive relevance for Albanian and other Balkan-type reservoir systems. The empirical basis of the study was the open-access Project Penobscot dataset, which was selected as a publicly available geophysical test site suitable for validating an integrated workflow for seismic attribute-based reservoir quality prediction. Open-access regional subsurface datasets directly comparable to Project Penobscot are currently limited for Albania and the wider Balkan petroleum domain; therefore, the Penobscot dataset was used as an empirical benchmark for workflow validation, while the geological applicability of the approach was interpreted with reference to clastic reservoir systems relevant to the Balkan region and Albania.

The dataset used for this study was obtained from the publicly available Project Penobscot project offshore Nova Scotia, Canada. The material base primarily included a 3D post-stack seismic volume $S(x, y, t)$, interpreted stratigraphic horizons H_i, stratigraphic markers, and well-log data $L(z)$, which formed the core basis for seismic attribute extraction and target calibration. Additional dataset components, including 2D seismic profiles and prestack information, were considered only as auxiliary support during interval familiarisation and verification and were not used as an independent basis for the reported predictive results. The 3D seismic cube $S(x, y, t)$ served as the main source for seismic attribute extraction, whereas the well-log data $L(z)$ served as the reference source for reservoir-related target parameters. The interpreted horizons H_i and stratigraphic markers were used to constrain the analysis to geologically consistent intervals and to maintain a stable relationship between seismic reflections and reservoir units.

A working multi-attribute set was constructed from the seismic volume to represent seismic descriptors specifically relevant to the geological setting of Albanian and other Balkan-type clastic reservoirs, where tectonic deformation, stratigraphic variability, internal heterogeneity, and discontinuous sand-body architecture affect reflection continuity, amplitude response, frequency behaviour, and impedance contrasts that are indirectly related to porosity, permeability, and facies organisation. This set included amplitude-related attributes A_{amp}, represented by instantaneous amplitude A_{inst} and RMS amplitude A_{RMS}; frequency-sensitive attributes A_{freq}, represented by instantaneous frequency f_{inst} and sweetness SW; geometric and continuity-related attributes A_{geom}, including coherence C and variance Var; and inversion-derived parameters A_{inv}, particularly acoustic impedance AI. The analytical dataset was represented by the predictor matrix (1):

$$X = [A_1, A_2, \dots, A_n]. \tag{1}$$

The vector of continuous target variables (2):

$$Y_c = [\phi, k, SI]. \tag{2}$$

The categorical target variable used for facies classification (3):

$$Y_f = F, \tag{3}$$

where ϕ – porosity; k – permeability; SI – the sandiness index; F – the facies class. Porosity is an estimation based on well log data and is used as the main indicator of the reservoir's storage capacity. Permeability is obtained from the reference petrophysical dataset and represents the permeability of the selected well intervals. The sandiness index is calculated from the sandy nature of the intervals. The facies class is also determined from the well log data and divides the intervals into different facies according to their lithology. Thus, these parameters represent both the continuous regression targets (ϕ, k, SI) and the categorical classification target (F). These target variables were selected because, taken together, they provide an operational representation of reservoir quality in clastic systems and allow subsequent engineering interpretation in terms of storage capacity, filtration potential, internal heterogeneity, and probable fluid-flow behaviour.

The analytical sample was non-random and condition-based. It was formed only from intervals for which consistency between $S(x, y, t)$, H_i, and $L(z)$ could be ensured. The inclusion criteria required acceptable seismic signal quality, stable time-depth alignment, interpretable stratigraphic correlation, and sufficiently complete well-log coverage. Intervals affected by major noise contamination, incomplete logging curves, unstable stratigraphic attribution, or ambiguous seismic-to-well ties were excluded. Following data cleaning, interval alignment, and preparation of the predictor and target variables for inclusion into the analysis, the dataset comprised 324 interval-level observations from 2 wells (L-30 and B-41) from the Project Penobscot dataset. Each observation in the dataset represented one individual interval within the wells. This predictor-target matrix served as the basis for subsequent model training and validation.

Data pre-processing, seismic attribute extraction, model development, validation, and result analysis were carried out using OpendTect, Petrel, Python 3.11, OriginPro 2024, and Microsoft Excel 365. The methodological workflow consisted of five successive stages: data preparation, attribute processing, feature selection, model training and validation, and integrated interpretation of predicted reservoir-quality indicators. At the first stage, seismic and well data were checked for consistency within a common interpretation framework. Seismic reflections were tied to the available well-log intervals using interpreted horizons and stratigraphic markers in order to ensure that predictor variables and target parameters referred to the same geological intervals. Only those intervals for which the time-depth relationship was sufficiently stable were retained for analysis. At the second stage, all continuous input variables were normalised using z-score transformation (4):

$$Z_i = \frac{X_i - \mu}{\sigma}, \tag{4}$$

where X_i – original feature value; μ – the mean; σ – standard deviation. To reduce multicollinearity within the predictor space, pairwise Pearson correlation screening was applied; variables with $|r| > 0.85$ were considered redundant. Highly correlated predictors were removed, after which recursive feature elimination was applied to retain a compact subset of informative variables for model training. At the third stage, the dataset was divided into training and testing subsets with an 80:20 ratio. The split was performed randomly at the interval level for the regression tasks and with stratification for the facies classification task in order to preserve class proportions. For regression tasks, Random Forest, XGBoost, and Gaussian Process Regression were used to predict continuous reservoir parameters. For facies classification, Support Vector Machine was applied. Model robustness and generalisation capability were assessed using 5-fold cross-validation. At the fourth stage, the predictive performance of regression models was evaluated using the coefficient of determination (5), root mean square error (RMSE) (6) and mean absolute error (MAE) (7):

$$R^2 = 1 - \frac{\sum_{i=1}^{n}(y_i - \hat{y}_i)^2}{\sum_{i=1}^{n}(y_i - \bar{y})^2}; \quad (5)$$

$$RMSE = \sqrt{\frac{1}{n}\sum_{i=1}^{n}(y_i - \hat{y}_i)^2}; \quad (6)$$

$$MAE = \frac{1}{n}\sum_{i=1}^{n} | y_i - \hat{y}_i |, \quad (7)$$

where y_i – reference value; $\hat{y}_i$ – predicted value; $\bar{y}$ – mean of reference values; n – the number of observations. For classification tasks, model quality was assessed using accuracy (8), precision (9), recall (10), and F1-score (11):

$$Accuracy = \frac{TP+TN}{TP+TN+FP+FN}; \quad (8)$$

$$Precision = \frac{TP}{TP+FP}; \quad (9)$$

$$Recall = \frac{TP}{TP+FN}; \quad (10)$$

$$F1 = 2 \cdot \frac{Precision \cdot Recall}{Precision + Recall}, \quad (11)$$

where TP, TN, FP, and FN denote true positive, true negative, false positive, and false negative predictions, respectively. In addition to mean, standard deviation, minimum, and maximum values, the coefficient of variation was calculated to compare the relative variability of the predicted reservoir parameters. The relative discriminative role of the continuous reservoir-quality parameters was interpreted on the basis of their normalised spread and coefficient of variation, with higher values indicating a stronger contribution to the differentiation of reservoir-quality groups. At the final stage, the trained models were applied to the attribute space to generate continuous and categorical prediction outputs. For integrated reservoir-quality interpretation, the predicted indicators were first transformed to a common normalised scale from 0 to 100. For the continuous variables, min-max normalisation was applied as follows (12):

$$V_i^{norm} = 100 \cdot \frac{V_i - V_{min}}{V_{max} - V_{min}}, \quad (12)$$

where V_i – predicted value of the corresponding parameter; V_{min}, V_{max} – the minimum and maximum values of that parameter within the analysed dataset. Facies class was incorporated as an ordinal categorical component reflecting the relative geological favourability of facies types for reservoir development. The integrated reservoir-quality index was then calculated as (13):

$$RQI = w_\phi \phi^{norm} + w_k k^{norm} + w_{SI} SI^{norm} + w_F F^{norm}, \quad (13)$$

where w_ϕ, w_k, w_{SI}, and w_F – weights assigned to the normalised components. In the absence of field-specific prior weighting constraints, equal weights were used ($w_\phi = w_k = w_{SI} = w_F = 0.25$). The resulting index was used to differentiate the analysed intervals into high-, moderate-, and low-quality groups. For integrated reservoir-quality interpretation, the predicted indicators were transformed to a common comparative scale and combined into a composite ranking scheme. Porosity, permeability, and sandiness index contributed to the integrated assessment as continuous variables, whereas facies class was incorporated as a categorical factor providing geological context for zone differentiation. On this basis, the analysed reservoir intervals were classified into high-, moderate-, and low-quality groups. The results presented in the paper were summarised through comparative model-performance metrics, descriptive statistics of the predicted parameters, and integrated reservoir-quality ranking. The interpretation focused on reservoir heterogeneity, storage capacity, permeability distribution, internal compartmentalisation, and probable fluid-flow behaviour within clastic reservoir systems.

Results

Seismic attribute space as a predictor basis for reservoir quality analysis

The resulting predictor space X, as defined in Equation (1), indicates that the reservoir quality prediction in the clastic oil fields can be made possible by a set of seismic attributes with different functions. The seismic volume that was processed along with the seismic data provided a set of attributes that collectively reflected the seismic responses associated with the lithology of the subsurface formation. This shows that the predictor space was appropriately defined to include the attributes that would best represent the main features of the reservoir in terms of its impact upon reservoir quality. Furthermore, the obtained attributes indicated that the individual groups of selected attributes provided slightly different information from one another. The amplitude attributes were used to recognise the contrasts within the subsurface from the strength of the seismic reflections. The frequency attributes were used to recognise the contrasts within the subsurface that were associated with the layering of the subsurface formations. The geometric attributes were used to recognise the contrasts within the subsurface that were associated with the discontinuities of the subsurface formations. Finally, the inversion attributes were used to recognise the contrasts within the subsurface that were associated with the lithology and porosity of the subsurface. The composition of the predictor space and the function of each of the attributes within that space are presented in Table 1.

Table 1. Composition and functional role of seismic attributes used in the study

Attribute group	Attribute	Notation	Analytical function in reservoir quality prediction
Amplitude	Instantaneous amplitude	A_{inst}	Reflects local reflection strength and contrasts in acoustic properties
	RMS amplitude	A_{RMS}	Characterises the total reflection energy within the analysis window
Frequency	Instantaneous frequency	f_{inst}	Reflects variations in layer thickness and vertical heterogeneity
	Sweetness	SW	Represents the combined amplitude and frequency structure of the signal
Geometric	Coherence	C	Detects discontinuities, body boundaries, and loss of continuity
	Variance	Var	Enhances local heterogeneity and internal segmentation
Inversion	Acoustic impedance	AI	Reflects elastic contrasts associated with lithology and porosity

Note: the predictor space presented in Table 1 corresponds to the final attribute subset retained after pairwise correlation screening and recursive feature elimination

Source: compiled by the authors based on the Project Penobscot dataset, seismic attribute extraction and interpretation performed in OpendTect and Petrel

As shown in Table 1, the constructed predictor space combined four complementary groups of features, none of which duplicated another in functional meaning. The amplitude attributes provided a basic characterisation of reflection strength and proved to be the most informative for identifying acoustic contrasts between intervals. This indicated their particular suitability for delineating zones of lithological change and intervals with differing reservoir quality. The frequency attributes, in turn, reflected the finer internal organisation of sedimentary bodies and proved important for characterising vertical heterogeneity, layering, and textural features of clastic sequences (Shevko *et al.*, 2021).

A different analytical role was demonstrated by the geometric attributes. Unlike the amplitude and frequency attributes, they proved to be the most suitable for identifying lateral boundaries, continuity disruptions, and internal segmentation of reservoir bodies. This is particularly important for the task of reservoir quality prediction, since the quality of a clastic reservoir is determined not only by its average petrophysical properties but also by the degree of spatial connectivity and heterogeneity (Cristea *et al.*, 2023). The inversion-derived attribute, represented by acoustic impedance, showed the clearest relationship with physically interpretable rock properties and therefore became a key link between seismic response and the prediction of continuous parameters, primarily porosity and permeability. The generalisation of the predictor-space structure showed that amplitude and inversion-derived attributes formed the main basis for estimating ϕ and k, whereas frequency and geometric features increased sensitivity to and , that is, to the internal organisation of the reservoir and facies variability. Therefore, the constructed space X proved sufficient for subsequent machine learning-based reservoir quality prediction, as it captured both direct and indirect seismic manifestations of lithology, heterogeneity, and reservoir architecture. This created a substantive basis for the next stage, namely, comparing the performance of machine learning models in predicting reservoir quality parameters. The resulting predictor structure is relevant to clastic reservoir systems of the Balkan type, where lithological variability, structural fragmentation, and internal heterogeneity require a multi-attribute basis for reservoir quality prediction.

Reservoir quality targets and analytical representation of the response variables

The analytical representation of the system response through the continuous target variables in Equation (2) and the categorical facies variable in Equation (3) indicates that reservoir quality in a clastic reservoir cannot be represented by a single parameter. The resulting structure of the target variables revealed the multi-component nature of reservoir quality, in which quantitative petrophysical properties are combined with lithological and facies-related characteristics. As a result, the system response acquired an integrated form, making it possible to consider reservoir quality not in isolation but as a combination of storage capacity, flow potential, the degree of development of sandy bodies, and the internal spatial differentiation of the reservoir. The composition of the target vector and the functional role of its components are presented in Table 2.

Table 2. Target reservoir-quality parameters used in the study

Parameter	Notation	Parameter description	Engineering role in reservoir characterisation
Porosity	ϕ	Fraction of pore space in the rock	Characterises the storage capacity of the reservoir for fluid accumulation
Permeability	k	Ability of the rock to transmit fluids	Determines flow potential and the possible intensity of fluid movement
Sandiness index	SI	Relative proportion of sandy material within the interval	Reflects the degree of development of potentially reservoir-prone bodies in clastics
Facies class	F	Assignment of the interval to a specific facies type	Allows accounting for spatial and lithological heterogeneity of the reservoir

Source: compiled by the authors based on the Project Penobscot dataset, analytical structuring of target variables performed in Python 3.11

As shown in Table 2, the quantitative core of the resulting representation was formed by porosity ϕ and permeability k. These parameters most directly reflected reservoir quality in terms of fluid storage and flow capacity. Their joint presence in the response vector demonstrated that reservoir characterisation requires the simultaneous consideration of both storage and filtration components. In the absence of either parameter, the assessment of reservoir quality would be incomplete, since high porosity does not necessarily imply high permeability, just as satisfactory permeability is not always accompanied by sufficient pore volume. At the same time, the sandiness index SI served as the parameter that linked the petrophysical response to the lithological structure of the reservoir. Its inclusion in the vector Y showed that variations in reservoir quality have not only a physical but also a clearly expressed sedimentological dimension. Unlike ϕ and k, which describe the properties of the rock as a medium for fluid storage and flow, SI reflected the degree of development of sandy bodies as the most prospective reservoir intervals. As a result, this parameter provided the connection between quantitative quality indicators and the lithological expression of the reservoir environment. The facies variable F complemented this system by introducing a spatial and structural level of interpretation. Its presence in the response vector demonstrated that reservoir quality in clastic deposits is determined not only by the magnitude of individual properties but also by the facies organisation of the environment in which these properties are realised. In this sense, F did not duplicate other components of the vector but defined the context of their spatial manifestation. The facies component thus enabled the transition from a purely parametric assessment to a structured representation of the reservoir as a heterogeneous system with internal differentiation. The generalisation of the resulting representation of the target vector showed that ϕ, k, SI and F form a sufficient and complementary set of indicators for reservoir quality characterisation. Porosity and permeability described its storage-flow core, the sandiness index refined the lithological prospectivity of intervals, and the facies class revealed the internal spatial heterogeneity of the system. Therefore, the continuous target vector Y_c represented in Equation (2) was utilised to define the continuous target variable that would be used to compare the different machine learning models for estimating the continuous reservoir parameters. This multi-component representation of the response space is particularly important for Balkan clastic reservoirs, where reservoir quality is controlled simultaneously by storage capacity, flow potential, sand-body development, and facies-related heterogeneity.

Model performance for prediction of continuous reservoir parameters

The comparison of regression results showed that the predictive accuracy of continuous reservoir-quality parameters was uneven both across models and across target variables. The evaluation metrics defined by equations (4)-(7) made it possible to compare the performance of the models for porosity, permeability, and sandiness index within a single analytical framework. The obtained values of R^2, RMSE and MAE indicated that the response of the models depended on the physical nature of the predicted parameter, with higher stability observed for porosity and sandiness index and lower stability for permeability. The comparative regression results are presented in Table 3.

Table 3. Regression performance of machine learning models for predicting porosity, permeability, and sandiness index

Model	ϕ R^2	ϕ RMSE	ϕ MAE	k: R^2	k: RMSE	k: MAE	SI: R^2	SI: RMSE	SI: MAE
Random Forest	0.84	0.028	0.021	0.71	18.6	13.9	0.81	0.061	0.046
XGBoost	0.88	0.024	0.018	0.76	16.9	12.4	0.85	0.054	0.039
Gaussian Process Regression	0.82	0.031	0.023	0.68	20.3	14.8	0.79	0.066	0.049

Note: the metrics are reported for the test set that was divided during the 80:20 split of the training set. Five-fold cross validation was used during the training of the models to ensure generalisation of the models

Source: compiled by the authors based on the Project Penobscot dataset, data preprocessing, model training, and metric calculation performed in Python 3.11, seismic interpretation support in OpendTect and Petrel

As presented in Table 3, XGBoost model achieved the highest overall predictive performance for each of the reservoir properties, based on the best values of each of the three regression metrics. For the prediction of porosity (ϕ), XGBoost achieved the highest value of the coefficient of determination ($R^2 = 0.88$), as well as the lowest values of the error metrics (RMSE = 0.024; MAE = 0.018). Random Forest also achieved relatively high values of each of the three regression metrics for the prediction of porosity, but with higher error values than XGBoost. Lastly, Gaussian Process Regression achieved an acceptable level of accuracy for the prediction of porosity, but with a lower R^2 value and higher error metrics than both the XGBoost and Random Forest models. The same ranking of the three models for the best performance relative to the prediction of permeability (k) was also achieved by each of the models, but with lower accuracy relative to the prediction of porosity. For permeability prediction, XGBoost achieved the best overall performance, with the highest R^2 value (0.76) and the lowest error metrics (RMSE = 16.9; MAE = 12.4). Random Forest models had slightly lower values for each of these metrics for the prediction of permeability, while Gaussian Process Regression achieved the lowest accuracy for permeability prediction. The relatively low accuracy of permeability prediction compared to porosity is likely due to the fact that permeability is a more difficult parameter to predict directly from seismic attributes than porosity.

For the sandiness index (*SI*), all three models achieved relatively high and strong values of each of the three regression metrics, but with XGBoost achieving the highest values. Overall, however, the accuracy of prediction for the sandiness index was higher for Random Forest and Gaussian Process Regression than for permeability. The sandiness index was more easily predicted than permeability, likely due to the fact that the sandiness index has a more stable relation to the attribute space than does permeability. Thus, each of the three models exhibited different levels of accuracy in the prediction of the three reservoir parameters. Porosity was the most easily predicted parameter with the models, followed by the sandiness index, and then permeability. The accuracy of each model in the prediction of each of these parameters indicates that the seismic attribute space is better able to represent storage (porosity and sandiness) than it is to represent flow (permeability). These differences in performance will inform the following stage of this analysis. The obtained ranking of regression performance is especially relevant for Balkan petroleum settings, where permeability prediction is expected to remain more uncertain than porosity and sandiness due to structural complexity and heterogeneous reservoir architecture.

Classification performance for facies prediction

The classification results showed that the facial variable *F* was reproduced by the model with an acceptable level of accuracy sufficient for further use in spatial interpretation of the reservoir. Evaluation by the metrics presented in formulas (8)-(11) made it possible to establish not only the general level of correctness of the classification, but also the degree of balance of the model between the accuracy of class recognition and the completeness of their selection. The obtained results proved that the facies organisation of the reservoir environment is reflected in the attribute space quite stably, although the accuracy of recognition of individual classes remained different. Comparative values of classification metrics are shown in Figure 1.

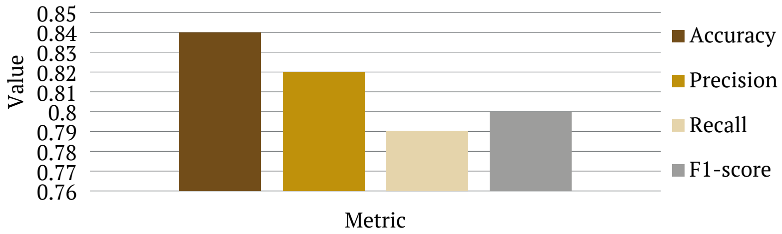

Figure 1. Classification performance metrics for facies prediction
Source: compiled by the authors based on the Project Penobscot dataset, classification performance assessed according to Equations (8)-(11), data processing in Python 3.11

As presented in Figure 1, the classification model achieved an overall accuracy of 0.84 with a precision of 0.82, a recall of 0.79 and an F1-score of 0.8. These results indicate that the model was able to generally stably classify the facies within the reservoir. Furthermore, the relatively balanced precision and F1-score score with the slightly lower recall indicates that the model was generally consistent in its predictions of the facies. Thus, while the model is adequate for predicting the facies within the reservoir, a more detailed analysis is required to determine specifically how the model performed in relation to each individual facies. Overall, the results of classification model indicate that the predictor space is informative enough to be utilised in the prediction of reservoir facies. The accuracy, precision, recall, and F1-score for the model indicate that the model is able to generally return the same structure of the reservoir facies as exist in the analysed reservoir intervals. Moreover, these results allow for the use of the model to predict the reservoir facies as an additional model to those that continuously predict parameters like porosity, permeability, and sandiness index; the determination of reservoir quality is not based upon the individual measurements of each of these parameters, but in relation to the structure of the reservoir facies itself. Furthermore, while these results are generally positive and indicate the ability of the model to appropriately classify the facies within the reservoir, some degree of caution must be applied in interpreting these results; the results are based only upon the classification of the reservoir intervals and does not include a confusion matrix or analyses of the classification of each individual class of reservoir facies. Despite these limitations, the incorporation of a model that predicts reservoir facies is still important in the reservoir description and geological representation of the reservoir. The incorporation of such a model allows for the description and determination of the structure of the analysed reservoir intervals. Finally, the applicability of this specific model and technique to reservoirs of the Balkan type is additionally motivated by the fact that the structure of those reservoirs tends to exhibit the same geological heterogeneity and structure as do the analysed reservoir intervals.

Distribution of predicted porosity, permeability, and sandiness index

After applying the machine learning models to the predictor space, the values of the continuous reservoir-quality parameters, as defined in Equation (2), namely, ϕ, k, and *SI*, were obtained. Unlike the previous subsection that focused upon the various performance metrics of the models, the results of the application of the models to the predictor space will be examined in this subsection. The obtained values of each of these parameters indicates that the predicted reservoir is not uniformly composed of the same type of sedimentary rocks and intervals; rather, there are differences in each of the parameters that indicate the inherent heterogeneity of the reservoir. The statistical characteristics of each of these parameters is summarised in Table 4.

Table 4. Statistical characteristics of predicted reservoir parameters

Parameter	Mean	Standard deviation	Minimum	Maximum	Coefficient of variation
Porosity, ϕ	0.184	0.037	0.112	0.267	0.201
Permeability, k (mD)	146.8	58.4	52.3	284.6	0.398
Sandiness index, SI	0.63	0.14	0.34	0.88	0.222

Source: compiled by the authors based on the Project Penobscot dataset, classification performance assessed according to Equations (7)-(10), data processing in Python 3.11

As shown in Table 4, porosity ϕ proved to be the most homogeneous among the reservoir parameters that were calculated. Porosity has a mean value of 0.184 and a standard deviation of 0.037. These values indicate that storage properties of the reservoir were the least contrastive of the parameters considered. Reservoirs did include intervals with relatively less prospective storage properties than others, and those with relatively better properties, but the contrast between minimum and maximum values was the least among the analysed parameters. This level of homogeneity was also established in the discussion of porosity stability in the previous stage of model evaluation. The homogeneity of this parameter indicates that the reservoir's capacity properties were represented more uniformly throughout the system than its flow-related properties.

Permeability k exhibited a completely different distribution within the reservoir. Permeability had the highest degree of variability of the parameters. Mean permeability value was calculated at 146.8 mD, standard deviation 58.4 mD and the coefficient of variation (a measure of variability relative to the mean) 0.398, the highest of all the calculated coefficients. These values indicate that permeability was the most contrastive parameter within the reservoir space. Minimum permeability of the reservoir was 52.3 mD, and the maximum value was 284.6 mD. Such contrast indicates that permeability is the most sensitive parameter to internal heterogeneity within the reservoir and that its value varies the most among different sections of the reservoir. Sandiness index SI exhibited intermediate variability within the reservoir. Mean sandiness index within the reservoir was 0.63, with values ranging from 0.34 to 0.88. While not as high as permeability, the range in sandiness index indicates differences between the lithologies within the reservoir. The reservoir has segments that exhibit different degrees of sandy bodies. The distributions of porosity, permeability, and sandiness indicate that the reservoir has multi-level heterogeneity within it. Porosity indicates the stability of the reservoir's storage properties, permeability the contrast in the flow properties of the reservoir, and the sandiness the distribution of sandy bodies within the reservoir. These three parameters indicate that the quality of the reservoir within this clastic system is based upon the interrelation of the storage, flow, and sand body properties. This pattern of heterogeneity is especially important to consider within the context of clastic reservoirs of the Balkan type.

Integrated interpretation of reservoir quality and fluid-flow potential

The integrated interpretation of the predicted parameters showed that reservoir quality within the analysed clastic system was controlled by the combined effect of porosity , permeability , sandiness index SI, and facies class F, rather than by any single indicator taken in isolation. When considered together, these variables formed a differentiated reservoir-quality pattern in which storage capacity, transmissibility, lithological prospectivity, and facies-controlled heterogeneity interacted to produce zones with clearly unequal engineering potential. The resulting configuration indicates that the studied reservoir space was internally structured into intervals of high, moderate, and low quality, each associated with a distinct combination of petrophysical and lithological characteristics. The integrated ranking of reservoir zones, obtained from the normalised predicted quality indicators according to Equations (12) and (13), is shown in Figure 2.

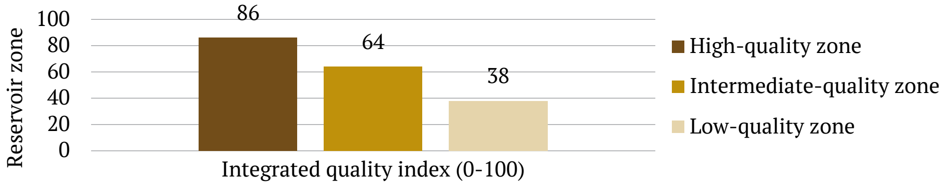

Figure 2. Integrated ranking of reservoir zones by predicted quality indicators
Source: compiled by the authors based on the integrated interpretation of predicted porosity, permeability, sandiness index, and facies class derived from the Project Penobscot dataset, seismic interpretation support in OpendTect and Petrel, data processing in Python 3.11

As shown in Figure 2, the integrated ranking divides the predicted reservoir space into three quality levels. The highest quality of reservoir zones reaches the highest integrated index of 86, the intermediate quality of reservoir zones has an index of 64, while the lowest quality of reservoir zones has the lowest integrated index of 38. The difference between the highest and the lowest ranked zones in terms of the integrated index is 48. The ranking of the quality of reservoir zones within the clastic reservoir system of the Balkan type shows that the prospective zones have higher levels of porosity, permeability, and sand-body development, while the lower ranked zones have lower permeability, porosity, and sand-body development. The integrated ranking of the quality of reservoir zones within the clastic reservoir system of the Balkan type is especially helpful in recognising the effect of the four different variables on the prospectivity of the reservoir zones. Permeability is the most discriminating variable in determining the quality of the reservoir zones, as indicated by the ranking results. The other variables of porosity, sandiness, and facies have other important contributions to the prospectivity of the zone. Porosity is the most important parameter in determining the storage capacity of the reservoir zones, while sandiness and facies are important in recognising the development of sandy bodies within the reservoir zones. The integration of these four variables is important in converting the separate predicted variables of reservoir quality to a model that can help to determine the probable behaviour of the reservoir in relation to the movement of fluids through the reservoir. Furthermore, the developed pattern is especially important in the evaluation of clastic reservoirs of the Balkan type.

The quality of the reservoir zones within these formations are often influenced by lithological variability, variability in the development of sandy bodies within the reservoir zones, and the heterogeneity of the sedimentary facies within the reservoir (Babayeva *et al.*, 2024). Thus, the workflow developed for the recognition of these four variables is relevant to the evaluation of the petroleum reservoirs of Albania and the Balkans region in general, even if the workflow is not applied to the specific data of Albania. Additionally, because of the importance of each of these four variables for the prediction of the quality of the reservoir zones within clastic reservoirs of the Balkan type, the developed workflow is transferable to those same reservoir systems, as well. Thus, the integrated ranking of the quality of reservoir zones within the clastic reservoir system of the Balkan type indicates that the most prospective zones for petroleum exploration and production will have high levels of porosity (ϕ), permeability (k), sand-body development (SI), and favourable facies, while the least prospective zones will contain low levels of those same variables. Thus, the machine learning and seismic attribute workflow developed for prediction of the quality of the reservoir zones within clastic oil fields is analytically suitable for application to those oil fields, including the Balkan-type oil fields, including those within Albania.

Overall, the obtained results demonstrate that the constructed multi-attribute seismic predictor space, combined with machine learning methods, provides a consistent and analytically reliable basis for reservoir quality prediction in clastic oil systems. The results confirmed that reservoir quality cannot be described by a single parameter, but emerges from the interaction of porosity, permeability, sandiness index, and facies structure. The models showed the highest predictive stability for the porosity and sandiness index, while permeability proved to be the most sensitive to heterogeneity within the reservoir rock. The classification of facies within the area also helped to reveal information about the reservoir that was not otherwise obtained from the prediction models. The distribution of the predicted reservoir parameters helped to reveal the different levels of heterogeneity existing within the reservoir, as well as the differing stability of reservoir properties like storage versus flow potential. The differentiated zones within the reservoir have different engineering potentials due to the reservoir characteristics like permeability and sandy bodies. Such an analysis helps to confirm the applicability of this workflow to these types of reservoirs and its relevance to the Balkans-type reservoirs specifically.

Discussion

Comparison of the obtained results with modern works in the field of seismic interpretation made it possible to more precisely outline their place in the current direction of reservoir characterisation, where the combination of multi-attribute analysis with machine learning algorithms is gaining more and more importance. Such a comparison revealed not only the commonality of methodological approaches, but also differences in which parameters of the reservoir were reproduced most stably, how important the role of facies control remained, and how the influence of the internal heterogeneity of the environment was interpreted. In this context, it is advisable to consider the obtained results sequentially, in the order of the involved sources, comparing the nature of the established regularities with the conclusions of the conducted research.

An increase in the accuracy of estimation of petrophysical properties in a lithologically variable environment was obtained in the work of J.O. Olutoki *et al.* (2024) by combining geostatistical inversion with extreme gradient boosting. A similar pattern was found in the conducted study, where XGBoost provided the best results for predicting porosity and sandiness index, which indicated the high efficiency of this algorithm in the tasks of detecting non-linear relationships between seismic attributes and reservoir properties. An increase in interpretive reliability under conditions of limited direct control was shown in a study by N. Abd-Elfattah *et al.* (2025), where machine learning algorithms were combined with the amplitude versus offset class II workflow for hydrocarbon prospectivity assessment. The obtained results revealed a close logic, since the multicomponent space of seismic predictors also provided stable reproduction of reservoir characteristics even in the presence of a complex internal structure and heterogeneous distribution of properties within the clastic system. Improvement of identification of promising intervals under conditions of structural and stratigraphic complexity was achieved in the work of M. Reda *et al*. (2024) by combining high-resolution seismic analysis and 3D modelling. In the conducted research, a related effect was obtained at the stage of integrated ranking of zones, when the greatest informativeness was provided not by the isolated interpretation of individual attributes, but by the combined analysis of porosity, permeability, sandiness index and facies structure. A more meaningful facies interpretation under the conditions of integration of mineralogical and porosity information was demonstrated in the work of P. Owusu *et al*. (2025), where machine learning was used for seismofacies analysis. Such an approach was consistent with the obtained results, as the facies classification did not duplicate the prediction of continuous parameters, but extended it by adding spatial context and clarifying the internal organisation of the reservoir.

A reduction in predictor redundancy and an improvement in the identification of sand bodies was established in a study by T.F. Ren *et al*. (2025), where Light Gradient Boosting Machine was combined with RFECV. The same methodical advantage was observed in the conducted study, since preliminary correlation screening and recursive feature elimination made it possible to form a compact and functionally disjoint set of attributes, on which the sandiness index was predicted more stable than permeability. Increased sensitivity to fine sand bodies in complex sedimentation conditions was obtained by J. Wang *et al*. (2025) thanks to the combination of self-organising map-optimisation of attribute space with seismic waveform inversion. The obtained results revealed a close trend, since it was the combination of amplitude, frequency, geometric and inversion indicators that provided acceptable sensitivity to lithological variability and internal heterogeneity of clastic intervals. The need for an integrated approach to reservoir characterisation was substantiated by G. Murtaza *et al*. (2025), who combined petrophysical, seismic and rock-physics analysis and showed the limitation of relying on only one type of data. The obtained results developed the same logic, since the quality of the reservoir was interpreted not through a single parameter, but through the interaction of porosity, permeability, sandiness and facies belonging within a single analytical scheme. The dependence of the reliability of seismofacies on the consideration of the wider sedimentary context was shown in the work of P.C. Kumar *et al*. (2026), where subsurface and outcrop data were integrated for the analysis of complex sedimentation systems.

A similar trend was found in the conducted study, where the interpretive value of the predicted parameters increased when they were considered not in isolation, but within the integral internal architecture of the clastic system. An improvement in the prediction of lithofacies and their spatial distribution in a deltaic reservoir was demonstrated by S.M. Badr *et al*. (2026) by integrating machine learning with seismic attributes. This was consistent with the obtained results, since it was the facies classification that made it possible to move from a set of individual predicted values to a spatially differentiated model of the reservoir with different degrees of perspective. An increase in the geological relevance of the prediction of reservoir properties was obtained in the work of K. Ren *et al*. (2026) by optimising seismic attributes in combination with spectral decomposition and automated machine learning. A similar conclusion emerged from the conducted study, where the best prognostic quality was achieved not due to the maximum expansion of the descriptor space, but due to the selection of features that reflected different, but not duplicated aspects of lithology, heterogeneity and reservoir architecture. A significant improvement in the prediction of sand bodies in complex structural and sedimentary conditions was shown by J. Liu *et al*. (2026), who combined multi-attribute seismic analysis with machine learning under facies constraint. The obtained results revealed the same pattern, as it was the inclusion of the facies component together with porosity, permeability and sandiness index that made it possible to move from individual predictions to a holistic model of reservoir quality with a clear separation of high, medium and low potential zones.

Improved accuracy of porosity estimation in heterogeneous siliciclastic rocks was obtained by M. Hussain *et al*. (2025) through the integration of conventional approaches, machine learning, and seismic inversion. A similar tendency was observed in the conducted study, where porosity proved to be the parameter with the highest predictive stability, while the combination of multi-attribute analysis and machine learning algorithms produced the best accuracy values specifically for this indicator. High efficiency of machine learning for predicting lithological and petrophysical parameters in hydrocarbon exploration tasks was demonstrated by D. Arkadiusz *et al*. (2025) using the Carpathian Foredeep case study. The obtained results revealed a similar pattern, as they also indicated that machine learning was most effective when applied not to the isolated prediction of a single variable, but to the simultaneous interpretation of several interrelated reservoir characteristics. The integration of seismic attributes and Hjorth parameters for seismic facies classification and total organic carbon prediction was implemented by R. Al Hasan *et al*. (2025), who showed that the expansion of the descriptor space increased interpretive sensitivity to the internal heterogeneity of the medium. A comparable effect was obtained in the conducted study, where a heterogeneous set of amplitude, frequency, geometric, and inversion-derived attributes made it possible to reproduce both continuous reservoir parameters and facies structure within a single analytical framework. The issue of training-data consistency and the need for its verification in the context of seismic deep learning tasks was examined in detail by A. Pradhan & T. Mukerji (2022). The authors showed that the quality of the predictions of the deep learning models depended on two factors: the validity of the training data and the absence of contradictions between the training data and geological expectations. These findings correspond to the study conducted herein, as the same analytical sample of seismic data was formed only from data segments with consistent time-depth relationships and signal quality, as well as good seismic well log ties.

A new approach to seismic-attribute optimisation based on forward modelling and machine learning was proposed by W. Li *et al*. (2023), who found that targeted feature selection improved the prediction quality of fluvial reservoirs. A similar conclusion followed from the obtained results, since the best predictive performance was achieved not through mechanical expansion of the attribute space, but through the selection of predictors representing different aspects of lithology, heterogeneity, and reservoir architecture without functional duplication. Petroleum prospect generation and evaluation based on machine learning and seismic attributes were examined by M. Farfour *et al*. (2025), who showed that data-driven analysis improved the quality of prospect evaluation in offshore conditions. The results obtained made it possible to not only rank the determined zones according to their quality but also to create a more comprehensive model of the reservoir based on these parameters.

A similar approach to the identification of prospective reservoirs and the risking of their exploration was presented by M. Farfour & D. Foster (2022). The authors used machine learning algorithms to predict a series of seismic attributes that made it possible to better explore the area of interest. The same principle can be seen in the development of a model that predicted lithology that provided more information than each of the individual seismic attributes alone. The use of machine learning to predict lithology based on well log data was performed by W. Jia *et al*. (2026). In their study, the authors found that the use of machine learning made it possible to stably reconstruct the lithological features of the explored area based on the inversion of the seismic data used to train the model. As such, it is not surprising that the inverted component of the model for reservoir quality was also essential to determine the lithology of the reservoir, mainly its porosity.

The capabilities of unsupervised machine learning combined with multi-attribute analysis for identifying low-saturation gas reservoirs were demonstrated by J. Chenin & H. Bedle (2022), who proved that even without rigidly predefined training labels, a multidimensional attribute space could reveal geologically meaningful patterns. A comparable observation was obtained in the conducted study, since facies differentiation and spatial zoning of reservoir quality also confirmed that the multi-attribute space contained sufficient information to reproduce the internal organisation of the clastic system.

The generalisation of the comparison with these sources showed that the obtained results extended the contemporary direction of integrated seismic interpretation oriented toward the combination of inversion, attribute optimisation, training-data quality control, and machine learning algorithms. At the same time, the conducted study specified that, for clastic systems, the most stable predictions were obtained for parameters more closely related to storage properties and lithological structure, whereas permeability remained the most sensitive to internal heterogeneity, segmentation, and the complexity of reservoir architecture.

Conclusions

The study showed that machine learning methods provide a viable and analytically sound basis for reservoir quality prediction in clastic oil fields. Reservoir quality could not be reliably characterised by any single seismic attribute, since it was controlled by the combined influence of storage capacity, flow potential, sand-body development, and facies characteristics. At the same time, the multi-attribute predictor space proved adequate for representing the main parameters of reservoir quality. The efficacy of various models was determined to be dependent upon the physical nature of the parameter that was to be predicted. The stability of the reservoir parameters was highest for the prediction of porosity, with the XGBoost algorithm achieving the highest R^2 value of 0.88, the lowest RMSE of 024, and the lowest MAE of 0.018. The sandiness index followed closely behind with an R^2 of 0.85, an RMSE of 0.054, and an MAE of 0.039. The permeability of the reservoir was the hardest to predict, with the best performing model achieving only an R^2 of 0.76, an RMSE of 16.9, and an MAE of 12.4. Finally, the classification of the reservoir facies exhibited a relatively steady quality in its predictions, with accuracies of 0.84, precision of 0.82, recall of 0.79, and an F1 score of 0.80.

Thus, the proposed methodology was applicable both to continuous prediction of reservoir properties and to facies classification. The predicted parameter distribution confirmed reservoir heterogeneity: porosity was the most stable parameter, whereas permeability showed the highest variability. The integrated assessment identified high-, moderate-, and low-quality intervals with indices of 86, 64, and 38, respectively. The most promising intervals were associated with higher porosity, higher permeability, stronger sand-body development, and more favourable facies characteristics. Future research in this area would be directed towards testing the accuracy of this methodology upon a dataset of reservoirs within Albania, collecting additional attributes related to seismic reflection and inversion analyses, increasing the accuracy in the prediction of permeability within those reservoirs, and performing uncertainty analyses regarding the quality predictions of those reservoirs.

Acknowledgements

None.

Funding

None.

Conflict of Interest

None.

References

[1] Abd-Elfattah, N., Dahroug, A., El Kammar, M., & Fahmy, R. (2025). Machine learning and AVO class II workflow for hydrocarbon prospectivity in the Messinian offshore Nile Delta Egypt. *Scientific Reports*, 15(1), article number 3566. doi: 10.1038/s41598-025-86765-7.

[2] Al Hasan, R., Saberi, M.H., & Riahi, M.A. (2025). Seismic facies classification and TOC prediction using seismic attributes and Hjorth parameters, in the Groningen field in northeastern Netherlands. *Discover Applied Sciences*, 7(10), article number 1202. doi: 10.1007/s42452-025-07794-5.

[3] Alexandridis, I., Oikonomopoulos, I.K., Carvajal-Ortiz, H., Gentzis, T., Kalaitzidis, S., Georgakopoulos, A.N., & Christanis, K. (2022). Discovery of a new source-rock interval within the Pantokrator Formation, Ionian Zone, western Greece: Insights from sulfur speciation and kinetics analyses. *Marine and Petroleum Geology*, 145, article number 105918. doi: 10.1016/j.marpetgeo.2022.105918.

[4] Ali, M., Changxingyue, H., Wei, N., Jiang, R., Zhu, P., Hao, Z., Hussain, W., & Ashraf, U. (2024). Optimizing seismic-based reservoir property prediction: A synthetic data-driven approach using convolutional neural networks and transfer learning with real data integration. *Artificial Intelligence Review*, 58(1), article number 31. doi: 10.1007/s10462-024-11030-8.

[5] Arkadiusz, D., Tomasz, T., Anita, L.Ś., & Krzysztof, S. (2025). Machine learning approaches for predicting lithological and petrophysical parameters in hydrocarbon exploration: A case study from the Carpathian foredeep. *Energies*, 18(17), article number 4521. doi: 10.3390/en18174521.

[6] Babayeva, T., Guliyev, A., İslamzade, T., İslamzade, R., Haciyeva, X., Ashurova, N., Aliyeva, A., & Maksudov, S. (2024). Impacts of irrigation with Cd-contaminated water from Sugovushan Reservoir, Azerbaijan on total cadmium and its fractions in soils with varied textures. *Eurasian Journal of Soil Science*, 13(2), 145-152. doi: 10.18393/ejss.1424421.

[7] Badr, S.M., Mohamed, F.H., Mansour, A.S., & Elessawy, A.A. (2026). Machine learning integration with seismic attributes for lithofacies prediction and distribution in Abu Madi reservoir, onshore Faraskour gas field, east Nile Delta, Egypt. *Journal of Petroleum Exploration and Production Technology*, 16(2), article number 24. doi: 10.1007/s13202-025-02125-1.

[8] Chen, Y., Zhao, L., Pan, J., Li, C., Xu, M., Li, K., Zhang, F., & Geng, J. (2021). Deep carbonate reservoir characterisation using multi-seismic attributes via machine learning with physical constraints. *Journal of Geophysics and Engineering*, 18(5), 761-775. doi: 10.1093/jge/gxab049.

[9] Chenin, J., & Bedle, H. (2022). Unsupervised machine learning, multi-attribute analysis for identifying low saturation gas reservoirs within the deepwater Gulf of Mexico, and Offshore Australia. *Geosciences*, 12(3), article number 132. doi: 10.3390/geosciences12030132.

[10] Cristea, V.-M., Baigulbayeva, M., Ongarbayev, Y., Smailov, N., Akkazin, Y., & Ubaidulayeva, N. (2023). Prediction of oil sorption capacity on carbonized mixtures of Shungite using artificial neural networks. *Processes*, 11(2), article number 518. doi: 10.3390/pr11020518.

[11] El-Dabaa, S.A., Metwalli, F.I., Maher, A., & Ismail, A. (2024). Unsupervised machine learning-based multi-attributes analysis for enhancing gas channel detection and facies classification in the serpent field, offshore Nile Delta, Egypt. *Geomechanics and Geophysics for Geo-Energy and Geo-Resources*, 10(1), article number 185. doi: 10.1007/s40948-024-00907-1.

[12] Farfour, M., & Foster, D. (2022). Machine learning and seismic attributes for prospect identification and risking: An example from offshore Australia. In *SEG international exposition and annual meeting* (article number D011S011R004). Houston: OnePetro. doi: 10.1190/image2022-3752064.1.

[13] Farfour, M., Hedjam, R., Foster, D., & Gaci, S. (2025). Machine learning and seismic attributes for petroleum prospect generation and evaluation: An example from offshore Australia. *Interpretation*, 13(4), 805-815. doi: 10.1190/INT-2024-0177.1.

[14] Ferreira, D.J., Dias, R.M., & Lupinacci, W.M. (2021). Seismic pattern classification integrated with permeability-porosity evaluation for reservoir characterization of presalt carbonates in the Buzios Field, Brazil. *Journal of Petroleum Science and Engineering*, 201, article number 108441. doi: 10.1016/j.petrol.2021.108441.

[15] Fociro, A., Fociro, O., Prifti, I., Muçi, R., & Pekmezi, J. (2023). Petrography and mineralogy of the Oligocene flysch in Ionian Zone, Albania: Implications for the evolution of sediment provenance and paleoenvironment. *Open Geosciences*, 15(1), article number 20220442. doi: 10.1515/geo-2022-0442.

[16] Hussain, M., Shakir, U., Naseer, Z., Amjad, M.R., Arshad, F., Kamal, M., & Radwan, A.E. (2025). Integrating conventional and machine learning aproaches with seismic inversion for optimized porosity estimation in heterogeneous siliciclastic rocks. *Physics and Chemistry of the Earth, Parts A/B/C*, 142, article number 104248. doi: 10.1016/j.pce.2025.104248.

[17] Jia, W., Liu, D., Zhang, G., Lan, T., Sun, Z., & Hu, H. (2026). Lithology prediction based on well-log data and seismic inversion result: A machine learning approach. *Journal of Applied Geophysics*, 247, article number 106131. doi: 10.1016/j.jappgeo.2026.106131.

[18] Kumar, P.C., Bedle, H., Kumar, J., Goswami, T.K., & Sain, K. (2026). Seismic facies characterization: Integrated subsurface-outcrop analysis for complex depositional systems in northeast India. *Artificial Intelligence in Geosciences*, 7(1), article number 100196. doi: 10.1016/j.aiig.2026.100196.

[19] Li, W., Yue, D., Colombera, L., Duan, D., Long, T., Wu, S., & Liu, Y. (2023). A novel method for seismic-attribute optimization driven by forward modeling and machine learning in prediction of fluvial reservoirs. *Geoenergy Science and Engineering*, 227, article number 211952. doi: 10.1016/j.geoen.2023.211952.

[20] Liu, J., Lin, C., Elders, C., & Faris, A. (2026). Sandbody prediction based on fusion of seismic multi-attributes and machine learning under sedimentary facies constraint – a case study of Chenguanzhuang area in Dongying depression, Bohai Bay basin. *Applied Sciences*, 16(7), article number 3341. doi: 10.3390/app16073341.

[21] Murtaza, G., Ali, N., Hussain, W., Iqbal, S.M., Azhar, M.U., Ahmad, T., Iltaf, K., & Ahmed, A. (2025). Integrating petrophysical, seismic and rock physics analyses for precise reservoir characterization. *Earth Systems and Environment*, 9(3), 2165-2187. doi: 10.1007/s41748-025-00654-7.

[22] Narayan, S., Sahoo, S.D., Kar, S., Pal, S.K., & Kangsabanik, S. (2024). Improved reservoir characterization by means of supervised machine learning and model-based seismic impedance inversion in the Penobscot field, Scotian Basin. *Energy Geoscience*, 5(2), article number 100180. doi: 10.1016/j.engeos.2023.100180.

[23] Oitseva, T. (2024). Geological structure and mineralogical composition of the Kara-Ayak rare metal ore occurrence (East Kazakhstan). In *International multidisciplinary scientific geoconference surveying geology and mining ecology management SGEM 2024* (pp. 71-78). Vienna: SGEM. doi: 10.5593/sgem2024/1.1/s01.10.

[24] Olutoki, J.O., Elsaadany, M., Siddiqui, N.A., Haque, A.E., Ali, S.H., Rashid, A., & Akinyemi, O.D. (2024). Estimating petrophysical properties using geostatistical inversion and data-driven extreme gradient boosting: A case study of late eocene McKee formation, Taranaki Basin, new Zealand. *Results in Engineering*, 24, article number 103494. doi: 10.1016/j.rineng.2024.103494.

[25] Owusu, P., Raef, A., & Sharaf, E. (2025). Carbonate seismic facies analysis in reservoir characterization: A machine learning approach with integration of reservoir mineralogy and porosity. *Geosciences*, 15(7), article number 257. doi: 10.3390/geosciences15070257.

[26] Pradhan, A., & Mukerji, T. (2022). Consistency and prior falsification of training data in seismic deep learning: Application to offshore deltaic reservoir characterization. *Geophysics*, 87(3), 45-61. doi: 10.1190/geo2021-0568.1.

[27] Rahma Putra, M.H., Hermana, M., Yogi, I.B., Hossain, T.M., Abdurrachman, M.F., & Kadir, S.J. (2024). Reservoir porosity assessment and anomaly identification from seismic attributes using Gaussian process machine learning. *Earth Science Informatics*, 17(2), 1315-1327. doi: 10.1007/s12145-024-01240-7.

[28] Reda, M., El-Gendy, N.H., Raef, A., Elmashaly, M.M., AlArifi, N., & Barakat, M.K. (2024). Advancing neogene-quaternary reservoir characterization in offshore Nile Delta, Egypt: high-resolution seismic insights and 3D modeling for new prospect identification. *Environmental Earth Sciences*, 83(20), article number 581. doi: 10.1007/s12665-024-11846-1.

[29] Ren, K., Li, W., Zhao, L., Wang, W., Wang, J., Wang, H., Li, Y., Qu, L., & Yue, D. (2026). Seismic-attribute optimization for improving reservoir prediction integrating the spectral decomposition and automated machine learning. *Journal of Applied Geophysics*, 248, article number 106167. doi: 10.1016/j.jappgeo.2026.106167.

[30] Ren, T.F., Feng, Z.B., Zhang, Y., Zhang, X., Jiang, L., Ning, Y.L., Wang, J., Ding, J., & Qi, Z.S. (2025). A seismic multi-attribute sandbody identification method based on the LightGBM-RFECV coupling algorithm. *Applied Geophysics*, 22(3), 757-769. doi: 10.1007/s11770-025-1292-y.

[31] Riyadi, Z.A., Olutoki, J.O., Hermana, M., Latif, A.H., Yogi, I.B., & Kadir, S.J. (2024). Machine learning prediction of permeability distribution in the X field Malay Basin using elastic properties. *Results in Engineering*, 24, article number 103421. doi: 10.1016/j.rineng.2024.103421.

[32] Shevko, V.M., Zharmenov, A.A., Aitkulov, D.K., & Terlikbaeva, A.Z. (2021). Complex processing of oxidized copper and zinc oxide ores with simultaneous production of several products. *Physicochemical Problems of Mineral Processing*, 57(1), 226-249. doi: 10.37190/ppmp/131091.

[33] Soto, J.I., *et al*. (2024). Contrasting styles of salt-tectonic processes in the Ionian Zone (Greece and Albania): Integrating surface geology, subsurface data, and experimental models. *Tectonics*, 43(1), article number e2023TC008104. doi: 10.1029/2023TC008104.

[34] Wang, J., Guan, D., Huang, X., He, Y., Li, H., Xu, W., Liu, R., & Feng, B. (2025). Integrated SOM multi-attribute optimization and seismic waveform inversion for thin sand body characterization: A case study of the paleogene lower E3d2 sub-member in the HHK depression, Bohai Bay basin. *Applied Sciences*, 15(9), article number 5134. doi: 10.3390/app15095134.

Аналіз сейсмічних атрибутів з використанням методів машинного навчання для прогнозування якості колекторів на родовищах осадових порід

Фахрі Махо

Доктор філософії у галузі водної інженерії, викладач
Політехнічний університет Тирани
1001, вул. Теодора Кеко, 28, м. Тирана, Албанія
https://orcid.org/0009-0002-0673-4577

Енкелейда Джиналі

Доктор філософії у галузі водної екологічної інженерії, доцент
Політехнічний університет Тирани
1001, вул. Теодора Кеко, 28, м. Тирана, Албанія
https://orcid.org/0009-0005-4942-3893

Анотація. Метою дослідження було оцінити ефективність аналізу сейсмічних атрибутів з використанням методів машинного навчання для прогнозування якості колекторів на кластичних та балканських нафтових родовищах. Валідаційне дослідження було проведено на основі загальнодоступних сейсмічних даних та даних про колектори в рамках проекту «Penobscot» для низки атрибутів у просторі предикторів, а також для чотирьох змінних якості колекторів. XGBoost показав найкращі результати регресії для всіх безперервних параметрів, з найвищою точністю для пористості (R^2 = 0,88, середньоквадратична похибка = 0,024, середня абсолютна похибка = 0,018), за якою слідував індекс піщаності (R^2 = 0,85, середньоквадратична похибка = 0,054, середня абсолютна похибка = 0,039), тоді як проникність залишилася найскладнішим для прогнозування параметром (R2 = 0,76, середньоквадратична похибка = 16,9, середня абсолютна похибка = 12,4). Класифікація фацій також продемонструвала стабільні результати: точність 0,84, прецизія 0,82, відтворюваність 0,79 та F1-показник 0,8. Розподіл прогнозованих параметрів виявив неоднорідну систему колектора, де пористість була найстабільнішим параметром, індекс піщаності демонстрував середню мінливість, а проникність – найвищий контраст. Комплексна інтерпретація прогнозованих показників дозволила розділити пласт на зони високої, середньої та низької якості з індексами 86, 64 та 38 відповідно. Отже, якість пласта в першу чергу визначається факторами, пов'язаними з потенціалом накопичення та протікання, піщаними тілами та фаціями, проте методи, доповнені технологіями машинного навчання, можуть ефективно допомогти інженерам-нафтовикам у складанні точних прогнозів щодо пластів у цих неоднорідних системах. Практична цінність дослідження полягає в можливості використання розробленого алгоритму для ефективного пошуку та визначення пріоритетності ділянок видобутку нафти й газу в родовищах за допомогою машинного навчання, зокрема в геологічно та структурно складних осадових системах

Ключові слова: пористість; середньоквадратична похибка; проникність; потенціал протікання; індекс піщаності; балканський тип

ISSN 1993-9973, e-ISSN 2415-332X

Vol. 26, No. 1
2026

PROSPECTING AND DEVELOPMENT OF OIL AND GAS FIELDS

https://pdogf.com.ua/en

Received: 15.12.2025. Revised: 17.04.2026. Accepted: 29.05.2026. Published: 29.06.2026.

UDC 622.24.053

DOI: 10.63341/pdogf/1.2026.30

Features of fretting corrosion damage drilling lines of hoisting mechanisms of mobile drilling rigs

Jaroslav Grydzhuk

Doctor of Technical Sciences, Professor
Ivano-Frankivsk National Technical University of Oil and Gas
76019, 15 Karpatska Str., Ivano-Frankivsk, Ukraine
https://orcid.org/0000-0002-1429-8640

Vasyl Popovych*

PhD in Technical Sciences, Associate Professor
Ivano-Frankivsk National Technical University of Oil and Gas
76019, 15 Karpatska Str., Ivano-Frankivsk, Ukraine
https://orcid.org/0000-0003-2438-8532

Orest Slabyi

PhD in Technical Sciences, Associate Professor
Ivano-Frankivsk National Technical University of Oil and Gas
76019, 15 Karpatska Str., Ivano-Frankivsk, Ukraine
https://orcid.org/0000-0002-1274-2875

Andrii Mykhailiv

Postgraduate Student
Ivano-Frankivsk National Technical University of Oil and Gas
76019, 15 Karpatska Str., Ivano-Frankivsk, Ukraine

Tetiana Voitsehivska

Assistant
Ivano-Frankivsk National Technical University of Oil and Gas
76019, 15 Karpatska Str., Ivano-Frankivsk, Ukraine
https://orcid.org/0000-0001-7967-4953

Andrii Kohut

Lead Engineer
Diagnostic Laboratory of the Research and Development Department of PJSC "Ukrnafta"
76019, 2m Pivnichnyi Blvd., Ivano-Frankivsk, Ukraine

Abstract. Downhole drilling, production, and servicing equipment is lowered, raised, and held in the well using the drilling system, the primary working element of which is the drilling line. During long-term operation, drilling lines undergo fretting corrosion damage, the mechanisms of action and development of which require additional research. The purpose of this study was to analyse the degradation processes by evaluating the features of fretting wear and fretting corrosion of wires, rods, and cores of drilling lines of lifting mechanisms of drilling rigs and their impact on the occurrence and development of damage. The analysis of publications on the selected topic in the research cycle, problem statement, collection of primary data on visual and non-destructive testing of lines from literature sources and examination data to assess their technical condition and study the impact of fretting corrosion damage was carried out. The methodology of research of drilling lines covered a complex of theoretical and practical approaches aimed at studying their characteristics,

Suggested Citation: Grydzhuk, Ja., Popovych, V., Slabyi, O., Mykhailiv, A., Voitsehivska, T., & Kohut, A. (2025). Features of fretting corrosion damage drilling lines of hoisting mechanisms of mobile drilling rigs. *Prospecting and Development of Oil and Gas Fields*, 26(1), 30-40. doi: 10.63341/pdogf/1.2026.30.

*Corresponding author (*vasyl.popovych@nung.edu.ua*)

assessing their technical condition, predicting durability and ensuring operational safety. It was established considering the relevance and practical necessity based on data from literature sources characterised by high citation, the requirements of international standards for the study of line damage in conditions of corrosion and wear effects. Some features of the abrasive effect of oxides on the condition of wires, rods, and cores of drilling lines were revealed. The residual stress-strain state of conjugated surfaces in lines due to the kinematics features of multilayer line winding on the drum was analysed. The analysis of external and internal fretting wear and fretting corrosion damage for drilling lines of lifting mechanisms of the UPA-60x mobile drilling rig was carried out. The prerequisites for the occurrence of a critical condition of the surfaces of drilling line elements due to fretting and corrosion damage were established. Considering the features and potential hazards of damage and destruction of elements of drilling lines due to fretting corrosion phenomena, practical recommendations for the use of lines with polymer-coated cores were given for further operation. The use of these lines in the oil and gas industry will help to: prevent water and dust from entering the cores, reduce the friction forces of the rods to the core and internal stresses, improve the stability of the line shape; absorb fluctuations in dynamic loads

Keywords: fretting wear; fretting corrosion; fatigue damage; drilling system; descent and lifting operations; friction

Introduction

Drilling and operation of new wells, and repair of existing ones, is impossible without a large number of lifting operations and intensive operation of drilling systems. During operation, the drilling lines of the hoisting mechanisms of drilling rigs are damaged due to wear and corrosion. Operation of drilling lines in an aggressive environment, in a wide range of loads, amplitudes, and frequencies of forced vibrations creates strict requirements for lines of drilling systems. This is explained by the fact that drilling systems are critical components of drilling, production, and well servicing installations, and their reliability directly affects both the safety of operating personnel and the technical and economic performance of the equipment.

X. Chang *et al.* (2022) experimentally investigated the degree of line wear as a function of the relative sliding speed on pulleys, the temperature of lines and pulleys, the level of vibration, and the nature of the load. It was found that the temperature of the steel line increased in proportion to the increase in the sliding speed, from approximately 52.7°C to 116.2°C. The maximum diametric value of wear was lowest (approximately 1.5 mm) when the sliding speed was 1.2 m/s. The line wear mechanisms were mainly adhesive and abrasive, and surface wear changed the morphology of steel line destruction and accelerated its destruction rate. X. Chang *et al.* (2022), based on a tribological test unit, investigated the amount of wear in the contact zone of the drilling line and pulleys. The effect of surface wear on fatigue life during bending of line samples was analysed. It was found that the coefficient of friction decreases with increasing sliding distance and reaches a minimum value (approximately 0.52) when the contact load was 700 N. The maximum temperature increase ranged from 50°C to 60°C when the contact load increased. The nature of line wear was uneven, the maximum wear width increased from 1.94 mm to 2.45 mm with contact load.

Deterioration of the mechanical properties of a drilling lines caused by different wear evolution was investigated by L. Guerra-Fuentes *et al.* (2020). The change in the wear rate of lines depending on the load was studied by X. Chang *et al.* (2025). S. Senyk *et al.* (2025) investigated that line wear leads to nonlinear degradation of tensile strength and bending fatigue. C. Debeleac *et al.* (2020) found that when the sliding distance between the cable and the pulley increases, the breaking force decreases from about 48 kN to 23 kN, and the number of fatigue bends of the line before disposal decreases from about 6,200 times to 200 times. The study by A. Mohamed *et al.* (2019) proposed a hybrid visual control method for detecting defects in drilling lines. P. Zhou *et al.* (2020) developed special equipment for visual inspection of lines. E. Kuhn *et al.* (2024) established a number of key empirical dependencies using such equipment. M. Heldin *et al*. (2021) found that this method was based on comparing and analysing the internal and external stresses of the line layers. By combined strain gauges, H. Karasu *et al*. (2024) established destructive stress levels and stages of line damage. K. Huang *et al*. (2025) made generalisations regarding the level of damage, destruction of wires and rods, and subsequent disposal of a drilling line.

To ensure trouble-free operation of drilling lines, methods based on increasing the safety margin and reducing the intended life of the line were used. In addition, the condition of the line must be constantly monitored, including with the help of non-destructive testing tools and methods. Therefore, a comprehensive analysis of the processes of loading, wear, and degradation that occur in the line will allow determining and scientifically substantiating the influence of various external and internal factors on its durability. The very existence of such a scientific concept is of important national economic and strategic importance for the domestic oil and gas industry. That is why the purpose of this study was to carry out an additional analysis of the processes of corrosion degradation, local wear of line elements, and their impact on the occurrence and development of damage. To achieve this goal, this study used general scientific methods, such as analysis, synthesis, comparison, abstraction and generalisation, and a systematic approach. The study of the state of drilling lines was carried out based on the analysis of fretting corrosion damage and comparison of their degradation parameters. The literature review, as the main method, included the collection, critical evaluation, and analysis of already published studies.

The literature for this analysis was selected based on criteria such as relevance and practical necessity. The search was carried out in international scientific databases, such as Scopus, Web of Science, Index Copernicus, and in electronic libraries of universities and specialised oil and gas publications. Keywords such as drilling lines, corrosion, wear, damage, and combined queries that include these terms together with the specification of operating conditions in aggressive environments were used for selection. Irrelevant papers were eliminated at the stage of initial revision based on the results of checking the completeness of the study, the method of analysis, and its correlation with the topic. The selected sources were characterised by high citation, compliance with the requirements of international standards, and relevance for studying the damage of lines under conditions of corrosion and wear effects.

Design features and performance characteristics

Drilling lines are flexible elements of the hoisting system that connect the travelling block with the crown block and ensure the execution of hoisting and lowering operations during drilling and well operation (Kryzhanivskyi *et al.*, 2003; Borysevych *et al.*, 2004; Kryzhanivskyi *et al.*, 2007). The drilling line is made of steel wire (crucible steel), which is tied into strands of single, double, or triple weaving. Lines are shifted from strands that are wound on the core, which gives the line a round shape and flexibility (Fig. 1). In the lines of drilling rigs, steel lines of round cross-section, single-layer, 6-strand double twisting are used, the wires of which are twisted into strands, and the strands into lines. Drilling lines for operational and deep exploration drilling are manufactured in three versions, which differ in the type of cores used.

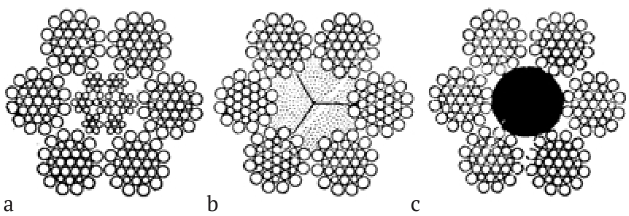

Figure 1. LK-DS type drilling lines with cores
Note: a – steel core; b – organic three-strand core; c – plastic core
Source: Ye. Kryzhanivskyi *et al*. (2007)

In lines with an organic core, lubrication is improved due to the impregnation of the fibrous core with a lubricant. Depending on the relative position of the wires in the strands, lines with point and linear contact of the wires are distinguished. Lines with a linear contact of wires are more durable. Tests show that their operating time is 1.5-2 times higher than that of lines with a point touch (Kryzhanivskyi *et al.*, 2003; Kryzhanivskyi *et al.*, 2007). Drilling lines belonging to the LK-DS type differ in that wires of different (D) and the same (S) diameters are used in separate layers of the strand. Line wires are made of steels (steel 50, 55, 60, 70) with heat treatment and a tensile strength of 1,700-2,000 MPa. In the direction of twisting, drilling lines of the following designs are made: cross right twist – Z; cross left twist – S. In the right Z twisting, the strands are placed from left to right, and in the left S – from right to left. Z-type lines are more common in operational drilling.

Drilling lines do not unwind, as they are made of pre-deformed wires and strands. As a result of preliminary deformation, the wires and strands have geometric shapes that correspond to their position in the finished line. The endurance of such a line, all other things being equal, is 25-30% higher than that of a conventional untwisted line. Line types: LK-DS-6×25+1-MO; LK-DS-6×19+1-SC and LK-DS-6×37-OC, where 6 – number of strands; 25, 19, 37 – number of wires in the strand; SC – steel core; OC – organic core. When drilling wells, LK-DS drilling lines with diameters of 25, 28, 32, 35, 38 mm are mainly used. The tribological and fatigue characteristics of the interaction of a curved steel rope and the groove of the drum of an offshore drilling rig winch were studied by S. O'Halloran *et al.* (2018) and Z. Wang *et al.* (2025). Z. Ren *et al.* (2018) and C. Lu *et al.* (2022) experimentally tested the effect of groove coverage angles, fatigue loads, and fatigue cycles on the tribological properties of the line (coefficient of friction, wear mechanism, volume loss, wear rate, etc.). Research findings by H. Liu *et al*. (2018), C. Wokem *et al*. (2018) showed that an increase in variable load and fatigue cycles leads to more serious damage to lines that are subject to bending fatigue, while an increase in the wrapping angle somewhat mitigates the severity of this grip damage.

The studies by Y. Shen *et al.* (2023), A. Lomakin (2024) and T. Ta *et al.* (2024) are devoted to theoretical and experimental approaches to the investigation of additional stresses that occur in steel rope elements when hitting blocks and drums. The researchers conducted a critical analysis and generalisation to determine additional stresses in the elements of steel ropes. It was noted that the current practice of determining additional stresses that occur in the line when it runs on a pulley or drum is far from the results obtained experimentally. The analysis of experimental approaches indicates the existence of various approaches that require generalisation and further development and implementation in the form of a comprehensive experimental study. D. Zhang *et al.* (2021), B. Kubiś *et al.* (2023) and Y. Peng *et al.* (2024) conducted unique fatigue tests of steel lines. The obtained findings and their interpretation revealed several important aspects of assessing the stress-strain state and wear of lines. As a result of the research, the characteristics of line elongation were established, showing three different periods (phases): a short initial period with a sharp increase in elongation associated with the winding of a new line, a long period with stable elongation, and a final phase characterised by accelerated elongation associated with rapidly progressive fatigue wear with the occurrence of a large number of wire breaks.

Features of wear and damage of drilling lines

During operation, drilling lines are subjected to stretching and repeated kinks on the pulleys of the crown block, hoist block, and drum winches, resulting in their fatigue destruction (Kryzhanivskyi *et al.*, 2003; Kryzhanivskyi *et al.*, 2007). The outer wires of the line are subject to wear on the pulleys and drum of the winch, so the process of their fatigue destruction is accelerated. Due to insufficient durability, the consumption of drilling lines and the waiting time for the drilling rig to replace worn lines increases, which negatively affects the technical and economic performance of drilling. The main reason for rejection or failure of drilling lines is wear, which is caused by contact and friction interaction, accompanied by corrosion processes (Fig. 2-3) (Transport Department of PJSC "Ukrnafta", 2023). During operation, drilling lines are subjected to two main types of wear.

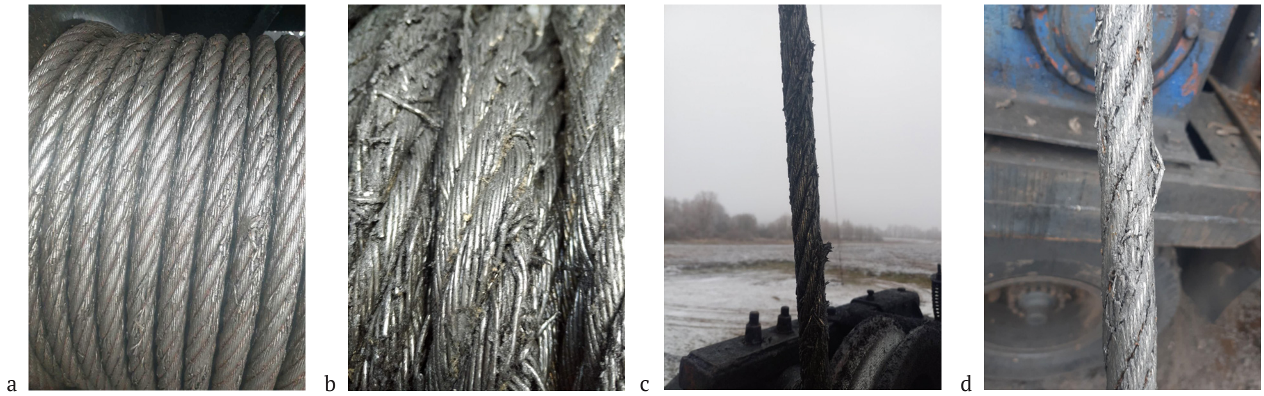

Figure 2. Appearance of the drilling line with signs of fretting damage and destruction of the wires of the drilling line of the UPA-60X unit
Note: a, b – local wear due to abrasion on the supporting structure; c, d – typical wire breaks as a result of bending fatigue
Source: Transport Department of PJSC "Ukrnafta" (2023)

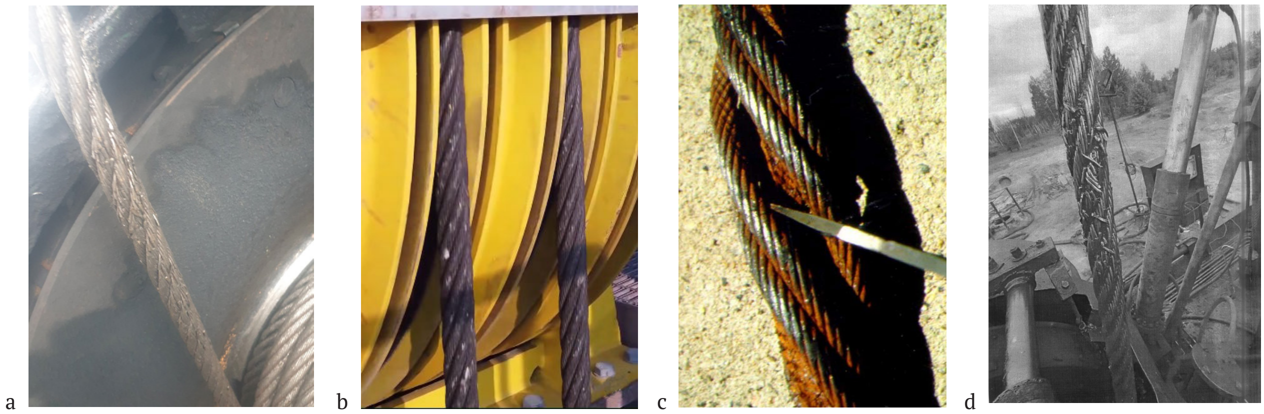

Figure 3. Appearance of the drilling line with signs of fretting and corrosion damage and destruction of the wires of the drilling line of the UPA-60X unit
Note: a – local corrosion; b – continuous surface corrosion; c – corrosion along the contact lines of strands; d – corrosion cracking with wire breakage
Source: Transport Department of PJSC "Ukrnafta" (2023)

External wear is a type of wear in which the drilling line comes into contact with external surfaces, such as drums, pulleys, guide elements, or any other parts of equipment with which it interacts. For drilling lines of drilling rigs, external wear is determined by the operating conditions of lifting equipment and the specifics of lifting operations. When the drill tool is lowered into the well (lowering the loaded hoisting block), the drilling line is unwound from the drum under load, and wound on the drum without load (lifting the unloaded drilling line). In this case, the non-stressed state in the line turns on the drum changes to the stressed state in the leading branch. In the process of lifting the drill tool from the well (lifting the loaded drilling block), the drilling line is wound on the drum under load, and unwound without load (lowering the unloaded drilling block).

Internal wear is a type of wear in which wires and strands come into contact with each other during operation. Actually, during the accelerated lifting of drilling or operational equipment in the line, the strands located on the outside of the line are most stretched. This is conditioned by the fact that the outer strands are subjected to a greater load than the inner ones, which are under less stress. When a line is bent, for example, around a pulley, those strands that are on the outside of the curve travel a longer path and experience more tension than the strands located inside. The amount of internal wear mainly depends on the amount of contact stresses in the wires in contact with each other, the method of twisting the wires and strands of the line, the amount of load, and the method of lubrication. In turn, the contact stresses in the wires that are in contact with each other depend on the shape of the cross-section of the drilling line. The drilling line loses its shape due to: non-compliance of the rope diameter with the profile of the pulley gutters and grooves on the drum; winding the line turns under the load of the first layer on the drum with a smooth surface; and multi-layer laying procedures. The latter causes compressive stresses and contact stresses: in the wires and turns of the lower layers in the zones of parallel laying of twists; in the zones of transition of the twist to twist and transition from one strand to another (Ivashko *et al.*, 2017; Chunming *et al.*, 2022).

Thus, both external and internal wear occurs mainly under the influence of variable tensile and bending loads. Such loads occur, as a rule, when the system is loaded: during drilling, during the period of increasing load in the drilling system, during acceleration when lifting the loaded hook, and during braking of the system when the drilling line is lowered. The oscillatory process is most pronounced during drilling, and during certain periods of lifting operations. In addition, the vibrational nature of the load occurs during the descent and ascent of the drilling block due to the uneven winding of the line on the drum, due to the specifics of the kinematics of multi-layer winding. As a rule, dynamic loads have a relatively high frequency compared to a change in the frequency of the main load (1-8 Hz) and a change in the amplitude of vibrations (stresses) within a wide range. The nature of dynamic loads in the elements of the drilling system during lifting operations is in principle different from the nature of vibrations that occur during drilling. In the first case, the source of forced vibrations is the uneven winding of the line on the drum, that is, the uneven movement of the leading branch. In this case, the maximum range of dynamic forces occurs in the leading and stationary branches, and the forces themselves in these branches are in antiphase. In the middle branches, the dynamic component of forces is minimal. In the second case, the source of forced vibrations of the system is a drill bit with a drill string, and these vibrations manifest themselves to a greater extent in rotary and combined drilling methods. Dynamic loads during this period in all branches of the drilling system are approximately the same and are in the same phase.

Therefore, the accumulation of both external and internal wear of drilling lines and the accompanying damage can be identified as fretting processes. Fretting (fretting fatigue) is the process of accumulation of damage and wear of materials of surfaces that come into contact and carry out vibrational relative movements with a small amplitude under the action of cyclic loading, which causes variable deformations of surface layers, setting and separation of particles, the appearance of oxides, accelerated crack appearance, their development, and destruction of the unit. Fretting wear and corrosion damage occurs in many detachable and all-in-one joints of mechanisms, machines, and structures (Ventsel *et al.*, 2007; Zakalov & Zakalov, 2011). The latter include rivet, thread, spline, key and pin connections, tight fit parts, steel ropes, hinges, couplings, leaf springs, valves, electrical contact regulators, cam mechanisms, gears, rolling bearings, gas turbine engine parts, etc.

Special attention is paid to fretting processes in drilling lines – flexible links of lifting mechanisms of drilling rigs, which are subjected to stretching and alternating bending during descent and lifting operations (Kryzhanivskyi *et al.*, 2003; Borysevych *et al.*, 2004; Kryzhanivskyi *et al.*, 2007). The branches of the drilling line go around the pulleys of the crown block and drilling block, which are components of the hoist system – the heavy-bearing part of the drilling rig. Consideration of the features of fretting corrosion damage is important both for assessing the tension forces in drilling lines and for predicting their durability. Surface damage due to wear during fretting serves as stress concentrators and reduces the endurance limit of the line material. V. Ivashchenko *et al.* (2017) characterised the wear process of wire line material: inside the line and out. A quantitative assessment of the influence of dynamic loads on the accumulation of fatigue factors is given, based on the line fatigue curve. Analytical dependences of the influence of design and operating parameters of drilling systems and their characteristics that affect the failure of the drilling line are presented.

Based on the results of experimental studies, it was found that for such a process, it is sufficient to move surfaces with an amplitude of 0.025 mm (1-2). As a result of the destruction of wire surfaces, miniature scratches, small point workings, and small grooves appear. Fretting corrosion is a local corrosion destruction that occurs during the cyclic mutual movement of two contacting surfaces and the action of a corrosive medium. It occurs due to the continuous destruction of the protective oxide film at the points of mobile contact of wire and rope strands. The result of physico-chemical interaction of drilling lines with the environment are: continuous (flowing over the entire surface of the metal) and local (localised on certain areas of the surface) corrosion; filamentous corrosion (flowing along the contact line of neighbouring wires); and corrosion cracking (occurring under the simultaneous influence of a corrosive medium and tensile residual or applied mechanical stresses). Fretting corrosion is caused not only by carbon steels, but also by corrosion-resistant steels.

Studies by L. Oleksiieva *et al.* (2022) showed that increased contact load leads to smoother wear of the line surface, while fatigue corrosion wear itself is mainly abrasive and adhesive in nature. In addition, surface wear leads to a decrease in the resistance of the lines to bending fatigue, and the deterioration of bending fatigue is more serious under a larger sliding contact load. I. Dmytrakh *et al.* (2003), H. Mouradi *et al.* (2018) and Xu. Chunming *et al.* (2022) investigated the fretting wear of steel ropes under the action of tensile and torsional forces. The research findings showed that the law of change in the coefficient of friction between steel wires of a line is proportional to the angle of intersection by the axis of the line of the axis of symmetry of the pulley. By investigating the hysteresis loop, it was found that the main mechanisms of wear of steel wires are fatigue and adhesive wear, and the worn surface of steel wires shows more obvious abrasive wear with a decrease in the angle of intersection of the line axis of the pulley symmetry axis.

Influence of operational factors on the intensity of fretting corrosion

The wear rate increases when drilling lines operate in aggressive environments, in particular, in aqueous solutions of mineral acids, alkaline solutions, and hydroxides. In this case, accelerated wear of the contacting surfaces of wires or line strands occurs due to fretting corrosion. On the surfaces of the contacting parts, protective oxide films are destroyed, and pure metal is exposed. Metal particles are separated (as in fretting), which are then oxidised (Fig. 4). Therefore, the products of wear during fretting corrosion are usually oxides. In the absence of lubrication with fretting corrosion products, the following oxides are mainly used: Fe_2O_3, FeO, Fe_3O_4. Oxides cause an abrasive effect that depends on the hardness of the oxides and the size of their particles in the wear products. According to the results of surveys (12), such indicated injuries are both local and large-scale in nature.

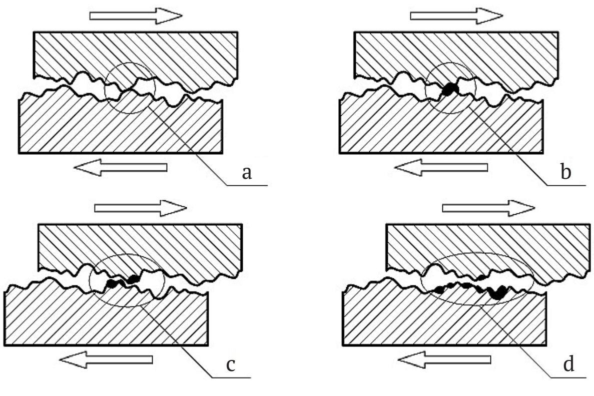

Figure 4. Mechanism of fretting wear of wire surfaces and simultaneous abrasive action of the results of their corrosion
Note: a – local contact of surfaces without corrosion; b – contact with spot corrosion; c – abrasive friction with corrosion elements; d – propagation of corrosion elements
Source: created by the authors based on O. Zakalov & O. Zakalov (2011)

According to Ye. Ventsel *et al.* (2007) and O. Zakalov & O. Zakalov (2011), the relative sliding rate of contacting surfaces during fretting corrosion is low. For harmonic vibrations with a frequency of 50 Hz and an amplitude of 0.025 mm, the average speed is 2.5 mm/s, and the maximum speed is 7.5 mm/s. If the oscillation amplitude is large (about 2.5 mm), the surface of damage caused by fretting corrosion will also be larger, and the rubbing surfaces will have both linear and volumetric defects (Fig. 5). Thus, the main criterion for the development of fretting corrosion damage should be considered the specified amplitude and speed of relative sliding motion of the contacting surfaces. Electrochemical processes of interaction of the contacting surfaces of lines with the environment, and the mechanical component (deformation process) are influential indicators of the intensity of development of fretting corrosion damage.

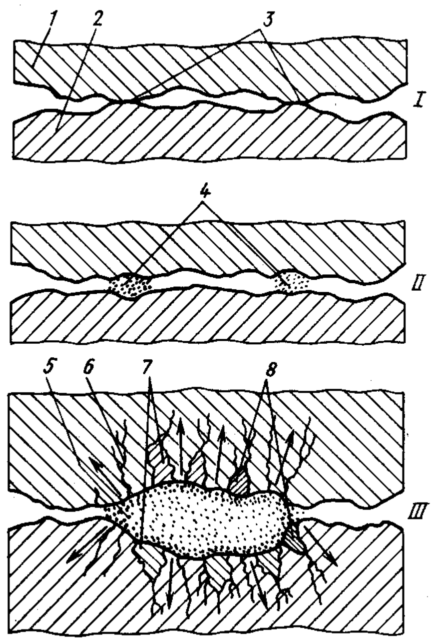

Figure 5. Diagram of wear and destruction of contacting surfaces during fretting corrosion
Note: 1, 2 – contacting surfaces; 3 – points of contact of surfaces; 4 – small caverns; 5 – general large cavern; 6 – cracks; 7 – volumes of broken metal; 8 – particles with a solid structure that have broken off
Source: O. Zakalov & O. Zakalov (2011)

With an increase in the speed of relative slipping of surfaces, the amplitude and frequency of their vibrations, and the level of load, the intensity of fretting corrosion destruction of these surfaces increases. With an increase in the relative sliding rates, metal oxides prevent the setting of rubbing surfaces, and the surfaces themselves have a low roughness. During the fretting corrosion destruction of surfaces, the following occurs. The crystal lattices of the surface layers of metal gradually loosen and collapse due to the action of friction forces during cyclic tangential shifts. There is a separation of metal particles, their mechanical grinding together with oxides into small particles without removing wear products. Detached metal particles, and places and areas of short-term setting of rubbing surfaces, undergo rapid oxidation. The chains of atoms captured during sliding are distorted and then broken, which causes individual atoms to separate from the crystal lattices and can further provoke the development of fatigue cracks. The rate of accumulation of wear products between steel surfaces and the development of new oxide films will depend on the physical and chemical properties of the materials and the newly formed chemical compounds. The accumulation of wear products and metal oxides in closed volumes leads to a local increase in pressure and point destruction of the metal in the form of pits – the so-called pitting. As practice shows, the hardness of metal oxides is greater than the hardness of pure rope metal, which explains their abrasive effect on the contacting surfaces of the wires themselves. The amount of abrasive action of oxides on the contacting surfaces depends on the hardness of oxides, the size of their particles in the wear products, and the adhesion forces of oxide films to the base metal.

From the very beginning, the contact of the rope wires occurs at separate points of the contacting surfaces (I) (Fig. 5). In the presence of vibration in the actual contact zone, the oxide films are destroyed, in place of which small cavities are formed, filled with oxide films (II). The latter, further increasing in size, merge into one large cavern (III), in which, due to an increase in the volume of oxides, pressure increases and small cracks form. In the future, small cracks can merge into larger ones, which causes chipping and large volumes of metal. In the chipped parts of the metal, due to the action of increased pressure, friction forces and increased temperature, new solid structures are formed. According to research by the Transport Department of PJSC "Ukrnafta" (2023), the intensity of fretting wear on surfaces in dry air is significantly higher than in wet air. In fretting corrosion, the wear rate in the presence of a liquid medium is much lower. Thus, in a liquid solution of sodium hydroxide, the weight of material lost due to friction is several times less than in air under normal atmospheric conditions. It is impossible to fully prevent and eliminate the manifestations of fretting corrosion. Assuming that it is impossible to get rid of the mutual micro-placement of wire surfaces in the rope, then it is possible to reduce the impact of fretting corrosion on the material by: reducing the friction force; reducing micro-placements; concentrating sliding in an intermediate medium.

Reducing the impact of fretting corrosion and design solutions to increase the durability of lines

The most effective method of combating this type of line destruction is the transfer of micro slip to the intermediate medium (Chunming *et al.*, 2022; Lomakin, 2024). Such a medium can be lubricants, special wire coatings, or polymer isotropic inserts. In fretting conditions, when the lubricant film does not renew during operation and quickly collapses, conventional viscous lubricants do not affect the coefficient of friction. The use of solid lubricants also does not give the desired results, although the friction force will decrease, the main purpose of coatings is to transfer the displacement process inside the coating, but the process of fretting destruction that has begun quickly turns into the base metal. The effectiveness of all coatings is determined by the service life, since sooner or later they are triggered.

Given that fretting is a process that determines the rate at which a line deteriorates, it is advisable to use lines with special rubber inserts that prevent the wires from rubbing against one another. In this case, a rational and effective measure is the use of lines, the core of which is coated with polymer (Wang *et al.*, 2018; Stalkanat, 2024). Steel ropes with a polymer-coated steel core consist of a layer of steels twisted around the metal core, on which a shell of polymer material is applied by extrusion. Plastic aggregate significantly reduces possible sliding between different elements and prevents changes in the geometric dimensions of lines (Fig. 6).

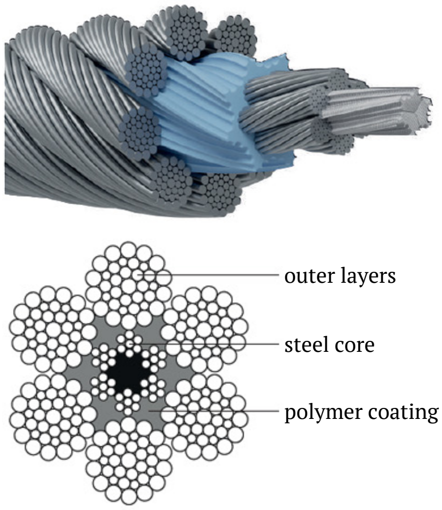

Figure 6. Steel rope with polymer coated steel core
Source: Stalkanat (2024)

The application of a polymer shell allows creating a mechanical connection that fixes the position of the corresponding elements of the steel wire rope, while simultaneously ensuring their necessary displacement; reducing internal corrosion caused by pollutants, which is achieved due to the increased tightness of the rope; and filling the free space between the outer rods and the core to prevent wear. The stabilising effect of the plastic-polymer coating is particularly evident when the rope is exposed to transverse pressure, torsion caused by a wide lateral deflection angle on pulleys or winches, and/or shock loads. The advantages of using polymer core coated ropes are as follows: preventing internal breaks; sealing grease in the rope; preventing water, dust, etc., from entering; reducing internal stresses; improving the stability of the line shape; absorbing dynamic load and partial damping. Adapted steel ropes can also be used based on the use of polymer shells.

The essence of this solution is to design and manufacture a lifting line in advance with geometric parameters as close as possible to those parameters that the line acquires in vertical hanging due to gravitational torsion (Patent No. 85078, 2008). Gravitational torsion of a rope is understood as the phenomenon of rotation, or tendency to rotation, which occurs in steel ropes under the action of a load (its own weight or suspended load), especially in those that have a one-way twist. This technique, developed under the supervision of Professor V.A. Malinovsky, is used in the manufacture of steel ropes that have already been tested in aggressive mine workings. The proposed design reduces the gravitational torsion of the line in the barrel and leads to a more uniform distribution of stresses between the wires in the line rods, which helps to increase fatigue strength, reduce the impact of fretting damage and service life.

Conclusions

As a result of the inspection and analysis, certain features of fretting wear and fretting corrosion of wires and strands of hoisting ropes of lifting mechanisms of drilling rigs, and their influence on the occurrence and development of damage and destruction, were revealed. In particular: a critical analysis of the phases of fretting corrosion processes that occur during the operation of hoisting ropes, and mechanisms of wear and damage of hoisting ropes in operational conditions was carried out; the search for opportunities to reduce the impact of fretting corrosion damage in hoisting ropes was carried out. It was established that the key factors of fretting corrosion wear of hoisting ropes were corrosion of the surface layers of wire and abrasive movement of corrosion products between the surfaces of wire and steel, and the main criterion for the development of fretting corrosion damage should be considered the amplitude and speed of relative sliding motion of the contacting surfaces.

Repeated kinks of the rope on the pulleys of the drilling block, crown block, and winch drum during descent and lifting operations create cycles of alternating stresses that lead to metal fatigue and, as a result, to wear and possible wire breakage. Dynamic loads, acceleration and braking, and changes in the weight of the drill string (during descent, ascent, drilling) create significant stresses that directly affect the intensity of wear. An incorrect angle of convergence of the rope between the winch drum and the crown block or deflecting pulley increases the lateral pressure and friction of the line against the edge of the groove, which causes intense abrasion. Multi-layer line winding on the winch drum (typical for mobile installations) leads to additional friction between the rope turns (line-to-line friction), which significantly increases wear.

Lack or insufficient lubrication is one of the main causes of premature wear. The lubricant reduces internal friction between wires and strands, and external friction on pulleys and drums, and protects against corrosion. Exposure to moisture, aggressive chemicals, namely aqueous solutions of mineral acids, alkaline solutions, hydroxides, and dustiness of the working environment leads to corrosion wear, which significantly reduces the strength of the line and accelerates its destruction. The increased speed of lifting operations increases dynamic loads and friction intensity, which accelerates wear. Considering the features and potential hazards of damage and destruction of elements of hoisting ropes due to fretting corrosion phenomena, it is proposed to use ropes with a polymer core coating for further operation. The use of these lines will help to: prevent the ingress of water and dust; reduce internal stresses; improve the stability of the line shape; absorb fluctuations in dynamic loads. Theoretical and experimental studies of the magnitude and speed of fretting corrosion wear, and the durability and residual life of drilling lines, depending on the amplitude frequency and phase frequency characteristics of vibrations and the dynamism coefficient of the drilling system are considered promising in this area.

Acknowledgements

None.

Funding

None.

Conflict of Interest

None.

References

[1] Borysevych, B.D., Smaha, B.I., Senchishak, V.M., & Popovych, V.Ya. (2004). *Fundamentals of theory and calculation of means of mechanization of cargo movement*. Ivano-Frankivsk: Ivano-Frankivsk National Technical University of Oil and Gas.

[2] Chang, X., Chen, X., Dong, Y., Lu, H., Tang, W., Zhang, Q., & Huang, K. (2022). Friction and wear behavior between crane wire rope and pulley under different contact loads. *Lubricants*, 10(12), article number 337. doi: 10.3390/lubricants10120337.

[3] Chang, X., Peng, Y., Zhu, Z., Lu, H., Tang, W., & Zhang, X. (2022). Sliding friction and wear characteristics of wire rope contact with sheave under long-distance transmission conditions. *Materials*, 15(20), article number 7092. doi: 10.3390/ma15207092.

[4] Chang, X., Shi, F., Chen, X., Peng, Y., Tang, Y., Xiao, W., & Hu, R. (2025). Mechanical property degradation of transmission wire rope caused by different wear evolution. *Lubricants,* 13(2), article number 59. doi: 10.3390/lubricants13020059.

[5] Chi, J., Ma, H.-J., Lee, G.-S., Park, J.-H., & Kim, D.-E. (2024). Effect of speed and number of sliding cycles on the film formation behavior of fluorine-based grease. *Lubricants*, 12(1), article number 26. doi: 10.3390/lubricants12010026.

[6] Chunming, X., & Peng, Y., & Zhu, Z.C., & Tang, W. (2020). Fretting behaviors of steel wires with tensile-torsional coupling force under different wire diameters and crossing angles. *Tribology Letters*, 68(3), article number 91. doi: 10.1007/s11249-020-01331-8.

[7] Debeleac, C., Nastac, S., & Anghelache, G.D.M. (2020). Experimental investigations regarding the structural damage monitoring of strands wire rope within mechanical systems. *Materials*, 13(15), article number 3439. doi: 10.3390/ma13153439.

[8] Dmytrakh, I.M., Syrotyuk, A.M., & Hrabovs'kyi, R.S. (2003). Surface cracking of steels in the process of cyclic deformation in aqueous media. *Materials Science*, 39(4), 455-461. doi: 10.1023/B:MASC.0000010930.41747.e0.

[9] Guerra-Fuentes, L., Torres-López, M., Hernandez-Rodriguez, M.A.L., & Garcia-Sanchez, E. (2020). Failure analysis of steel wire rope used in overhead crane system. Engineering Failure Analysis, 118, article number 104893. doi: 10.1016/j.engfailanal.2020.104893.

[10] Heldin, M., Heinrichs, J., & Jacobson, S. (2021). On the critical roles of initial plastic deformation and material transfer on the sliding friction between metals. *Wear*, 477, article number 203853. doi: 10.1016/j.wear.2021.203853.

[11] Huang, K., Li, G., Chang, X., Zhou, Z., Peng, Y., & Deng, R. (2025). Fretting friction and wear characteristics of the internal spiral contact steel wires in the hoisting wire rope under different service conditions. *Lubricants*, 13(10), article number 453. doi: 10.3390/lubricants13100453.

[12] Ivashchenko, V.T., Liakh, M.M., Zhuravlov, D.Yu., & Mykhailiv, V.V. (2017). Factors influencing the failure of drilling rig drilling ropes. *Prykarpatsky Bulletin of the National Taras Shevchenko Society*, 2, 292-300.

[13] Karasu, H., & Demirsoy, M. (2024). Corrosion cracking resistance of hoisting ropes. *Materials Testing*, 66(3), 347-358. doi: 10.1515/mt-2023-0219.

[14] Kryzhanivskyi, Ye.I., Borysevych, B.D., & Smaga, B.I. (2007). *Hoisting machines and continuous transport machines (fundamentals of theory and calculation)*. Ivano-Frankivsk: Ivano-Frankivsk National Technical University of Oil and Gas.

[15] Kryzhanivskyi, Ye.I., Mironov, Yu.V., & Romanyshyn, L.I. (2003). *Mobile units for drilling, repairing, and servicing wells: Overview analysis of designs, structural-compositional, and kinematic schemes: Parameter studies: Design recommendations*. Ivano-Frankivsk: Ivano-Frankivsk National Technical University of Oil and Gas.

[16] Kubiś, B., Szade, P., & Tytko, A. (2023). Fatigue life of compacted wire ropes for applications in deep mining. *Management Systems in Production Engineering*, 31(1), 95-101. doi: 10.2478/mspe-2023-0012.

[17] Kuhn, E. (2024). Energy dissipation in tribological stressed greases. *Processes,* 12(1), article number 17. doi: 10.3390/pr12010017.

[18] Liu, H., Zhang, D., Cao, S., Shen, Y., Hou, X., & Xu, L. (2011). Fretting corrosion wear behaviors of steel wires in hoisting ropes in alkaline condition. *Applied Mechanics and Materials*, 99-100, 1014-1017. doi: 10.4028/www.scientific.net/AMM.99-100.1014.

[19] Liu, Y., Dong, J., Ye, X., Mao, R., & Wang, J. (2025). Comparative analysis of dynamic characteristics between magnetorheological grease and graphite magnetorheological grease. *Materials Today Communications*, 42, article number 111322. doi: 10.1016/j.mtcomm.2024.111322.

[20] Lomakin, A.O. (2024). Theoretical and experimental approaches to the study of additional stresses in steel rope elements when running onto sheaves and drums. *Engineering*, 33, 30-37.

[21] Lu, C., Jiang, X., Chen, X., & Mo, J. (2022). Experimental study on the evolution of friction and wear behaviours of railway friction block during temperature rise under extreme braking conditions. *Engineering Failure Analysis*, 141, article number 106621. doi: 10.1016/j.engfailanal.2022.106621.

[22] Mohamed, A., Hamdy, M., Bayoumi, M., & Osman, T. (2019). Synthesis and tribological properties of nanogrease. *Industrial Lubrication and Tribology*, 70(3), 512-518. doi: 10.1108/ILT-08-2017-0228.

[23] Mouradi, H., El Barkany, A., & El Biyaali, A. (2018). Steel wire ropes failure analysis: Experimental study. *Engineering Failure Analysis*, 91, 234-242. doi: 10.1016/j.engfailanal.2018.04.019.

[24] O'Halloran, S.M., Harte, A.M., Shipway, P.H., & Leen, S.B. (2018). An experimental study on the key fretting variables for flexible marine risers. *Tribology International*, 117, 87-97. doi: 10.1016/j.triboint.2017.08.019.

[25] Oleksiieva, L.A., & Ilenko, Ye.Yu. (2022). On the issue of wear resistance of rope wire. *Scientific Works of Kharkiv National Air Force University*, 4(74), 36-39. doi: 10.30748/zhups.2022.74.15.

[26] Patent No. 85078. (2008). *Wire rope*. Retrieved from https://iprop-ua.com/inv/aaua0sa2/.

[27] Peng, H., Zhao, D., Shangguan, L., Li, S., Cheng, R., & Li, Y. (2024). The optimization study of rheological characteristics of wind power grease based on gel-state. *Gels*, 10(4), article number 253. doi: 10.3390/gels10040253.

[28] Ren, Z., Lu, Z., Yu, Q., & Jiang, Y. (2018). Failure analysis and safety protection of a certain type of wire ropes under high-speed impact loads. *MATEC Web of Conferences*, 142, article number 03001. doi: 10.1051/matecconf/201814203001.

[29] Senyk, S., Gocman, K., Wachowski, M., & Kałdoński, T. (2025). Role of base grease type on the lubrication performance of hexagonal boron nitride nanoparticles and microparticles. *Materials*, 18(10), article number 2196. doi: 10.3390/ma18102196.

[30] Shen, Y., Wang, Y., Lin, J., Zhang, P., Gao, X., & Wang, Z. (2023). Study on anti-wear and friction-reducing compounding additives in lithium greases. *Industrial Lubrication and Tribology*, 75(5), 546-553. doi: 10.1108/ILT-07-2022-0350.

[31] Stalkanat. (2024). *Steel ropes*. Odesa: Private Joint-Stock Company "Stalkanat".

[32] Ta, T., Horng, J., Huang, M.-W., Torskaya, E.V., & Kuo, C.-W. (2024). Tribological characteristics and vibration response of grease lubricated contacts under environmental particles and water impact. *Wear*, 550-551, article number 205403. doi: 10.1016/j.wear.2024.205403.

[33] Transport Department of PJSC "Ukrnafta". (2023). *Expert report based on the results of the expert inspection of equipment No. 0203-EO-0309-23-IF*. Retrieved from https://www.ukrnafta.com/.

[34] Ventsel, Ye.S., Lysikov, Ye.M., & Yevtushenko, A.V. (2007). *Fundamentals of tribology and chemotology*. Kharkiv: UkrDAZT.

[35] Wang, D., *et al*. (2025) Bending tribo-fatigue behaviors between steel wire rope and rope groove material of offshore rig winch drum. *Tribology International*, 204, article number 110477. doi: 10.1016/j.triboint.2024.110477.

[36] Wang, Z., Chetwynd, D.G., & Mao, K. (2018). Friction characterics tics of polymers applicable to small-scale devices. *Tribology International*, 119, 698-706. doi: 10.1016/j.triboint.2017.11.036.

[37] Wokem, C., Joseph, T., & Curley, M. (2018). Fatigue life prediction for cables in cyclic tension. *Journal of Strain Analysis for Engineering Design*, 53(3), 141-155. doi: 10.1177/0309324717753211.

[38] Zakalov, O.V., & Zakalov, I.O. (2011). *Fundamentals of friction and wear in machines*. Ternopil: Ivan Puluj Ternopil National Technical University.

[39] Zhang, Y., Zhang, Q., Wang, C., Chang, X., & Chen, G. (2021). Preparation and tribological properties of lanthanum stearate modified lubricating oil for wire rope in a mine hoist. *Materials,* 14(19), article number 5821. doi: 10.3390/ma14195821.

[40] Zhou, P., Zhou, G., Li, Y., He, Z., & Liu, Y. (2020) A hybrid data-driven method for wire rope surface defect detection. *IEEE Sensors Journal*, 20(15), 8297-8306. doi: 10.1109/jsen.2020.2970070.

Особливості фретинг-корозійних пошкоджень талевих канатів вантажопідйомних механізмів мобільних бурових установок

Ярослав Гриджук
Доктор технічних наук, професор
Івано-Франківський національний технічний університет нафти і газу
76019, вул. Карпатська, 15, м. Івано-Франківськ, Україна
https://orcid.org/0000-0002-1429-8640

Василь Попович
Кандидат технічних наук, доцент
Івано-Франківський національний технічний університет нафти і газу
76019, вул. Карпатська, 15, м. Івано-Франківськ, Україна
https://orcid.org/0000-0003-2438-8532

Орест Слабий
Кандидат технічних наук, доцент
Івано-Франківський національний технічний університет нафти і газу
76019, вул. Карпатська, 15, м. Івано-Франківськ, Україна
https://orcid.org/0000-0002-1274-2875

Андрій Михайлів
Аспірант
Івано-Франківський національний технічний університет нафти і газу
76019, вул. Карпатська, 15, м. Івано-Франківськ, Україна

Тетяна Войцехівська
Асистент
Івано-Франківський національний технічний університет нафти і газу
76019, вул. Карпатська, 15, м. Івано-Франківськ, Україна
https://orcid.org/0000-0001-7967-4953

Андрій Когут
Провідний інженер
Лабораторія діагностики НДПІ ПАТ “Укрнафта”
76019, бульв. Північний, 2м, м. Івано-Франківськ, Україна

Анотація. Глибинне бурове, експлуатаційне та ремонтне обладнання спускається, підіймається та утримується у свердловині за допомогою талевої системи, основним виконавчим елементом якої є талевий канат. В процесі тривалої експлуатації талеві канати зазнають фретинг-корозійних пошкоджень, механізми впливу та розвитку яких вимагають додаткових досліджень. Метою даної статті було проаналізувати процеси деградації шляхом оцінки особливостей фретинг-зношування та фретинг-корозії дротин, сталок та осердь талевих канатів вантажопідйомних механізмів бурових установок та їх вплив на виникнення та розвиток пошкоджень. Проведено аналіз публікацій за обраною тематикою в циклі досліджень, постановку проблеми, збір первинних даних візуального та неруйнівного контролю канатів із літературних джерел і даних експертизи для оцінки їх технічного стану та вивчення впливу фретинг-корозійних пошкоджень. Методологія досліджень талевих канатів охоплює комплекс теоретичних та практичних підходів, спрямованих на вивчення їхніх характеристик, оцінку технічного стану, прогнозування довговічності та забезпечення безпеки експлуатації. Вона сформована з врахуванням актуальності та практичної необхідності на основі даних літературних джерел, що характеризуються високою цитованістю, вимогам міжнародних стандартів щодо дослідження пошкоджуваності канатів в умовах корозійного та зношувального впливу. Виявлено окремі особливості абразивного впливу оксидів на стан дротин, сталок та осердь талевих канатів. Проаналізовано залишковий напружено-деформований стан спряжених поверхонь у канатах, обумовлений особливостями кінематики багатошарового намотування канатів на барабан. Проведено аналіз зовнішнього та внутрішнього фретинг-зношування та фретинг-корозії пошкоджень для талевих канатів вантажопідйомних механізмів мобільної бурової установки УПА-60Х. Встановлено передумови виникнення критичного стану поверхонь елементів талевих канатів внаслідок фретинг-корозійних пошкоджень. З урахуванням особливостей та потенційних небезпек пошкодження та руйнування елементів талевих канатів внаслідок фретинг-корозійних явищ для подальшої експлуатації надано практичні рекомендації щодо застосовування канатів з осердями покритими полімером. Застосування зазначених канатів у нафтогазовій галузі дасть можливість: запобігти попаданню води, пилу на осердя, зменшити сили тертя сталок до осердя та внутрішні напруження, покращити стабільність форми каната; поглинати коливання динамічних навантажень

Ключові слова: фретинг-зношування; фретинг-корозія; втомне пошкодження; талева система; спуско-підйомні операції; тертя

ISSN 1993-9973, e-ISSN 2415-332X

Vol. 26, No. 1
2026

PROSPECTING AND DEVELOPMENT OF OIL AND GAS FIELDS

https://pdogf.com.ua/en

Received: 20.11.2025. Revised: 01.05.2026. Accepted: 29.05.2026. Published: 29.06.2026.

UDC 621.793:539.538

DOI: 10.63341/pdogf/1.2026.41

Microstructural evolution and wear resistance of Ti-based MAX phases doped with X-elements for use in drilling and hydrocarbon production

Marine Sasuntsyan*

PhD in Technical Sciences, Associate Professor
National Polytechnic University of Armenia
0009, 105 Teryan Str., Yerevan, Armenia
https://orcid.org/0009-0000-6769-114X

Nina Sahakyan

PhD in Technical Sciences
National Polytechnic University of Armenia
0009, 105 Teryan Str., Yerevan, Armenia
https://orcid.org/0009-0007-6511-7129

Serob Hayrapetyan

PhD in Technical Sciences, Researcher
National Polytechnic University of Armenia
0009, 105 Teryan Str., Yerevan, Armenia
https://orcid.org/0009-0008-4576-2371

Suren Aghbalyan

Postgraduate Student
National Polytechnic University of Armenia
0009, 105 Teryan Str., Yerevan, Armenia
https://orcid.org/0000-0001-9987-8515

Abstract. The purpose of the study was to establish how doping with various X elements affects the microstructural evolution of Ti-based MAX-phase alloys and how these changes affect hardness, thermophysical and tribological properties. The methodology provided for obtaining the base and doped series of Ti-Al-C alloys and their study by X-ray phase analysis, scanning electron microscopy, energy dispersion analysis, digital morphometry, microindentation, resonance determination of elastic modulus, dilatometry, thermogravimetric analysis, tribological tests, and statistical data processing. As a result, it was found that the base series retains the dominance of Ti_3AlC_2 at 87% and is characterised by the most ordered lamellar microstructure with an average grain size of 8.3 μm. Iron doping reduces the proportion of Ti_3AlC_2 to 62%, increases the TiC content to 28%, and is accompanied by the appearance of Fe_3Al, grain grinding to 5.7 μm, violation of the lamellar architecture, and the development of a heterogeneous carbide-intermetallic ensemble. This provides a maximum microhardness of 5.1 GPa, but simultaneously leads to a decrease in the elastic modulus to 191 GPa, density to 4.17 g/cm^3, electrical conductivity to 2.1×10^4 S/m, an increase in the coefficient of linear thermal expansion to 9.7 × 10-6 1/°C, mass loss according to the results of thermogravimetric analysis to 8.6%, and the worst tribological indicators. Silicon doping preserves Ti_3AlC_2 at 74%, is accompanied by the formation of Ti^5Si_3, supports a more ordered intergranular organisation with an average grain size of 6.9 μm and forms the most balanced complex of properties: microhardness 4.2 GPa, modulus of elasticity 214 GPa, density 4.44 g/cm^3, electrical conductivity 3.2×10^4 S/m, coefficient

Suggested Citation: Sasuntsyan, M., Sahakyan, N., Hayrapetyan, S., Aghbalyan, S. (2026). Microstructural evolution and wear resistance of Ti-based MAX phases doped with X-elements for use in drilling and hydrocarbon production. *Prospecting and Development of Oil and Gas Fields*, 26(1), 41-55. doi: 10.63341/pdogf/1.2026.41.

*Corresponding author (*sasuntsyanmarine@gmail.com*)

of linear thermal expansion 7.5×10^{-6} 1/°C, mass loss according to the results of thermogravimetric analysis – 3.4%, mass loss at friction – 3.4%, wear – 0.28 C.U., and the coefficient of friction – 0.47. The practical significance of the results lies in the possibility of their use in the development and selection of wear-resistant Ti-based MAX materials and coatings for drilling and oil and gas production equipment

Keywords: carbide development; tribological behaviour; grain size; modulus of elasticity; thermal conductivity; hardness

Introduction

Ti-based MAX-phases-layered carbides or carbonitrides of transition metals with the general formula $M_{n+1}AX_n$, doped with X-elements, attract increasing attention in materials science and engineering as a class of materials in which the layered crystal structure is combined with high chemical and thermal stability, satisfactory mechanical characteristics, and the ability to work under difficult contact load conditions. Interest in such systems increases in those applications where the material must simultaneously withstand abrasive effects, friction heating, cyclic stress changes, and long-term operation in an aggressive environment. These conditions include the processes of drilling and extraction of hydrocarbons, in which the durability of structural elements and coatings is determined not by a separate parameter, but by a set of interrelated characteristics. In this mode of operation, the analysis covers the stability of lamellar morphology, the state of grain boundaries, the distribution of secondary phases, hardness, thermal conductivity, and the nature of wear under external loads. Therefore, doping with X elements should not be considered as a local compositional change, but as a factor capable of rearranging the phase equilibrium, microstructural organisation, and functional behaviour of Ti-based MAX phases.

An important foundation for this understanding was laid by N.N. Aghajanyan *et al*. (2023), who investigated the self-propagating high-temperature synthesis of MAX phases in the Ti-Zr-Al-C system. The paper showed that variations in the composition of the initial mixture and synthesis conditions directly affect the phase composition, lattice parameters, and microstructure features, and therefore, composite control is one of the basic mechanisms for controlling structure formation. Further disclosure of this approach was contained in the paper by G.N. Muradyan (2023), where Ti-Al-C-based MAX phases were considered in the framework of synthesis in the hydride cycle. The study clearly linked the phase state of the material with the conditions of development and the course of reaction processes, which is why the technological route was not a background circumstance, but an active factor in the development of the final structure. A broader generalising view was suggested by S. Aydinyan (2023), who analysed the synthesis of MAX phases by combustion and emphasised that the microstructure and properties of such materials are determined by the production method itself. As a result, the lamellar organisation, the level of defects, and the presence of side phases appear as a natural result of a particular technological scheme, and not as random accompanying phenomena. A significant contribution to understanding the role of substitution in Ti-based MAX systems was made by M. Berrabah *et al*. (2025), who synthesised and characterised a new solid solution . Combining microstructural analysis with the study of transport properties showed that NB doping affects not only phase stability, but also functional parameters of the material.

A similar content vector result was obtained by M. Shahbaz *et al*. (2024) during the study of chromium-aluminium carbide MAX phases. The paper confirmed that a change in the chemical composition can lead to the development of structurally different MAX-like phases, so the choice of a doping element takes on the significance of a directional phase design tool. The functional measurement of TI-containing carbide systems was further revealed in the paper by B. Liu *et al*. (2026), where the Ti-C composite interlayer formed in situ was associated with increased corrosion resistance and electrical conductivity. This formulation of the question shifted attention to the role of microstructural architecture in the organisation of conducting pathways and once again emphasised that transport characteristics in multiphase Ti-based systems are structurally determined. A direct approach to tribological problems was traced in the study by H. Wu *et al*. (2025), devoted to the effect of Nb content on the properties of laser-deposited Ti-Al-CMAX-phase composite coatings. The results showed that the change in the doping component is accompanied by a simultaneous rearrangement of the phase ensemble, microstructure, and friction behaviour, and this indicates a complex nature of wear resistance development. This line was supported by Y. Lu *et al*. (2024), who investigated CoNi coatings reinforced with Ti_2AlC and Ti_3AlC_2, using analyses of nanostructure, tribological properties, and density functional theory calculations. The study showed that the presence of the MAX-phase component is associated with an improvement in the tribological response, while interfacial interaction and the nature of structural organisation affect the mechanisms of wear. The influence of technological parameters on the development of the durability of Ti-Al-C systems was traced in detail by H. Hong *et al*. (2025). The researchers proved that the powder composition and processing parameters significantly change the microstructure and tribological behaviour of coatings, therefore, wear resistance was formed as a result of the joint action of the composition and technology. A related aspect of functional tribological optimisation was presented in the study by X. Gui *et al*. (2025) on Cu-Ti_2AlC coatings. The paper showed that the High-Velocity Oxy-Fuel spraying parameters affect the wear mechanisms and efficiency of the MAX-phase component, which once again emphasises the multi-factor nature of the behaviour of MAX-phase systems in friction mode.

The totality of these studies has shown that ideas about phase formation, microstructural development, transport characteristics, and tribological behaviour of Ti-based MAX systems have already acquired sufficient depth, but these lines of analysis are mostly deployed not in a single research field, but in partially separate areas. As a result, the complete scheme of interpretation of Ti-Al-X MAX phases, within which microstructural evolution, hardness, thermal conductivity and wear resistance would be considered as interrelated consequences of doping with various X elements, remains insufficiently developed. In many studies, the phase composition and features of synthesis are described without a sufficiently detailed tribological interpretation, whereas in studies focused on wear, the behaviour of the material is not always associated with the evolution of lamellar morphology, the state of grain boundaries, and the redistribution of secondary phases. This is what makes it necessary to study where the effect of X elements in Ti-based MAX phases will be analysed through the relationship between structure, hardness, and wear resistance under conditions typical of drilling and hydrocarbon production. The purpose of the study was to establish the features of the influence of various X-elements on the microstructural evolution of Ti-based MAX-phase alloys and related changes in hardness, thermophysical, and tribological properties.

Materials and Methods

The study was conducted during 2025 at the Basic Research Laboratory of Materials Science and Metallurgy at the National Polytechnic University of Armenia (Yerevan). It was of a comparative nature and covered three series of Ti-based MAX alloys in the Ti-Al-C system: base without doping, Fe-doped and Si-doped. This design allowed comparing the effect of the type of doping element on the phase composition, microstructure, mechanical, thermophysical and tribological characteristics of the material under the same synthesis conditions. Dispersed powders of titanium (Ti, 99.5%, <45 µm, Alfa Aesar, USA), aluminium (Al, 99.9%, <50 µm, Sigma-Aldrich, Germany), carbon in the form of graphite (99.9%, <20 µm, Merck, Germany), and powder doping additives Fe and Si of high purity (Alfa Aesar, USA) were used as starting components. At the stage of model study of compositions, Fe and Si were considered as X-elements, which differ in the nature of interaction with the Ti-Al-C matrix, the ability to form secondary phases, and the effect on the stability of the lamellar structure. The base series without doping was used as a reference, and the doped series was formed under comparable synthesis conditions, which helped to correctly link the detected differences with the action of the doping factor.

Before mixing, the powder components were dried at 100°C for 24 hours. The charge was prepared in a Retsch PM100 planetary ball mill (Germany) at 300 rpm for 6 hours in an argon atmosphere using steel balls with a mass ratio of balls to powder of 10:1. This regime ensured sufficient uniformity in the distribution of components and reduced the risk of local segregation. After mixing, the powder compositions were compacted by cold isostatic pressing into cylindrical samples with a diameter of 20 mm at a pressure of 200 MPa on an AIP KIP-100 installation (Japan). Further development of the dense structure and the course of phase formation were provided by vacuum sintering in the Carbolite Gero STF 15/610 (UK) furnace at a temperature of 1,350°C with an exposure time of 2 hours and a heating rate of 10°C/min, after which the furnace was cooled to room temperature. To obtain representative results, three series of samples were prepared that differed in the type of doping element: basic without doping, Fe-doped and Si-doped, under the same pressing and sintering conditions. The phase composition of the synthesised materials was determined by X-ray diffraction on a Bruker D8 Advance diffractometer (Germany) using CuKα- radiation ($\lambda = 1.5406$ Å) in the range 2θ from 20° to 80°, with a step of 0.02° and an accumulation time of 1 s per point. Phase identification was performed using a PDF-4+ database, and primary diffraction processing, reflex comparison, and phase composition refinement were performed in HighScore Plus. This approach allowed recording the main MAX phase, carbide and intermetallic components, and to assess trends towards stabilisation or destabilisation of the layered structure depending on the nature of the doping element.

Microstructural analysis was performed using a Tescan VEGA3 scanning electron microscope (Czech Republic) equipped with an energy-dispersive X-ray analyser Oxford Instruments X-MAX (United Kingdom). Polished cross-sections and fractographic surfaces were investigated, which allowed assessing the nature of morphology, spatial phase distribution, localisation of secondary inclusions, the state of interfacial boundaries, and signs of structural destabilisation. Energy dispersion analysis was used to clarify the local chemical composition of individual zones. The average grain size was determined by linear cross-section using scanning electron microscopy images. For this purpose, digital morphometry of scanning electron microscopy (SEM images) was performed in the Fiji software environment, followed by statistical processing of the measured values for each series of samples. This allowed moving from descriptive analysis of the microstructure to quantitative comparison of the degree of its rearrangement in different series of samples. The mechanical unit of the study included measurements of microhardness and elastic modulus. Microhardness was determined on a Buehler Micromet 5101 device (USA) at a load of 50 g; for each series, 10 measurements were performed in different sections of the section, which allowed considering the local inhomogeneity of the structure. The elastic modulus was evaluated by the resonant method on the IMCE RFDA system (Belgium) at longitudinal and transverse resonant frequencies. The density of the samples was determined by the Archimedes method, which allowed linking mechanical parameters with the degree of compaction, porosity, and features of the phase composition.

Functional characteristics included determination of electrical conductivity, coefficient of linear thermal expansion, and oxidative heat resistance. Electrical conductivity was measured by the four-probe method on a Loresta GP MCP-T610 instrument (Japan). The coefficient of linear thermal expansion was determined on a Linseis L75 PT dilatometer (Germany) in the temperature range from 25°C to 800°C. Oxidative heat resistance was analysed by thermogravimetric analysis on a Jupiter Netzsch STA 449 F3 (Germany) in an air atmosphere heated to 1,000°C at a rate of 10 °C/min with continuous recording of mass changes. This allowed comparing the functional parameters with the phase composition, the state of grain boundaries, and the distribution of secondary phases.

To assess wear resistance, tribological tests were carried out under dry friction conditions using the ball-on-disk method, with a 6 mm diameter AISI 52100 steel counter-body. The tests were performed at a normal load of 5 N, a sliding speed of 0.1 m/s, and a total friction path of 300 m at room temperature. At least three repetitions were performed for each series of samples. During the tests, the coefficient of friction was recorded, and after the test was completed, the mass loss and the amount of wear were determined. Thus, wear resistance was interpreted as an integral manifestation of the phase composition, microstructure, hardness, density, and functional stability of the material under tribological interaction conditions.

The methodological scheme of the study was based on a sequential combination of phase, microstructural, mechanical, thermophysical, and tribological analysis. The phase composition was considered as the structural basis of properties; microstructure – as a spatial expression of the phase development flow and doping consequences; hardness and modulus of elasticity – as indicators of hardening and rigidity; density – as an indicator of compaction and porosity; electrical conductivity, coefficient of thermal expansion and oxidative heat resistance – as characteristics of functional stability; and wear resistance – as a generalised result of the interaction of all these parameters in the friction mode.

The statistical stage of the study was aimed at describing the obtained values and checking the differences between the sample series. The mean value and standard deviation were determined for each indicator. The normality of the distribution was checked according to the Shapiro-Wilk criterion, and the uniformity of variances was checked according to the Leuven criterion. Differences between the three independent series were evaluated by univariate analysis of variance followed by the Tukey post hoc test. The distribution deviated from the normal one, the Kraskel-Wallis criterion with multiple pairwise comparisons was applied. The initial ordering of experimental arrays, calculation of descriptive statistics, and verification of inter-series differences were performed by Jamovi, while the construction of graphs, diagrams, and comparative visualisations was performed in GraphPad Prism 10. For each indicator – microhardness, elastic modulus, density, electrical conductivity, coefficient of linear thermal expansion, oxidation resistance, and wear parameters – generalising statistics were determined and intra-batch scattering values were estimated. The differences obtained were interpreted considering the phase composition, microstructural rearrangement, and functional properties of the material. The statistical significance level was assumed to be $p < 0.05$. In general, the applied method provided a reproducible study of the microstructural evolution of Ti-based MAX-phase alloys with various X-elements and created grounds for a holistic comparison of the structure, mechanical, thermophysical and tribological properties within a single materials science interpretation.

Results

Doping and phase stability of Ti-based MAX phases during X-element doping

The results of X-ray phase analysis showed that doping with different X-elements is accompanied by an unequal rearrangement of the phase composition of Ti-based MAX phases. The main differences were related to the proportion of the Ti_3AlC_2 phase, the intensity of carbide development, and the appearance of intermetallic components, which allows considering the phase balance as a primary structural indicator of stability or destabilisation of the layered MAX architecture. The quantitative ratio of phases in the base and doped series is shown in Table 1.

Table 1. Phase composition of Ti-based MAX series of phases doped with various X elements

Sample series	Main MAX-phase Ti_3AlC_2, %	Carbide phases (TiC), %	Intermetallic phases, %	Other phases, %
Base series without doping	87	10	0	3
Fe doping	62	28	7 (Fe_3Al)	3
Si doping	74	12	11 (Ti_5Si_3)	3

Source: created by the authors based on the results of X-ray phase analysis performed on Bruker D8 Advance with diffraction processing in HighScore Plus

As shown in Table 1, the base series without doping was characterised by the highest proportion of the Ti_3AlC_2 phase – 87%, which indicates the dominance of the layered MAX structure under the accepted synthesis conditions. The proportion of TiC in this series was 10%, while intermetallic components were not fixed, and other phases accounted for only 3%. This ratio indicates that in the reference material, the main MAX phase retains the role of a structural matrix, while the secondary components are limited in nature and do not determine the overall phase organisation of the alloy. In the Fe-doped series, the phase balance shifted most noticeably. The proportion of Ti_3AlC_2 decreased to 62%, i.e., by 25 percentage points compared to the baseline series, while the TiC content increased to 28%.

Simultaneously, the intermetallic phase Fe_3Al appeared in the structure in an amount of 7%. This combination indicates a pronounced destabilisation of the layered MAX architecture, since a decrease in the proportion of the main phase is accompanied by increased carbide formation and a noticeable redistribution of components towards the intermetallic component. In phase equilibrium, this means that Fe acts as a doping element that does not support the dominance of Ti_3AlC_2, but stimulates the development of a more rigid, but less structurally integral carbide-intermetallic ensemble. The Si-doped series showed a different nature of phase rearrangement. The proportion of Ti_3AlC_2 decreased to 74%, i.e., there was also a deviation from the base composition, but it was less sharp than with Fe doping. The TiC content was 12%, and the intermetallic component was represented by the Ti_5Si_3 phase in the amount of 11%. In contrast to Fe doping, no sharp increase in the carbide phase was observed in this case, and the main MAX phase retained its dominant position in the structure. Such a phase balance indicates not a deep destabilisation, but a partial phase modification, in which the layered matrix is preserved, but supplemented by an interfacial intermetallic component (Kvasnytskyi *et al.*, 2020).

Comparing the three series allows distinguishing different scenarios of phase stability. The base series corresponds to a state in which Ti_3AlC_2 dominated, and the secondary phases have a subordinate value (Mukhamedova *et al.*, 2022). Fe doping forms a scenario of the deepest phase destabilisation, since it is accompanied by a simultaneous decrease in the proportion of the main MAX phase, a sharp increase in TiC and the appearance of Fe_3Al. Si doping occupied an intermediate position: it also changes the phase composition, but does not put the system in the mode of predominant carbide formation, but retains Ti_3AlC_2 as the main phase. It is this difference between Fe and Si that is fundamental, since it sets different trajectories for further microstructural evolution – from breaking down the lamellar architecture to partially preserving it. Taken together, the results of phase analysis showed that the nature of the doping element directly determines the degree of stability of the Ti-based MAX phase. Fe promotes the destabilisation of Ti_3AlC_2 and the enhanced development of carbide and intermetallic components, while Si provides a milder type of phase adjustment, in which the main MAX phase is maintained at a higher level. The established phase balance is the initial structural prerequisite for further analysis of the morphology, mechanical characteristics, thermophysical properties, and wear resistance of doped Ti-based MAX phases.

Microstructural evolution and morphology of doped Ti-based MAX phases

The results of scanning electron microscopy, energy dispersion analysis, and digital morphometry showed that do ping with various X-elements changes the microstructural prganisation of Ti-based MAX phases not only quantitatively, but also morphologically. The degree of preservation of the lamellar architecture, the nature of interfacial boundaries, the localisation of secondary inclusions, and the average grain size were most sensitive to changes in the composition. The generalised morphometric parameters of the microstructure are shown in Table 2.

Table 2. Morphometric parameters of the microstructure of Ti-based MAX phases with different types of doping

Sample series	Dominant morphology	Nature of secondary phase distribution	State of interfacial boundaries	Average grain size, μm
Base series without doping	Lamellar, plate	Uniform, limited	Clearly defined	8.3
Fe doping	Broken, heterogeneous, with rounded inclusions	Heterogeneous, with local concentrations of carbides and intermetallides	Partially blurred, sometimes destabilised	5.7
Si doping	Lamellar with intergranular intermetallic modification	Localised along grain boundaries	Mostly preserved, structurally ordered	6.9

Source: formed by the authors based on the results of SEM analysis, energy dispersion analysis, and digital morphometry in Fiji

As shown in Table 2, the base series without doping was characterised by the most ordered microstructure. It was characterised by lamellar plate morphology, uniform and limited distribution of secondary phases, and well-defined interfacial boundaries. This combination of features corresponds to a structure in which the layered MAX matrix retains its integrity, and secondary components do not acquire a decisive role in the organisation of the material. Fe doping was accompanied by the deepest microstructural rearrangement. The dominant morphology lost its ordered lamellar structure and passed into a disturbed, heterogeneous state with rounded secondary inclusions. The distribution of secondary phases became heterogeneous, with local concentrations of carbides and intermetallides, and the interfacial boundaries were partially blurred and acquired signs of destabilisation. Taken together, this suggests that Fe not only changes the number of secondary phases, but also rearranges the very principle of microstructural organisation, shifting it from lamellar to a more fragmented type (Ratov *et al.*, 2023). Si doping demonstrated a different scenario of microstructural evolution. In this series, the lamellar architecture was generally preserved, although it was supplemented by an intergranular intermetallic modification. The secondary phases had a predominantly localised distribution along the grain boundaries, while the interfacial boundaries themselves remained predominantly ordered. This means that Si is not associated with the destruction of the layered framework, but with its partial intergranular reconstruction, which preserves the overall structural integrity of the material. The change in the average grain size requires a separate comparison, since it is this indicator that quantifies the differences between the identified morphological scenarios. For a clearer comparison of morphometric differences between the series, the values of the average grain size are shown in Figure 1.

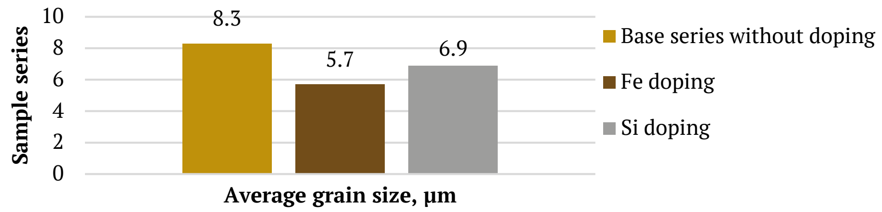

Figure 1. Change in the average grain size in Ti-based MAX phases when doping with various X elements
Source: compiled by the authors based on the results of morphometric analysis of the microstructure in Fiji

Figure 1 shows that the base series without doping had the largest average grain size – 8.3 μm. This is consistent with its most ordered lamellar morphology and well-defined interfacial boundaries. Fe doping reduced the average grain size to 5.7 μm, that is, it gave the lowest value among all the studied series. This decrease occurred simultaneously with the greatest morphological destabilisation, which indicates the grinding of the structure not as an isolated effect, but as part of the overall rearrangement associated with intensive carbide and intermetallic formation. Si doping occupied an intermediate position: the average grain size was 6.9 μm, that is, it was smaller than in the base series, but larger than in the Fe-doped material. This indicates moderate restriction of grain growth without drastic destruction of the lamellar architecture. In a comparable dimension, the data obtained reflect three different scenarios of microstructural evolution. The base series corresponds to the state with a structurally stable lamellar organisation and the largest average grain size. Fe doping forms a scenario of the deepest destabilisation, which combines grain grinding, blurring of interfacial boundaries, and heterogeneous localisation of secondary phases. Si doping occupies an intermediate position, combining grain growth restriction with relative preservation of the layered framework and ordered intergranular localisation of secondary inclusions. Thus, the results of microstructural analysis showed that the nature of the doping element determines not only the grain size, but also the type of morphological rearrangement itself, namely, this rearrangement further forms the mechanical, thermophysical and tribological properties of the doped Ti-based MAX phases.

Effect of phase-structural adjustment on microhardness, elastic modulus, and density

Generalisation of the results of the mechanical unit of the study showed that changes in the phase composition and microstructural organisation of Ti-based MAX phases directly affect the indicators of microhardness, elastic modulus and density. The most significant in this aspect were the differences between the series in which doping was accompanied either by destabilisation of the lamellar MAX matrix with enhanced carbide and intermetallic formation, or partial preservation of the layered architecture with intergranular modification. That is why mechanical characteristics in this subsection are considered not as isolated parameters, but as a quantitative expression of the phase-structural rearrangement of the material. A comparison of microhardness, elastic modulus, and density in the base and doped series is shown in Figure 2.

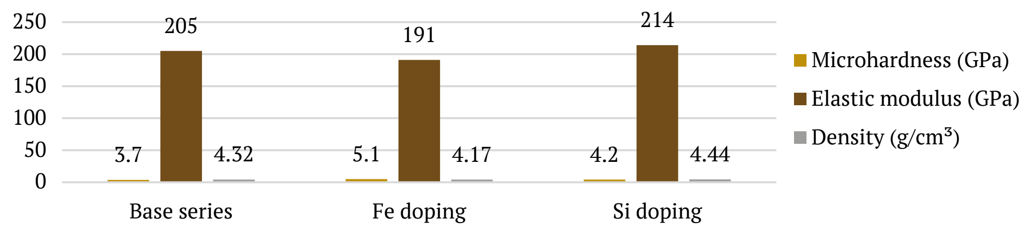

Figure 2. Comparison of microhardness, elastic modulus, and density in Ti-based MAX-phase series
Source: compiled by the authors based on the results of microhardness measurements on Buehler Micromet 5101, determination of elastic modulus on IMCE RFDA, and density estimation by the Archimedes method

Figure 2 shows that the mechanical response of Ti-based MAX phases when doping with various X elements is formed not according to a single scenario, but through different combinations of local hardening, structural rigidity, and compaction of the material. The basic series occupies a relatively balanced position: microhardness is 3.7 GPa, modulus of elasticity – 205 GPa, density – 4.32 g/cm^3. This corresponds to a state in which the layered MAX matrix retains structural integrity without a sharp dominance of secondary phases. The most noticeable contrast is observed in the Fe-doped series. It shows the maximum microhardness – 5.1 GPa, but simultaneously has the lowest values of the elastic modulus – 191 GPa and density-4.17 g/cm³. This combination indicates that Fe increases the local indentation resistance, which is consistent with an increase in the proportion of TiC and the appearance of Fe_3Al, but this strengthening is achieved not through structural ordering, but through a more rigid and simultaneously less integral carbide-intermetallic framework. A decrease in density indicates a lower degree of compaction and a higher probability of porosity or defect, and a decrease in the elastic modulus indicates a weakening of the continuity of the layered matrix despite an increase in hardness. The Si-doped series demonstrates a different type of mechanical response. The microhardness here is 4.2 GPa, i.e., it exceeds the base series, but remains lower than the Fe-doped variant. This particular series has the highest modulus of elasticity – 214 GPa and the highest density – 4.44 g/cm³. This distribution of indicators indicates that Si does not provide maximum local hardening, but provides a more favourable combination of rigidity and structural compaction. This is in good agreement with previous phase and microstructural results, where Si was associated with less drastic destabilisation of Ti_3AlC_2 and more ordered intergranular modification. An increase in microhardness does not in itself mean an improvement in the entire complex of mechanical properties (Adjamskiy *et al.*, 2022). Fe doping forms a local hardening scenario against the background of structural destabilisation, while Si doping provides a more balanced mechanical profile with increased stiffness and density. In this sense, the mechanical response of Ti-based MAX phases is determined not by a single indicator, but by a cumulative phase-structural rearrangement, which is implemented differently depending on the nature of the doping element. That is, the mechanical response of Ti-based MAX phases is determined not by one single parameter, but by a cumulative rearrangement of the phase composition, morphology, and interfacial organisation. An increase in microhardness is accompanied by various structural scenarios: in the case of Fe – carbide-intermetallic hardening with loss of part of the structural integrity, in the case of Si – moderate hardening against the background of maintaining a more ordered lamellar base. Density in this context reflects not only the degree of compaction, but also the general nature of the microstructural organisation, in particular, the relationship between the preservation of the matrix phase and the development of secondary inclusions. Consequently, the results of mechanical analysis confirm that phase-structural rearrangement determines not only the local strain resistance, but also the overall level of rigidity and structural integrity of doped Ti-based MAX phases.

Thermophysical and functional properties of doped Ti-based MAX phases

The results of the thermophysical and functional unit of the study showed that doping with various X-elements changes not only the phase and microstructural state of the Ti-based MAX phases, but also the method of thermal and electrical response of the material under thermal load conditions. Electrical conductivity, coefficient of linear thermal expansion, and oxidative heat resistance were the most sensitive to phase-structural adjustment, while thermal conductivity was considered as an integral indicator, the value of which was determined by the preservation or violation of the layered architecture, the state of grain boundaries, and the spatial distribution of secondary phases. Table 3 summarises the thermophysical and functional characteristics of the base and doped series of Ti-based MAX phases.

Table 3. Thermophysical and functional characteristics of Ti-based MAX phases when doping with various X elements

Sample series	Electrical conductivity, S/m	Coefficient of linear thermal expansion, $\times 10^{-6}$ 1/°C	Mass loss based on thermogravimetric analysis, %
Base series without doping	3.5×10^4	8.1	5.8
Fe doping	2.1×10^4	9.7	8.6
Si doping	3.2×10^4	7.5	3.4

Source: created by the authors based on the results of electrical conductivity measurements on Loresta GP MCP-T610, dilatometric analysis on Linseis L75 PT, and thermogravimetric analysis on Netzsch STA 449 F3 Jupiter

As shown in Table 3, the base series without doping was characterised by the most balanced combination of functional parameters. The electrical conductivity was 3.5×10^4 S/m, the coefficient of linear thermal expansion was 8.1×10^{-6} 1/°C, and the mass loss according to the results of thermogravimetric analysis was 5.8%. This ratio corresponds to a structure in which Ti_3AlC_2 retains its dominant position, and the secondary phases do not critically disrupt either the conducting paths or the stability of the material when heated. In a functional sense, the base series sets a reference level relative to which the area and depth of changes caused by doping can be estimated. The Fe-doped series showed the least favourable complex of thermophysical and functional characteristics. The electrical conductivity was reduced to 2.1×10^4 S/m, i.e., a significant part of the conductivity was lost compared to the base series. The coefficient of linear thermal expansion increased to 9.7×10^{-6} 1/°C, and the mass loss for TGA reached 8.6%, which is the maximum value among the studied series. This combination of indicators is consistent with the previously established phase-structural destabilisation: an increase in the proportion of TiC, the appearance of Fe_3Al, a decrease in the average grain size and blurring of interfacial boundaries form a more heterogeneous environment for charge and heat transfer, and simultaneously reduce resistance to high-temperature oxidation. Consequently, Fe doping is accompanied not only by a rearrangement of the phase composition, but also by a systemic deterioration in the functional profile of the material. The Si-doped series, on the contrary, showed the most stable type of thermophysical behaviour. The electrical conductivity in it was 3.2×10^4 S/m, that is, it remained close to the base series, the coefficient of linear thermal expansion decreased to 7.5×10^{-6} 1/°C, and the mass loss by TGA was minimal – 3.4%. Taken together, this indicates that SI doping does not lead to deep destruction of the conductive framework of the MAX matrix, but, on the contrary, is associated with higher dimensional stability and better resistance to oxidative degradation. Figure 3 summarises the thermogravimetric curves of the base and doped series of Ti-based MAX phases, which allows comparing not only the final level of degradation, but also the course of the oxidation process over the entire temperature range.

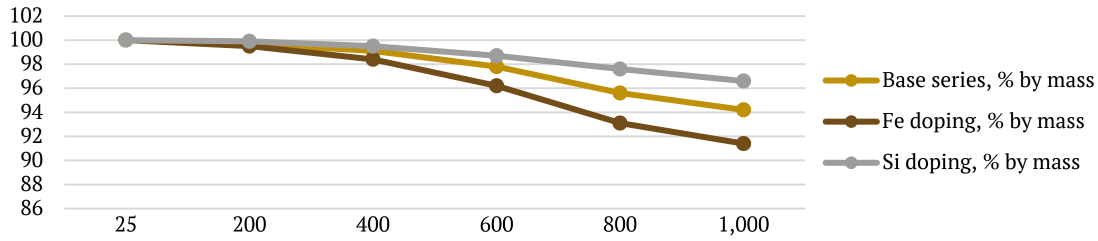

Figure 3. Change in the mass of Ti-based MAX-phase samples based on the results of thermogravimetric analysis

Source: created by the authors based on the results of thermogravimetric analysis performed on a Netzsch STA 449 F3 Jupiter

As can be seen from Figure 3, the change in the mass of the samples during heating occurred in different scenarios depending on the type of doping, and the differences between the series were observed not only in the final mass loss, but also in the course of the thermogravimetric process itself. The base series showed a moderate decrease in residual mass as the temperature increased: at the initial heating sites, the changes are insignificant, while in the region of higher temperatures, the degradation becomes more intense and up to 1,000°C, the residual mass decreases to 94.2%. Such a curve corresponded to a material with a relatively stable phase base, but without additional factors that would significantly restrain the oxidation processes at the final stages of heating. The Fe-doped series showed the least stable behaviour. Already in the intermediate temperature sections, its curve passed below the base one, and in the region of high temperatures, the mass decline became the most pronounced. By 1,000°C, the residual mass decreased to 91.4%, which corresponds to the maximum loss among all the studied series. This nature of the curve indicates that Fe doping not only increases the overall level of oxidative degradation, but also makes the mass loss process more intense over the entire temperature range. In a structural sense, this is consistent with the greatest phase and microstructural destabilisation established earlier: an increase in the proportion of TiC, the appearance of Fe_3Al, grain grinding, and a violation of the lamellar architecture, which creates a less stable material when heated. The Si-doped series, on the contrary, is characterised by the wettest curve and the smallest decrease in residual mass. Throughout the entire temperature range, its values remained higher than those of the base and Fe-doped series, and at 1,000°C, the residual mass is 96.6%. This indicates that Si doping provides the highest oxidative heat resistance among the studied variants. It is important to note that this behaviour was observed not only at the end point, but throughout the heating process, i.e., Si is associated not with a local, but with a systemic slowdown in degradation processes. The results confirmed that the type of doping element determines not only the final level of mass loss, but also the shape of the thermogravimetric response of the material. Fe doping established a scenario of accelerated oxidative degradation, the base series retained an intermediate behaviour, while Si doping formed the most stable curve with minimal mass loss.

Wear resistance and wear mechanisms of Ti-based MAX phases in dry friction mode

The results of tribological tests showed that the behaviour of Ti-based MAX phases in the dry friction mode is determined not by a separate mechanical indicator, but by the integral action of the phase composition, microstructural organisation, hardness, density, and thermophysical stability of the material. It is in the tribological mode that it is most clearly shown how much the structural adjustment caused by doping is favourable or, conversely, destabilising from the standpoint of the actual operational response of the material. To compare the base and doped series, Figure 4 summarises the indicators of mass loss, wear value, and coefficient of friction, which allows estimating wear resistance as the final result of the entire pre-set phase-structural and functional evolution.

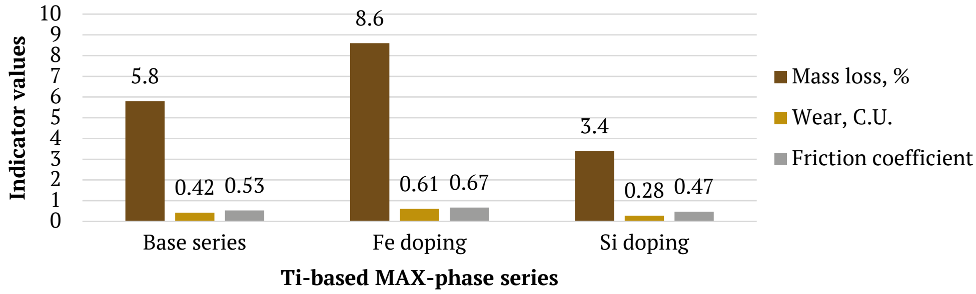

Figure 4. Comparison of mass loss, wear and coefficient of friction indicators in the base and doped Ti-based MAX phase series

Source: compiled by the authors based on the results of tribological tests in the dry friction mode and subsequent statistical processing in Jamovi and GraphPad Prism 10

Figure 4 showed that the tribological behaviour of Ti-based MAX phases is determined by the combined effect of phase composition, microstructure, and functional characteristics, not just the level of hardness. The base series occupied an intermediate position in all three indicators: mass loss was 5.8%, wear – 0.42 C.U., the coefficient of friction – 0.53. This distribution corresponds to a relatively stable lamellar structure dominated by Ti_3AlC_2, which provided moderate wear resistance without a pronounced tribological advantage. The Fe-doped series occupied the least favourable position: it was characterised by the greatest mass loss – 8.6%, maximum wear – 0.61 C.U. and the highest coefficient of friction – 0.67. This indicates that the increase in microhardness was not accompanied by an increase in wear resistance. This discrepancy is associated with phase-structural destabilisation, since the growth of the proportion of TiC and Fe_3Al, grain grinding, and inhomogeneity of the interfacial space formed a rigid but less integral surface layer. The Si-doped series, on the contrary, occupied the best position in terms of tribological indicators. For it, the minimum values of mass loss were recorded – 3.4%, wear – 0.28 C.U. and the coefficient of friction – 0.47. This indicates that SI doping provided the most stable surface layer in the dry friction regime, which is consistent with better preservation of the lamellar architecture, ordered grain boundaries, and generally a more balanced structural and functional state of the material (Baklanov *et al.*, 2022).

Thus, the results of tribological analysis showed that the highest wear resistance is demonstrated by the Si-doped series, which is characterised by the most balanced combination of phase composition, microstructural organisation, rigidity, density, and thermal stability. It is in this series that the higher content of the main phase Ti_3AlC_2 is preserved, the lamellar architecture is less disturbed, and the secondary phases are localised in a more orderly manner, without deep destabilisation of the interfacial space. As a result, the surface layer works more stably during friction, is less susceptible to discolouration and better counteracts the accumulation of local damage, which is reflected in the minimum values of mass loss, wear and coefficient of friction. The base series retains an intermediate level of wear resistance, which is conditioned by the relatively ordered layered structure and the dominance of Ti_3AlC_2, but without the additional structural effect that would increase the wear resistance. Such a material does not show a sharp destabilisation, but it does not form the optimal combination of rigidity, compaction and thermal stability that is observed during Si doping (Malecha *et al.*, 2025). Therefore, its tribological behaviour is more stable than as effective as possible. Fe doping, despite the increase in microhardness, is accompanied by less favourable tribological behaviour due to deeper phase-structural destabilisation. An increase in the proportion of TiC and Fe_3Al, a decrease in the average grain size, a heterogeneous distribution of secondary phases, and a partial violation of interfacial boundaries form a microstructure in which local hardening is combined with a decrease in overall structural integrity. In the dry friction mode, this is manifested in unstable contact, an increased tendency to micro-destruction of the surface layer, and a worse agreement between hardness and actual wear resistance. That is, Fe increases the resistance to local indentation, but does not provide stable resistance to surface destruction (Shevko *et al.*, 2020). As a result, it is the nature of microstructural rearrangement that determines whether doping is transformed into an increase in operational stability, or, conversely, into an increase in the tendency to surface destruction in the dry friction mode. For Ti-based MAX phases, the principle is not the maximum increase in a particular mechanical parameter, but the preservation of structural order, controlled development of secondary phases, and stability of the surface layer under load. That is why the most promising type of doping from the standpoint of tribological application is that which does not destroy the layered MAX framework, but modifies it without losing its structural integrity (Nedeva, 2025).

In general, the results obtained showed that doping of Ti-based MAX phases with different X elements sets not just differences in individual indicators, but different scenarios for the structural and inherent evolution of the material. The base series retained the most stable layered MAX architecture with Ti_3AlC_2 dominance, moderate mechanical characteristics, balanced thermophysical parameters, and intermediate wear resistance. Fe doping caused the deepest phase and microstructural destabilisation, which was manifested in a decrease in the proportion of Ti_3AlC_2, an increase in TiC and Fe_3Al, grain grinding, disruption of lamellar organisation, and the development of a heterogeneous interfacial space. This led to a local increase in microhardness, but also was accompanied by a decrease in elastic modulus, density, electrical conductivity, deterioration of thermal stability, and the least favourable tribological behaviour. Si doping, on the contrary, provided a more controlled type of phase modification: while maintaining the dominance of Ti_3AlC_2 and the development of Ti_5Si_3 in the intergranular space, the structure remained more ordered, the grain organisation – more stable, and the complex of mechanical, thermophysical and tribological characteristics – the most balanced. That is why the Si-doped series demonstrated the highest wear resistance, the best oxidation heat resistance and the most favourable combination of rigidity, density, and functional stability. Thus, the key factor in the operational efficiency of Ti-based MAX phases was not the maximum increase in a particular property, but the type of microstructural adjustment that determines whether the integrity of the layered MAX frame is preserved under mechanical, thermal, and tribological loads.

Discussion

The complex of established regularities showed that doping of Ti-based MAX phases changed not one individual characteristic, but the entire chain "phase composition-microstructure – mechanical response – functional stability – wear resistance". This logic fits well with the advanced concept of materials engineering, where the operational effect is determined not by local reinforcement itself, but by the way structural modification rearranges the behaviour of the material under load conditions. The generalised emphasis on the role of complex control of the structure and surface state of the material echoed the conclusions of H. Sun *et al*. (2025), where advanced coating technologies were considered as a tool for purposeful development of durability, wear resistance, and stability of properties. This statement corresponded to the dependence found here, in which it was the nature of phase-microstructural rearrangement that determined whether the operational profile of the Ti-based MAX phase improved or, conversely, became less stable.

The contrast between local reinforcement and overall structural integrity correlated well with the results of W. Maziarz *et al*. (2024), where TiC-containing nanocomposites also showed increased stiffness due to solid secondary phases. However, such rigidity was not considered as a self-sufficient advantage, since the properties were also determined by how homogeneous the microstructural organisation remained, which conceptually coincided with the less favourable behaviour of the Fe-doped series. The milder and structurally controlled modification scenario was consistent with the observations of T. Ma *et al*. (2022), where Ti_2AlC-containing composites were interpreted as systems in which reinforcement is achieved without destroying the base frame of the material. This logic was also traced here: Si doping did not put the system in the deepest destabilisation mode, but retained the dominant role of the MAX phase while simultaneously improving the complex of properties. The role of interfaces and phase boundaries in the development of the mechanical response was consistent with the study by Y. Zhou *et al*. (2023), where the properties of laminated Ti/Al composites were directly related to the state of interfacial interaction. This parallel was also important for Ti-based MAX phases, since it was the nature of grain boundaries and the way secondary phases were localised that distinguished the destabilised Fe-containing variant from the more ordered Si-modified state. The emphasis on the spatial organisation of reinforcement phases echoed the conclusions of Z. Yuan *et al*. (2022), where the properties of titanium composites were determined not only by the presence of reinforcing components, but also by their distribution in the matrix and structural uniformity. In this sense, the heterogeneous interfacial space during Fe doping and intergranular localised modification during Si doping corresponded to two different scenarios of evolution, which led to differences in mechanical and tribological behaviour. A favourable combination of rigidity and functional stability found a conceptual parallel in the results of S. Zhou *et al*. (2026), where Cu-Ti_3AlC_2 composites were considered as systems with structural synergy between the MAX phase and the matrix. A close emphasis was also observed here, since the best property profile was implemented not where the solid phases were most abundant, but where a more consistent structural organisation of the entire system was preserved. The fact that wear resistance was determined not only by the hardness, but also by the stability of the surface layer correlated with the results of X. Zeng *et al*. (2022), where the tribological efficiency of self-lubricating coatings was related to the combination of composition, microstructure, and contact mode. This is why the highest microhardness of the Fe-doped series did not translate into better wear resistance, while the Si-containing material showed more stable behaviour under dry friction conditions.

The idea of the importance of preserving a MAX-like framework was consistent with the results of L. Cao *et al*. (2024), where high-entropy ceramics $(TiVNbTaM)_2AlC$ were interpreted as systems in which the composition was significant primarily due to the effect on the structural stability of the MAX phase. This formulation was consistent with the distinction found here between Fe doping as a destabilisation scenario and Si doping as a more controlled phase modification scenario. The balance between the MAX phase and the carbide component resonated well with the paper by A. Deng *et al*. (2025), where the properties of M_2AlC-MC composites were explained precisely by the ratio of the matrix MAX phase and rigid carbides. In this context, the unfavourable profile of the Fe-doped material was associated not only with the presence of TiC, but also with the fact that the carbide and intermetallic components began to displace the structure-forming role of Ti_3AlC_2. The dependence of oxidation resistance on the method of phase modification correlated with the results of Y. Xu *et al*. (2025), where an increase in oxidation resistance in Ti_2AlC was achieved through solid solutions that suppressed degradation processes. A similar emphasis was observed here: the wettest thermogravimetric curve and the lowest mass loss during Si doping indicated systemically higher stability, rather than the local effect of a single phase. A similar logic was also reflected in the paper by A. Zhang *et al*. (2024), where an improvement in the oxidative stability of Ti_2AlC coatings was associated with modification without destruction of the base MAX framework. It was this interpretation that corresponded to the conclusion established here that the most promising type is the type of doping that does not destabilise the layered architecture, but modifies it while maintaining structural integrity. Further development of the tribological block was in good agreement with the results of L. Cai *et al*. (2024), where the effect of solid-soluble elements on Ti_3AlC_2 was considered due to the self-lubricating effect and temperature-dependent friction stability over a wide range. This statement directly echoed the fact found here that favourable tribological behaviour was determined not only by the hardness, but also by the ability of the structurally modified MAX-phase to maintain a stable contact regime and restrain progressive surface destruction. A close accent could be traced in the paper by J. Li *et al*. (2024), where a-site doping of Ti_3AlC_2 was interpreted as a factor altering the tribological response by rearranging the MAX structure itself, rather than simply increasing the strength. This corresponded to the pattern established here, in which the type of doping element determined whether the structural modification turned into an increase in wear resistance, or, conversely, into an increase in the tendency to surface destruction.

The role of Ti_3AlC_2 as a structurally active component capable of changing the microhardness and tribological characteristics of the composite system correlated with the results of V. Desai *et al*. (2025), where Al7075/Ti_3AlC_2 surface composites after friction stir processing were also interpreted through a combination of microstructural rearrangement, local hardening, and changes in the friction mode. This logic also corresponded to the distinction found here between local reinforcement and integral wear resistance, since the very fact of the presence of the MAX phase was important only if its structurally favourable integration. A similar parallel was traced in the paper by M. Li *et al*. (2026), where Ti_3AlC_2 as an additive to WC-Co hard alloys simultaneously affected the mechanical and tribological characteristics of the system. This conceptually coincided with the dependence established here, in which the MAX-containing component did not act in isolation, but through a change in the entire structural and inherent profile of the material, including contact stability under friction. The oxidative behaviour of the established series correlated well with the results of S. Badie *et al*. (2021), where for Ti_2AlC, the breakaway oxidation mechanism was explained by a change in the structural state of the surface layer and a violation of its protective function. This statement was consistent with the fact that the deterioration of oxidative heat resistance during Fe doping reflects not only a greater mass loss, but also a deeper instability of the structural phase state during heating.

A more applied parallel to the behaviour of MAX phases in the form of coatings was observed in N. Laska *et al*. (2024), where the oxidation of Ti_2AlC-based coatings on γ-TiAl was also interpreted due to the relationship between the microstructure, the stability of the MAX component, and the preservation of the protective properties of the system. This was consistent with the conclusion established here that better oxidative stability was realised where a more ordered structural framework and controlled localisation of secondary phases were preserved. Tribological consequences of the introduction of Ti_2AlC as a strengthening component found a parallel in S.W. Hua *et al*. (2023), where Ti_2AlC-reinforced coatings on Ti6Al4V showed a change in wear resistance due to the microstructural organisation and the nature of particle distribution in the Matrix. This emphasis directly echoed the relationship found in this study, in which it was the type of distribution of secondary phases and the degree of preservation of the layered architecture that determined whether the tribological effect would be favourable. The functional aspect related to electrical conductivity correlated with the results of M. Mandegari *et al*. (2023), where the dual MAX-phase Ti_3AlC_2-Ti_2AlC system was interpreted as a material with high electrical conductivity due to the preservation of a structurally favourable phase coupling. This was consistent with the fact established here that a more stable MAX framework during Si doping was accompanied by preservation of electrical conductivity, while deeper phase-microstructural destabilisation during Fe doping led to its noticeable decrease. The temperature stability of the MAX phases over a wider heating range was consistent with the conclusions of M. Potoczek *et al*. (2023), where the oxidative behaviour of Ti_2AlC MAX-phase foams in the range of 600-1,000°C also depended on the structural features and course of degradation processes with increasing temperature. A similar logic was also traced here, since the shape of the thermogravimetric curve was just as important as the final mass loss, and the most stable scenario was associated with a more ordered structural state of the Si-doped series. As a result, comparison with the sources confirmed that for Ti-based MAX phases, the decisive factor is not the increase in a particular property, but the type of structural modification that simultaneously determines oxidative stability, conductivity, and behaviour under friction conditions. That is why the compositional scenario in which doping did not destroy the MAX framework, but provided its controlled modification while maintained a complete microstructural organisation remained the most promising.

Conclusions

As part of the study, it was found that doping of Ti-based MAX phases with various X elements determines not isolated changes in individual parameters, but integral scenarios of phase-microstructural evolution, which directly form the mechanical, thermophysical and tribological characteristics of the material. X-ray phase analysis showed that the baseline series retains the dominance of Ti_3AlC_2 at 87%, while Fe doping reduces its proportion to 62% and is accompanied by increased carbidisation (TiC – 28%) and the appearance of Fe_3Al (7%), which corresponds to the scenario of the deepest phase destabilisation. Si doping, on the contrary, forms a milder type of phase modification: the proportion of Ti_3AlC_2 remains at 74%, TiC is 12%, and the appearance of Ti_5Si_3 (11%) does not put the system in the dominant carbide formation mode. Microstructural analysis confirmed that the base series is characterised by the most ordered lamellar organisation with clear interfacial boundaries and an average grain size of 8.3 μm, while Fe doping is accompanied by the most pronounced morphological destabilisation, grain grinding up to 5.7 μm, heterogeneous distribution of secondary phases, and partial blurring of boundaries.

In the Si-doped series, the lamellar architecture is preserved with intergranular intermetallic modification and an intermediate average grain size of 6.9 μm, which indicates a restriction of grain growth without deep destruction of the structural framework. The mechanical unit of the study showed that Fe doping provides a maximum microhardness of 5.1 GPa, but is also accompanied by a decrease in the elastic modulus to 191 GPa and density to 4.17 g/cm^3, that is, local hardening is implemented against the background of general structural destabilisation. Si doping forms a different type of mechanical response: with a moderate microhardness of 4.2 GPa, it provides maximum values of the elastic modulus of 214 GPa and a density of 4.44 g/cm^3, which indicates a more favourable combination of rigidity and compaction. Thermophysical and functional analysis showed that the Fe-doped series has the least favourable profile: the conductivity decreases to 2.1×10^4 S/m, the coefficient of linear thermal expansion increases to 9.7×10^{-6} 1/°C, and the mass loss by TGA reaches 8.6%, which indicates the lowest oxidative heat resistance. Si doping, on the contrary, provides the most stable functional state: the electrical conductivity is 3.2×10^4 S/m, the coefficient of linear thermal expansion was reduced to 7.5×10^{-6} 1/°C, and the mass loss by TGA was limited to 3.4%, which corresponds to the best resistance to oxidative degradation. Tribological tests in the dry friction mode confirmed that wear resistance is determined not by the hardness level itself, but by the aggregate structural organisation of the material: the Fe-doped series, despite the highest microhardness, showed the greatest mass loss of 8.6%, maximum wear of 0.61 C.U. and the highest coefficient of friction – 0.67, while the Si-doped series showed a minimum mass loss of 3.4%, wear of 0.28 C.U., and the coefficient of friction – 0.47.

Thus, the results proved that the least favourable scenario for Ti-based MAX phases is associated with Fe doping, which enhances the carbide-intermetallic rearrangement, destabilises the lamellar architecture, and degrades the complex of mechanical, thermophysical, and tribological characteristics. The most balanced structural and functional profile is formed by Si doping, which provides partial preservation of Ti_3AlC_2, more ordered intergranular organisation, high rigidity, better oxidative heat resistance, and the highest wear resistance. Thus, the key factor in the operational efficiency of Ti-based MAX phases was not the maximum increase in a particular property, but the type of microstructural adjustment that determines whether the integrity of the layered MAX frame is preserved under mechanical, thermal and tribological loads.

Further research should be aimed at expanding a number of doping X-elements, varying their concentrations, clarifying the mechanisms of intergranular stabilisation, and checking the behaviour of Ti-based MAX phases in more complex modes of thermocyclic and tribocorrosive loading, characteristic of drilling and hydrocarbon production conditions.

Acknowledgements

None.

Funding

None.

Conflict of Interest

None.

References

[1] Adjamskiy, S., Kononenko, G., Podolskyi, R., & Baduk, S. (2022). Studying the influence of orientation and layer thickness on the physico-mechanical properties of Co-Cr-Mo alloy manufactured by the SLM method. *Science and Innovation*, 18(5), 85-94. doi: 10.15407/scine18.05.085.

[2] Aghajanyan, N.N., Dolukhanyan, S.K., Ter-Galstyan, O.P., Muradyan, G.N., & Hovhannisyan, A.A. (2023). Self-propagating high-temperature synthesis of MAX phases in Ti-Zr-Al-C system (C: P15). *Ceramics International*, 49(14), 24165-24170. doi: 10.1016/j.ceramint.2022.11.041.

[3] Aydinyan, S. (2023). Combustion synthesis of MAX phases: Microstructure and properties inherited from the processing pathway. *Crystals*, 13(7), article number 1143. doi: 10.3390/cryst13071143.

[4] Badie, S., Sebold, D., Vaßen, R., Guillon, O., & Gonzalez-Julian, J. (2021). Mechanism for breakaway oxidation of the Ti_2AlC MAX phase. *Acta Materialia*, 215, article number 117025. doi: 10.1016/j.actamat.2021.117025.

[5] Baklanov, V., Zhanbolatova, G., Skakov, M., Miniyazov, A., Sokolov, I., Tulenbergenov, T., Kozhakhmetov, Y., Bukina, O., & Orazgaliev, N. (2022). Study of the temperature dependence of a carbidized layer formation on the tungsten surface under plasma irradiation. *Materials Research Express*, 9(1), article number 016403. doi: 10.1088/2053-1591/ac4626.

[6] Berrabah, M., Cabioc'h, T., Brunet, V.G., Chartier, P., Epifano, E., & Dubois, S. (2025). Synthesis, microstructural characterization and transport properties of a new $(Ti_2Nb)AlC_2$ ternary nanolaminate carbide solid solution. *Journal of the European Ceramic Society*, 46(3), article number 117894. doi: 10.1016/j.jeurceramsoc.2025.117894.

[7] Cai, L., Li, J., Luo, B., Yang, J., He, N., & Jia, J. (2024). Self-lubricating effect of solid solution elements on tribological performance of Ti_3AlC_2 over a wide temperature range. *Journal of the American Ceramic Society*, 107(5), 3103-3116. doi: 10.1111/jace.19662.

[8] Cao, L., Zhang, Q., Du, L., Fu, S., Wan, D., Bao, Y., Feng, Q., & Hu, C. (2024). Synthesis and characterization of high entropy $(TiVNbTaM)_2AlC$ (M=Zr, Hf) ceramics. *Journal of Advanced Ceramics*, 13(2), 237-246. doi: 10.26599/JAC.2024.9220847.

[9] Deng, A., Niu, Y., Zhang, B., Lin, N., Ma, C., Huang, Z., & Yin, J. (2025). Synthesis, microstructure and mechanical properties of M_2AlC-MC (M = Ti, Ta, Nb) composite. *Journal of Alloys and Compounds*, 1014, article number 178745. doi: 10.1016/j.jallcom.2025.178745.

[10] Desai, V., Badheka, V., Zala, A., Parekh, T., & Jamnapara, N.I. (2025). Al7075/Ti_3AlC_2 MAX-phase surface composite generated by friction stir processing: Microstructure, microhardness, and tribological characteristics. *Tribology-Materials, Surfaces & Interfaces*, 19(4), 265-276. doi: 10.1177/17515831251358689.

[11] Gui, X., Sun, L., Chen, C., Yang, Y., Gao, W., Gyawali, G., Liu, X., Ding, J., & Zhang, S. (2025). Optimizing current-carrying tribological performance of Cu-Ti_2AlC coatings: Role of kerosene flow rate in HVOF spraying and wear mechanism analysis. *Tribology International*, 111377. doi: 10.1016/j.triboint.2025.111377.

[12] Hong, H., Yang, P., Gui, X., Yang, Y., Liu, X., Ding, J., Gyawali, G., Yang, K., & Zhang, S. (2025). Enhancing the durability of Ti-Al-C coatings: The role of powder composition and processing variables. *Journal of Materials Research and Technology*, 34, 2956-2963. doi: 10.1016/j.jmrt.2024.12.226.

[13] Hua, S.W., Pang, M., Chen, J., Zhao, J., & Ji, F.Q. (2023). Microstructure and tribological performance of laser cladding Ti_2AlC particle reinforced coatings on Ti6Al4V. *Journal of Materials Engineering and Performance*, 32(18), 8452-8466. doi: 10.1007/s11665-022-07714-3.

[14] Kvasnytskyi, V., Korzhyk, V., Kvasnytskyi, V., Mialnitsa, H., Dong, C., Pryadko, T., Kurdyumov, G.V., Matviienko, M., & Buturlia, Y. (2020). Designing brazing filler metal for heat-resistant alloys based on NI3AL intermetallide. *Eastern-European Journal of Enterprise Technologies*, 6(12), 6-19. doi: 10.15587/1729-4061.2020.217819.

[15] Laska, N., Swadźba, R., Nellessen, P., Helle, O., & Anton, R. (2024). Oxidation behavior of Ti_2AlC MAX phase-based coating on a γ-TiAl alloy TiAl48-2-2 produced by DC magnetron sputtering. *Surface and Coatings Technology*, 480, article number 130601. doi: 10.1016/j.surfcoat.2024.130601.

[16] Li, M., Wei, D., Gong, M.F., Guo, Z.Y., Mo, D.Y., & Wu, W.G. (2026). Effect of Ti_3AlC_2 as an additive on the mechanical and tribological properties of WC-Co cemented carbide. *Strength of Materials*, 57, 1260-1271. doi: 10.1007/s11223-026-00855-z.

[17] Liu, B., Zhang, C., Su, Y.F., Tang, P., Kuang, T.C., Lin, S.S., & Shi, Q. (2026). In situ induced Ti-C composite interlayer for enhanced corrosion resistance and electrical conductivity in a-C: Ti films on SS316L bipolar plates. *SSRN*. doi: 10.2139/ssrn.6017176.

[18] Lu, Y., Peng, Y., Chang, X., & Kong, D. (2024). Ti_2AlC and Ti_3AlC_2 reinforced CoNi coatings by laser cladding: Nanostructures, tribological properties and density functional theory calculations. *Journal of Manufacturing Processes*, 131, 736-749. doi: 10.1016/j.jmapro.2024.09.031.

[19] Ma, T., Li, Q., Wang, Y., Wang, X., Dong, D., & Zhu, D. (2022). Microstructure and mechanical properties of micro-nano Ti_2AlC-reinforced TiAl composites. *Intermetallics*, 146, article number 107563. doi: 10.1016/j.intermet.2022.107563.

[20] Malecha, D., Zubko, M., Żabiński, P., & Małecki, S. (2025). Analysis of the lead refining method using aluminium. *Metallurgical and Materials Transactions A: Physical Metallurgy and Materials Science*, 56(8), 2957-2975. doi: 10.1007/s11661-025-07813-5.

[21] Mandegari, M., Nasouri, K., & Ghasemi-Mobarakeh, L. (2023). Synthesis of low-cost Ti_3AlC_2-Ti_2AlC dual MAX phase with high-electrical conductivity using economical raw materials and novel compositions. *Materials Today Communications*, 36, article number 106868. doi: 10.1016/j.mtcomm.2023.106868.

[22] Maziarz, W., Wójcik, A., Chulist, R., Bigos, A., Kurtyka, P., Szymański, Ł., Jimenez Zabaleta, A., García de Cortázar, M., & Olejnik, E. (2024). Microstructure and mechanical properties of Al/TiC and Al/(Ti,W)C nanocomposites fabricated via in situ casting method. *Journal of Materials Research and Technology*, 28, 1852-1863. doi: 10.1016/j.jmrt.2023.12.126.

[23] Mukhamedova, N., Kozhakhmetov, Y., Skakov, M., Kurbanbekov, S., & Mukhamedov, N. (2022). Microstructural stability of a two-phase (O + B2) alloy of the Ti-25Al-25Nb system (at.%) during thermal cycling in a hydrogen atmosphere. *AIMS Materials Science*, 9(2), 270-282. doi: 10.3934/MATERSCI.2022016.

[24] Muradyan, G.N., Dolukhanyan, S.K., Aleksanyan, A.G., Ter-Galstyan, O.P., Mnatsakanyan, N.L., Asatryan, K.V., Mardanyan, S.S., & Hovhannisyan, A.A. (2023). Synthesis in hydride cycle of Ti-Al-C based MAX phases from mixtures of titanium carbohydrides and aluminium powders. *Ceramics International*, 49(14), 24171-24178. doi: 10.1016/j.ceramint.2022.11.125.

[25] Nedeva, D. (2025). Preparation, properties, and application of titanium carbide coatings. *Zeitschrift für Naturforschung A*, 80(10), 993-1008. doi: 10.1515/zna-2025-0152.

[26] Potoczek, M., Dąbek, J., & Brylewski, T. (2023). Oxidation behavior of Ti_2AlC MAX-phase foams in the temperature range of 600-1000°C. *Journal of Thermal Analysis and Calorimetry*, 148(10), 4119-4127. doi: 10.1007/s10973-023-11990-z.

[27] Ratov, B.T., *et al*. (2023). Features structure of the $C_{diamond}$-(WC-Co)-ZrO_2 composite fracture surface as a result of impact loading. *Journal of Superhard Materials*, 45(5), 348-359. doi: 10.3103/S1063457623050088.

[28] Shahbaz, M., Sabir, N., Amin, N., Zulfiqar, Z., & Zahid, M. (2024). Synthesis and characterization of chromium aluminium carbide MAX phases (CrxAlCx-1) for potential biomedical applications. *Frontiers in Chemistry*, 12, article number 1413253. doi: 10.3389/fchem.2024.1413253.

[29] Shevko, V.M., Karataeva, G.E., Badikova, A.D., Tuleev, M.A., & Uteeva, R.A. (2020). Comprehensive processing of basalt together with magnetite concentrate in order to obtain ferrous alloy and calcium carbide. *Archives of Foundry Engineering*, 20(4), 41-54. doi: 10.24425/afe.2020.133346.

[30] Sun, H., Song, B., Sun, X., Cui, X., Liu, Z., Cong, M., & Wang, L. (2025). Recent representative progress of surface coating technology. *The Chemical Record*, 25(8), article number e202500054. doi: 10.1002/tcr.202500054.

[31] Wu, H., Xiao, H., Chen, N., Chu, M., Lin, B., Zhang, Z., Fu, G., & Mo, T. (2025). Effect of Nb content on the tribological properties of laser-cladded Ti-Al-C MAX phase composite coatings. *Tribology International*, 204, article number 110426. doi: 10.1016/j.triboint.2024.110426.

[32] Xu, Y., Ma, G., Li, Z., Zhang, Y., Zhang, A., Wang, Z., & Wang, A. (2025). Valence-dependent TiO_2 inhibition for enhancing oxidation resistance in Ti_2AlC via Zr/Nb solid solution. *Corrosion Science*, 257, article number 113351. doi: 10.1016/j.corsci.2025.113351.

[33] Yuan, Z., Liu, H., Ma, Z., Ma, X., Wang, K., & Zhang, X. (2022). Microstructure and properties of high entropy alloy reinforced titanium matrix composites. *Materials Characterization*, 187, article number 111856. doi: 10.1016/j.matchar.2022.111856.

[34] Zeng, X., Xiong, Y., Liu, Z., Tong, X., Hu, C., Bian, J., Cao, Q., & Cheng, X. (2022). Preparation and characterization of self-lubricating CaF_2@ZrO_2/YSZ composite coating. *Journal of Thermal Spray Technology*, 31(7), 2126-2135. doi: 10.1007/s11666-022-01424-x.

[35] Zhang, A., Wang, K., Zhang, Y., Ma, G., Yang, W., Zhou, G., Ke, P., & Wang, A. (2024). Towards developing Ti_2AlC coatings with improved oxidation resistance via Nb solid solution. *Journal of Alloys and Compounds*, 1002, article number 175524. doi: 10.1016/j.jallcom.2024.175524.

[36] Zhou, S., Xiang, H., Fang, C., Xu, W., Sun, K., & Zhou, Y. (2026). Ultrasonic-assisted hot-press sintering of Cu-Ti_3AlC_2 composites. *Npj Advanced Manufacturing*, 3(1), article number 7. doi: 10.1038/s44334-026-00067-y.

[37] Zhou, Y., Wang, Z., Zhao, J., & Jiang, F. (2023). Effect of ultrasonic amplitude on interfacial characteristics and mechanical properties of Ti/Al laminated metal composites fabricated by ultrasonic additive manufacturing. *Additive Manufacturing*, 74, article number 103725. doi: 10.1016/j.addma.2023.103725.

Еволюція мікроструктури та зносостійкість фаз МАХ на основі титану, легованих елементами Х, для застосування у бурінні та видобутку вуглеводнів

Маріне Сасунцян

Кандидат технічних наук, доцент
Національний політехнічний університет Вірменії
0009, вул. Терян, 105, м. Єреван, Вірменія
https://orcid.org/0009-0000-6769-114X

Ніна Саакян

Кандидат технічних наук
Національний політехнічний університет Вірменії
0009, вул. Терян, 105, м. Єреван, Вірменія
https://orcid.org/0009-0007-6511-7129

Сероб Айрапетян

Кандидат технічних наук, науковий співробітник
Національний політехнічний університет Вірменії
0009, вул. Терян, 105, м. Єреван, Вірменія
https://orcid.org/0009-0008-4576-2371

Сурен Агбалян

Аспірант
Національний політехнічний університет Вірменії
0009, вул. Терян, 105, м. Єреван, Вірменія
https://orcid.org/0000-0001-9987-8515

Анотація. Метою дослідження було з'ясувати, як легування різними елементами групи Х впливає на еволюцію мікроструктури сплавів на основі титану з фазою МАХ, а також як ці зміни позначаються на твердості, теплофізичних та трибологічних властивостях. Методологія передбачала отримання базової та легованої серій сплавів Ti-Al-C та їх дослідження методами рентгенофазового аналізу, скануючої електронної мікроскопії, енергодисперсійного аналізу, цифрової морфометрії, мікроіндентації, резонансного визначення модуля пружності, дилатометрії, термогравіметричного аналізу, трибологічних випробувань та статистичної обробки даних. У результаті встановлено, що базова серія зберігає домінування Ti_3AlC_2 на рівні 87 % і характеризується найбільш впорядкованою пластинчастою мікроструктурою із середнім розміром зерен 8,3 мкм. Легування залізом зменшує частку Ti_3AlC_2 до 62 %, збільшує вміст TiC до 28 % і супроводжується появою Fe_3Al, подрібненням зерен до 5,7 мкм, порушенням пластинчастої архітектури та розвитком гетерогенного карбідно-інтерметалічного ансамблю. Це забезпечує максимальну мікротвердість 5,1 ГПа, але одночасно призводить до зниження модуля пружності до 191 ГПа, щільності до 4,17 г/см³, електропровідності до $2{,}1\times10^4$ См/м, збільшення коефіцієнта лінійного теплового розширення до $9{,}7\times10^{-6}$ 1/°C, втрати маси за результатами термогравіметричного аналізу до 8,6 % та найгірші трибологічні показники. Легування кремнієм зберігає вміст Ti_3AlC_2 на рівні 74 %, супроводжується утворенням Ti_5Si_3, сприяє формуванню більш впорядкованої міжзернової структури із середнім розміром зерен 6,9 мкм та забезпечує найбільш збалансований комплекс властивостей: мікротвердість 4,2 ГПа, модуль пружності 214 ГПа, щільність 4,44 г/см³, електрична провідність $3{,}2\times10^4$ См/м, коефіцієнт лінійного теплового розширення $7{,}5\times10^{-6}$ 1/°C, втрата маси за результатами термогравіметричного аналізу – 3,4 %, втрата маси при терті – 3,4 %, знос – 0,28 о.з., а коефіцієнт тертя – 0,47. Практичне значення отриманих результатів полягає у можливості їх використання при розробці та підборі зносостійких МАХ-матеріалів на основі титану та покриттів для бурового та нафтогазовидобувного обладнання

Ключові слова: розробка карбідів; трибологічні властивості; розмір зерен; модуль пружності; теплопровідність; твердість

ISSN 1993-9973, e-ISSN 2415-332X

Vol. 26, No. 1
2026

PROSPECTING AND DEVELOPMENT OF OIL AND GAS FIELDS

https://pdogf.com.ua/en

Received: 21.01.2026. Revised: 31.03.2026. Accepted: 29.05.2026. Published: 29.06.2026.

UDC 622.276, 622.279

DOI: 10.63341/pdogf/1.2026.56

Application of electric submersible pumps for post-fracturing gas well clean-up in depleted reservoirs

Lesia Moroz*

PhD in Technical Sciences, Associate Professor
Ivano-Frankivsk National Technical University of Oil and Gas
76019, 15 Karpatska Str., Ivano-Frankivsk, Ukraine
https://orcid.org/0000-0002-5183-4940

Yehor Selinny

Postgraduate Student
Ivano-Frankivsk National Technical University of Oil and Gas
76019, 15 Karpatska Str., Ivano-Frankivsk, Ukraine
https://orcid.org/0009-0002-7376-6050

Abstract. Given the long-term operation and depletion of most Ukrainian fields, the development of effective methods to restore their productivity is a priority for Ukraine's energy sector. This study focused on optimising the clean-up process of wells with abnormally low reservoir pressure after stimulation by hydraulic fracturing. The aim of the study was to introduce a technology for the successful extraction of fracturing fluid, which would significantly expand the criteria for well selection and enable the successful execution of hydraulic fracturing operations during the final stage of gas field development. The three alternative mechanised development technologies (electrical submersible pumps deployed on coiled tubing, cable, or jointed tubing) were compared through a theoretical techno-economic analysis to select the optimal method, considering the current state of Ukraine's gas production industry. The study was based on engineering calculations, nodal analysis, and hydrostatic imbalance evaluation for a typical deep well with depleted reservoir pressure (4,150 metres, 6.0 MPa). Hydrostatic imbalance calculations for the hypothetical well revealed a critical overbalance on the reservoir, which rendered development impossible without artificial lift. The hydrostatic pressure of the fluid column significantly exceeded the reservoir pressure, causing fluid fallback and subsequent fracture damage due to colmatation. Based on theoretical data, a comparative analysis of these technologies established that the rigless pump-on-cable option was technically unsuitable for depths exceeding 3,000 metres, whilst coiled-tubing deployment was economically unviable if a workover rig was already installed at the wellhead. The installation of an electrical submersible pump on jointed production tubing proved to be a pragmatic and economically sound solution. The parameters of the required assembly were calculated, and the complete cycle from the hydraulic fracturing stage to bringing the well on stream was modelled. A pragmatic approach was proposed that allowed the extraction of the fracturing fluid without overbalancing the reservoir, using available resources with minimal additional costs, which was critical for the cost-effectiveness of stimulation operations on depleted reservoirs

Keywords: reservoir; stimulation; flow rate; fracture; production; workover; coiled tubing

Introduction

The vast majority of gas and gas-condensate fields, particularly within the Dnieper-Donets Basin (DDB), are characterised by depleted reservoirs and significant colmatation of the near-wellbore zone in wells. This problem is one of the key issues, as it leads to a decrease in flow rates and well shut-ins. In conditions where drilling new wells becomes highly risky, and in some cases unprofitable, stimulation technologies are implemented to maintain production

Suggested Citation: Moroz, L., & Selinny, Ye. (2026). Application of electric submersible pumps for post-fracturing gas well clean-up in depleted reservoirs. *Prospecting and Development of Oil and Gas Fields*, 26(1), 56-64. doi: 10.63341/pdogf/1.2026.56.

*Corresponding author (*lesia.moroz@nung.edu.ua*)

from the existing well stock. Improving existing and implementing new gas and condensate production technologies is a priority task for the industry, particularly through the improvement of hydraulic fracturing (HF) technology, which has been actively implemented in Ukrainian fields for over 20 years.

In their abstracts, researchers I.I. Lartseva *et al*. (2025) reported on the current state of development of the largest deposits in Ukraine and characterised them as "depleted". The experience of conducting HF was described, concluding that the implementation of HF technology could be a key step in extracting Ukraine's oil and gas resources and contributing to its energy stability. In their research, A.V. Shcherbyna (2024) demonstrates that the implementation of a complex of well interventions, particularly HF and additional perforation, had a significant impact on well productivity. The author also notes that the main driver for increasing production rates is conducting HF on new wells and the existing well stock, which confirms the expediency of applying HF to enhance production and stabilise development rates.

The article by Yu.V. Lazebna *et al*. (2022) examines the exploration prospects and development challenges of tight gas reservoirs in the DDB. The authors analysed the geological parameters of the Paleozoic complex (structure, degree of catagenesis, organic carbon content, reservoir properties, and burial depths) and concluded that there is a high probability of gas presence in basin-centred reservoirs. At the same time, it is emphasised that such deposits are hard-to-recover due to the low porosity and permeability of the rocks; therefore, their development is impossible without applying stimulation methods. Among modern technologies, HF is highlighted as the most optimal stimulation method for this task. According to the authors, the use of foam fracturing technology can serve as a starting point for the active development of hard-to-recover tight gas reserves, particularly from basin-centred reservoirs.

According to researchers I. Kuper *et al*. (2025), the main problem for well productivity is the presence of the skin effect. The paper analyses how restrictions in the near-wellbore zone affect well performance and presents the modelling of the pumping technology itself, which minimises the negative impact on the near-wellbore zone. The proper selection of fracturing fluid, proppants, and control of fracture geometry through the modelling of pumping parameters allow for the complete elimination of near-wellbore flow capacity restrictions accumulated over years of production. B. Chen *et al*. (2022) emphasised that HF is critically important for oil and gas production from low-permeability reservoirs. The study analyses modern methods of modelling HF technology, describes the physical processes occurring during HF, and presents the capabilities of modern software. One of the problems arising during the pumping process is described as fluid leak-off into the formation, which leads to dynamic changes in fracture geometry and complicates the HF operation. However, for reservoirs with reduced formation pressure, there is an additional problem, namely fluid flowback to the surface after fracture propping.

In their work, researchers V.S. Biletskyi *et al*. (2025) described modern stimulation methods, including a characterisation of the HF process. The paper describes modern development trends in HF technology aimed at improving modelling and pumping process monitoring technologies, while also highlighting the focus on developing and applying environmentally safe fluids. In the article by A. Abdelaziz *et al*. (2023), a study was conducted and a digital model of fracture propagation during HF was created. Based on data obtained from laboratory experiments, it was established that under real conditions, fractures propagate chaotically, forming complex channel networks that are both induced by pumping and act as extensions of pre-existing faults within the reservoir. Researchers L.B. Moroz *et al*. (2023b) established the impact of polymer concentration in the working fluid on fracture dimensions and conductivity during HF. For all fluid types used in the modelling, an increase in polymer concentration led to an increase in the primary geometric parameters, such as fracture width and height, and a decrease in its length.

The analysed studies cover a wide range of aspects associated with HF stimulation technology. The articles describe the expediency of implementing HF in Ukrainian fields and confirm the high potential for increasing production from gas and gas-condensate reservoirs at the late-life stage of development. Existing research broadly covers the specific challenges of executing high-quality HF operations and shows ways to improve this technology. However, available studies do not sufficiently focus on the recovery of residual technological fluid from the reservoir after fracture propping. It is at this stage that a fundamental technological problem arises: the reservoir energy of a depleted reservoir is insufficient to autonomously lift the HF fluid to the surface. Standard practice in such cases is well clean-up using a coiled tubing unit (CTU) with the injection of an inert gas (nitrogen) below the fluid level to aerate the fluid column. However, as global practice shows, under conditions of severe reservoir depletion, when the hydrostatic pressure of the fluid column significantly exceeds the formation pressure, this technology becomes ineffective. The objective of this study was to conduct a techno-economic analysis of existing artificial lift technologies for well fluid extraction to determine the feasibility and possibility of their further use during the clean-up of wells stimulated by HF.

Materials and Methods

The study was conducted using engineering modelling and techno-economic analysis based on the methodology outlined by S.V. Matkivskyi & L.I. Khaydarova (2021), since it calculated the impact of electrical submersible pump (ESP) parameters on the production characteristics of water-loaded gas wells and proved that at high water-gas ratios, an ESP can operate stably and assist in lifting liquid to the surface. The selection of this methodology for investigating novel ways of recovering technological fluid after HF is justified, as the processes of recovering formation fluid and residual fracturing fluid are quite similar, despite their fundamentally different origins. A prolonged period usually elapses between the HF operation and the start of well clean-up, which includes a technological shut-in for gel breaking, as well as a period of operations for packer retrieval, tubing string replacement, and workover rig dismantling, which in total can take up to 1 month. During the final well preparation period, the pumped fluid is evenly distributed within the well drainage zone, which provides grounds for equating the reservoir conditions in this case to those of a naturally water-loaded gas well. A typical deep gas well from one of the depleted DDB fields (synthetic well No. 202), which is a candidate for HF, was selected as the base object (Table 1).

Table 1. Initial parameters of the facility (reference well No. 202)

No.	Parameter	Value	Unit
1	Field name	Field 1	Name
2	Well No.	202	No.
3	HF intervals	4,120-4,140	m
4	Perforator type and shot density	ZPK-62m; 18 hol./m.	
5	Formation pressure	60	atm
6	Reservoir temperature	103	°C
7	Porosity	14	%
8	Permeability	0.15	mD
9	Formation fluid viscosity (in-situ)	0.015055	mPa·s
10	Gas formation volume factor	0.010287	m^3/m^3
11	Saturation pressure	280	atm
12	Gas compressibility factor (Z)	0.8917	
13	Production casing	168	mm
14	Production casing wall thickness	12	mm

Source: created by the authors

Based on the experience of conducting HF operations in analogous horizons, the design parameters of the HF operation necessary for further calculations on the research topic were adopted using the methodology of L. Moroz *et al*. (2023a). Before starting the HF operation, a packer assembly is run on a work string; therefore, kill fluid remains in the wellbore. The wellbore volume must be taken into account, as to initiate the fracture and create a "pad", it is necessary to displace the kill fluid with the fracturing fluid, which is accompanied by forcing the former into the productive horizon. The total fluid volume, including the volume of the kill fluid used during the workover in the well preparation process, is 240 m^3. Another important parameter for conducting justified calculations is the average density of the fluid pumped into the formation during the HF process; a value of 1,030 kg/m^3 was adopted. For the modelling and theoretical substantiation of the study, Schlumberger (n.d.b) software was used. The capabilities of this software suite, highlighted on the company's official resource, allowed for the full execution of the entire cycle of calculations necessary to substantiate the method proposed in the study, without the use of additional tools. The formulas used for the calculations in this work are presented below.

Hydrostatic pressure of the fluid column on the formation:

$$P_g = \rho \times g \times H, \tag{1}$$

where P_g is the hydrostatic pressure of the fluid column on the formation; ρ is the fluid density; g is the acceleration due to gravity; H is the depth to the middle of the perforation interval (under conditions where the gas-producing part of the formation is not determined, the middle of the perforation interval is assumed).

Excessive overbalance in a fluid-filled well:

$$P_e = P_g - P_r, \tag{2}$$

where P_e is the excessive overbalance on the formation; P_r is the measured formation pressure before the start of operations.

Dynamic fluid level:

$$h_d = H - \frac{P_{bh}}{\rho_l \times g}, \tag{3}$$

where P_{bh} is the bottom-hole pressure; ρ_l is the fluid density.

Pump system head:

$$H_p = h'_d + h_2 + h_f - h_g, \tag{4}$$

where H_p is the head; h'_d is the distance from the wellhead to the dynamic fluid level; h_2 is the required head at the wellhead (assuming Pm = 0.5 MPa backpressure on the gathering line $h_2 = 50$ m); h_f represents friction head losses during fluid flow in the tubing of length L; h_g is the fluid lift height in the tubing due to gas energy ($h_g = 0$ since fluid without gas is pumped at the first stage).

Motor shaft power:

$$N = (Q \times \rho \times g \times H_p)/\eta, \tag{5}$$

where N is the motor shaft power; Q is the fluid flow rate; η is the system efficiency.

Results and Discussion

The key factor that precludes well clean-up is the hydrostatic imbalance between the formation pressure and the pressure of the fluid column in the well before the start of clean-up operations. First, the pressure of the HF fluid column on the formation was calculated. In conditions where no surveys were conducted during the well's operation to determine the exact part of the formation directly producing gas, the midpoint of the perforation interval is assumed in the calculations to minimise the margin of error. For the well under consideration, $H = 4{,}130$ m:

$$P_g = 1{,}030 \times 9.81 \times 4{,}130 = 41.6 \text{ MPa}.$$

Thus, knowing the formation pressure measured before the start of operations, the excessive overbalance applied to the formation with the well filled to the wellhead with kill fluid was determined:

$$P_e = 41.6 - 6.0 = 35.6 \text{ MPa}.$$

As a result, a significantly high value of excessive overbalance on the formation was obtained. This indicates that standard fluid recovery methods, such as well clean-up using compressor equipment or a CTU to inject inert gas below the fluid level, are unsuitable for the conditions of this well. To ensure the pumping of 25 m³/day of HF fluid and create sufficient drawdown on the formation, a standard ESP assembly (size 3 or 4) run on a 73 mm (2 7/8") tubing string is used. The first stage in designing the ESP installation is determining the setting depth and the dynamic fluid level that must be maintained to cool the motor. To create a drawdown on the formation (with $P_r = 6.0$ MPa), the dynamic fluid level in the well must be lowered to a value corresponding to a pressure below the formation pressure. $P_{bh} = 5.8$ MPa is assumed (a drawdown of 0.2 MPa). The required dynamic fluid level from the wellhead is:

$$h_d = 4{,}130 - \frac{5.8 \times 10^6}{1{,}030 \times 9.81} = 3{,}555 \text{ m}.$$

According to the technological solutions for the installation of ESP described by M.A. AL-Hejjaj *et al*. (2023), the pump setting depth must ensure sufficient submergence below the fluid level to create sufficient intake pressure for the motor (≈5-10 atm). Thus, the adopted ESP setting depth is $L_p = 3{,}650$ m. This provides 95 m of submergence at the pump intake at the initial stage, and as the fluid in the wellbore gradually changes into a gas-liquid mixture, it will provide a power reserve at the final stage of well clean-up. To subsequently determine the rated motor power of the ESP assembly, the required head was calculated using formula (4) for determining the well's theoretical system curve. The friction head losses in a 73 × 62 mm tubing string ($d_{in} = 0.062$ m) with a length of 3,650 m at a flow rate of $Q = 25$ m³/day will be approximately 150 m. The total required head is:

$$H_p = 3{,}555 + 50 + 150 = 3{,}755 \text{ m}.$$

Motor shaft power:

$$\text{N} = \frac{(0.00029 \times 1{,}030 \times 9.81 \times 3{,}755)}{0.4} = 27{,}507 \text{ W} = 27.5 \text{ KW}.$$

Based on the performed calculations, the clean-up of well No. 202 requires a standard size 3 (Ø 3.38") ESP assembly capable of generating a head of ~3,800 m at a flow rate of 25 m³/day. To select the ESP for fluid recovery, the built-in "ESP design" function was used, which allows for the automatic selection of the optimal system considering the specified wellbore conditions. Based on the well model parameters, the REDA MT2A-30 ESP system was selected, which, operating at 53% of its rated load, ensures the pumping of 25 m³/day of HF fluid from the formation (Fig. 1).

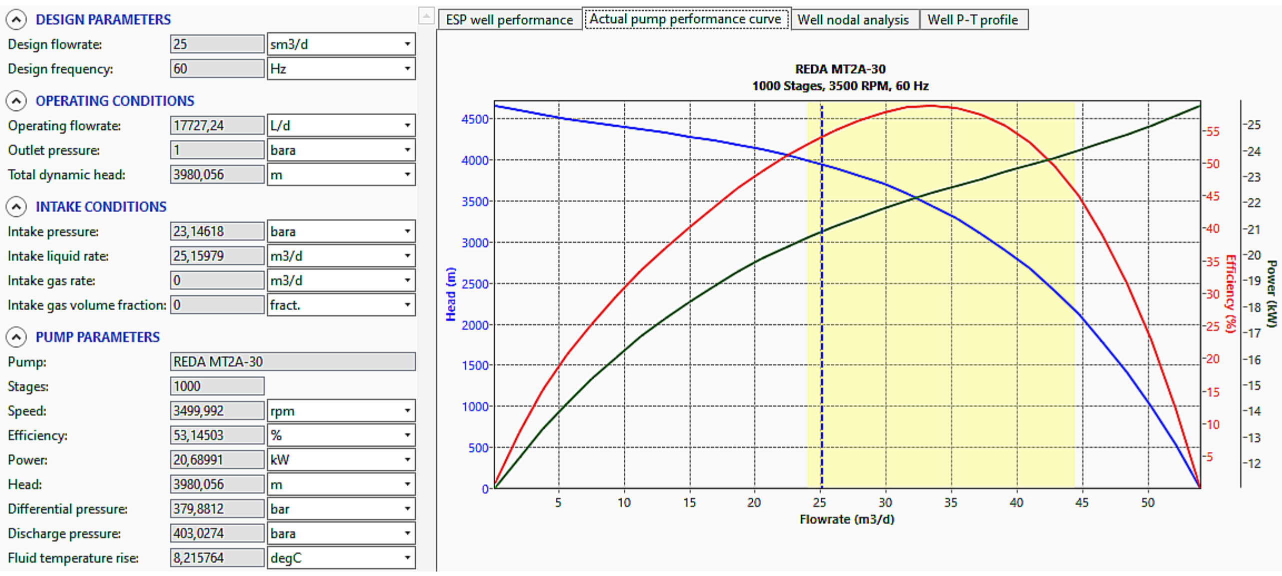

Figure 1. Pump performance curve of the REDA MT2A-30 ESP

Source: created by the authors

To validate the research findings, a model of well No. 202 was developed with an ESP installed on a jointed tubing string with a nominal diameter of 73 mm; the formation properties were specified, along with the condition that 240 m³ of HF fluid was pumped into the near-wellbore zone (Fig. 2).

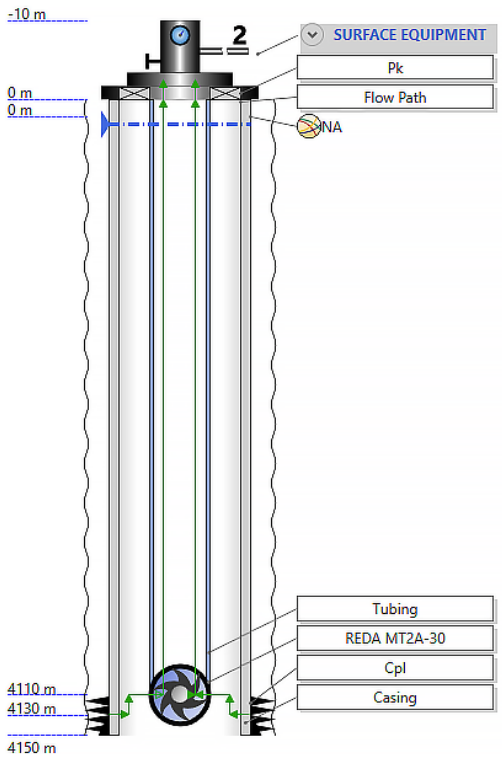

Figure 2. Conceptual well model

Source: created by the authors

Given that the HF was performed in a gas-bearing formation, the fluid will gradually become saturated with gas during the recovery process. It is necessary to verify whether the selected pump can continue to lift water as the gas-liquid ratio increases. Based on the sensitivity analysis conducted, it was determined that the pump can ensure stable fluid pumping even as the gas-liquid ratio in the production stream increases up to 400 cm³/cm³ (Fig. 3).

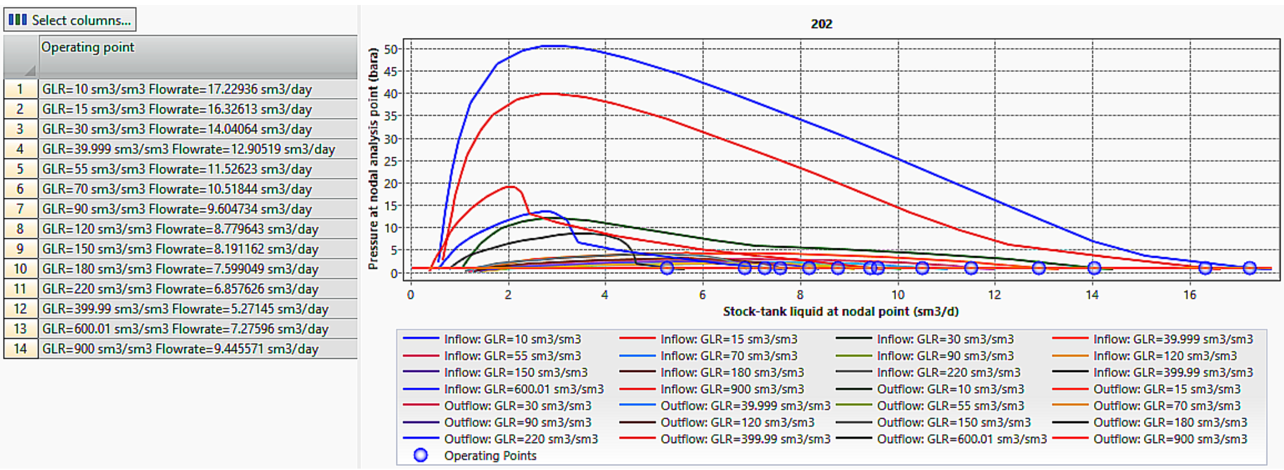

Figure 3. Sensitivity analysis of pump performance with increasing gas-liquid ratio

Source: created by the authors

Through simulation, it was determined that the REDA MT2A-30 ESP system, run on a tubing string with a nominal diameter of 73 mm, ensures the recovery of the fluid pumped during the HF operation. As the gas-liquid ratio increases, the liquid rate slightly decreases; however, the pump operation remains stable even at a gas-liquid ratio of 400 cm³/cm³. This will be sufficient for well clean-up, as under these parameters, after the pump is retrieved, the well will be capable of naturally unloading water and continuing to clean up during the production phase. This study has proven that the use of an ESP allows for well clean-up after HF if there is insufficient reservoir energy to lift the fluid. Therefore, the method of temporarily installing an ESP system on jointed tubing is a technically and economically justified solution.

Based on the selected technology, the complete well clean-up cycle is as follows: after performing the HF operation and isolating the pay zone by leaving a sand plug, a workover rig is used to replace the packer-tubing assembly utilised for the HF with a production tubing string equipped with an entry guide and an ESP assembly. Fluid recovery is conducted for approximately 10 days until gas breakthrough occurs and the pump operation becomes ineffective. After this, the well is killed to ensure safe tripping operations, and the ESP is retrieved. To bring the well on stream, a production tubing string with an entry guide is run in hole, and a standard clean-up is performed using compressor equipment or a CTU.

In their study, O.A. Pashchenko *et al*. (2024) proposed a comprehensive approach to calculating the operational parameters of HF, based on a combination of geomechanical rock properties, fluid and proppant properties, and injection rates. The authors developed a methodology for determining the breakdown pressure, fracture geometry, near-wellbore permeability, and the expected production gain following the HF operation. Special attention is given to optimising proppant selection depending on in-situ stress gradients, as well as to developing an automated algorithm for the rapid selection of pumping parameters. The proposed approach allows for enhancing operational efficiency and serves as a foundation for developing software tools for automated HF design in field conditions.

M. Zhulaj & O. Serbin (2024) analysed the advanced methods and approaches actively implemented by Ukrainian companies to enhance oil and gas production efficiency and secure Ukraine's energy independence. It was established that modern technologies, such as HF, can effectively increase production even in depleted reservoirs. Although the cost of applying these technologies is substantial, their payback period becomes significantly shorter amid rising energy prices. For example, fracturing operations can increase production volumes by 20-50%, allowing the costs to be recovered within a few years.

Studies by F. Jahn *et al*. (2026) confirm that in low-pressure reservoirs, the well clean-up technique involving fluid column aeration relies heavily on the assistance of reservoir energy. However, when reservoir energy is insufficient, this leads to fluid fallback into the perforation interval and inefficient solids cleanout. In the present case, where gel degradation residues are present in the wellbore and directly within the created fracture, the re-exposure of the highly permeable fracture to such fluid leads to its plugging. Furthermore, research by I. Kuper *et al*. (2025) indicates that the incomplete removal of fracturing fluid induces a skin effect and can reduce the initial gas rate by 40-60%.

To address the given objective, the industry's available artificial lift technologies, which could potentially be used for the recovery of residual post-frac fluid, were considered. One such advanced rigless ESP deployment technology reviewed is the system proposed by leading companies Schlumberger (n.d.a) and Baker Hughes (2021), which involves deploying an ESP on power-cable coiled tubing (CT) using a CTU. At first glance, the use of this technology appears optimal as an existing "off-the-shelf solution", but it has several drawbacks. The rental cost of the specialised CT-deployed ESP package is extremely high, and the 3.38" (85.8 mm) ESP assembly is designed to operate inside the production casing. Therefore, after fluid recovery, the well must be killed to install the production tubing string. This offsets the benefits of using a CTU and significantly complicates the operations.

It is also critical to consider the technical risks associated with CT operations. Specifically, deploying and operating an ESP imposes significantly higher mechanical loads on the CT string than standard interventions. As described by Vechietti *et al*. (2022), a CT string parted during retrieval, causing a well control incident. Regaining control required pumping a high-viscosity fluid to form a resin plug. In post-fracturing scenarios, where any fracture plugging is impermissible, such risks completely ruin the stimulation results.

Considering the drawbacks of using a CTU, the possibility of deploying an ESP assembly on a wireline is being considered. The existing technology, presented by J. Algerøy (2018), is primarily designed for rapid pump replacement in oil wells. It involves the prior deployment of a specialised tubing string equipped with a docking station. The ESP assembly itself (motor, protector, and pump) is run inside the tubing on a special load-bearing wireline. The main drawback of this technology, even if adapted for the current research objective, is the technical depth limitation. The maximum load the cable can withstand allows for ESP installation at depths of up to 3,000 meters, which is insufficient for wells developing gas reservoirs in the DDB.

In this case, the most promising approach for implementation is deploying the ESP on a tubing string. A method widely used in the oil industry that requires no additional technology implementation costs. This method involves using a standard ESP assembly as a temporary tool deployed by a workover rig. This approach is supported by case studies from A. Salah *et al*. (2025), where ESP installation was successfully used to lift gas-liquid streams. When compared to a gas lift system under standard operating conditions, the ESP efficiency was comparable; however, with an increasing water cut, the use of an ESP proved to be more effective. The primary advantage of applying this method to the study conditions is the low operational cost. ESP deployment does not require additional equipment or the involvement of expensive specialised packages demanded by the other described technologies. In most cases, during HF operations in Ukrainian fields M.A. Mysliuk & V.P. Kravets (2024), a workover rig is on standby on location. Furthermore, standard off-the-shelf ESPs are used, which are significantly cheaper than specialised slim-hole systems.

The obtained research result is validated by real-world challenges in global practice. In their study, A. Albahri *et* *al*. (2025) demonstrate that when applying the correct engineering approach to ESP optimisation, the system will operate continuously under high gas-water ratio conditions. The authors propose ESP design modifications and adjustments to mitigate the impact of phase separation as fluid passes through the pump stages. Additionally, one of the proposed solutions involves deploying the assembly below the perforation interval to reduce gas interference; however, for the given research conditions, specifically the significant well depth, implementing this approach will be problematic.

In global practice, deploying ESPs in high-GOR oil wells following HF is a widely adopted method. In their study, F. Leon *et al*. (2022) describe that when selecting the optimal pump stages, similar to the case of the current research, the ESP operates stably while lifting gas-liquid streams. One of their field trials involved installing an ESP in a fractured well, which demonstrated that the technology maintains high operational reliability even when subjected to abrasive proppant flowback.

However, the primary challenge of deploying ESPs to lift fluids with a high gas volume fraction remains the overheating of motor components. This issue is detailed by T. Chu *et al*. (2022) and aligns perfectly with the findings of the current study. Under conditions of a high gas fraction, ESP performance degrades, and motor cooling becomes insufficient. The researchers calculated that an increase in the free gas fraction to 40% results in a 50% drop in performance. They concluded that the ESP maintains stable operation at a gas ratio of up to 350 cm^3/cm^3, whereas at higher values, the motor rotational speed must be reduced to prevent overheating. These documented outcomes corroborate the modelling results obtained in this research.

An analysis of recent global studies confirms that deploying ESPs for gas well clean-up following HF presents no significant limitations in terms of equipment capabilities. While various case studies document ESP deployment for lifting gas-liquid streams to the surface, the specific scenario addressed by the proposed solution, characterised by a progressive increase in the gas-water ratio, has not been covered in existing literature. This validates the relevance of the research topic and highlights substantial potential for future studies. The availability of reliable post-fracturing clean-up technology, even under depleted reservoir pressure conditions, unlocks immense potential for applying stimulation methods in depleted Ukrainian fields. This, in turn, will ensure sustained gas production over the long term.

Conclusions

In order to resolve the issue of well clean-up under conditions of excessive overbalance, where conventional clean-up methods, such as direct air injection from the wellhead or using a CT unit to deliver inert gas to the bottomhole, result in the fluid column being forced back into the productive formation through the existing high-permeability fracture, thereby severely undermining the ultimate effectiveness of the stimulation, available global practices of artificial lift methods using ESP systems for fluid removal were reviewed. A comparative analysis of advanced technologies for temporary ESP deployment revealed substantial technological limitations and their impracticality for resolving the given objective. When deploying via CT, the well completion must be free of a production tubing string, as the outer dimensions of commercially available ESPs exceed the drift diameter of the production tubing. An additional risk in this scenario is CT parting during pump operation due to the extra loads exerted on it. Fishing the parted tubing would require killing the well, leading to deep colmatation (plugging) of the bottom-hole formation zone, which completely negates the stimulation effect. An alternative method, which eliminates ESP size constraints and reduces the risk of operational failures, involves deploying the pump on a wireline. In this setup, the pump requires a seating nipple on the tubing string, while both its installation and power supply are facilitated via the wireline cable. However, a major drawback that precludes the implementation of this method is the strict limitation on the ESP setting depth; the pump would be positioned significantly above the dynamic fluid level in the well, rendering its efficiency negligible under such conditions.

The proposed approach of deploying standard ESP systems which are widely used in oil production, on jointed production tubing eliminates the aforementioned drawbacks and can be implemented without additional capital expenditures. Particularly when operating in depleted reservoirs, the application of robust and relatively cost-effective solutions significantly enhances the economic viability of such projects. The results of calculations, software modelling, and the review of recent literature on the research topic demonstrate that the ESP deployment technique for recovering residual fracturing fluid despite presenting certain operational challenges, such as motor overheating and limitations when operating with high gas volume fractions, ultimately enables conducting stimulation operations in depleted reservoirs. If this technology is successfully implemented in the field, and fracturing candidate criteria are adjusted (specifically regarding current reservoir pressure), the number of stimulation jobs will increase. This will help maintain high gas production from existing wells. For further technology development, future research should focus on reducing the number of tripping operations during ESP deployment and retrieving the pump without killing the well.

Acknowledgements

None.

Funding

None.

Conflict of Interest

None.

References

[1] Abdelaziz, A., Ha, J., Li, M., Magsipoc, E., Sun, L., & Grasselli, G. (2023). Understanding hydraulic fracture mechanisms: From the laboratory to numerical modelling. *Advances in Geo-Energy Research*, 7(1), 66-68. doi: 10.46690/ager.2023.01.07.

[2] Albahri, A., Babiker, M.S., Aljaradi, A., Al-Harthi, A., Al Nabhani, S., & Al-Shandoudi, B. (2025). Optimizing ESP performance in high GVF wells: A case study. In *ADIPEC* (article number SPE-230173-MS). Abu Dhabi: ADIPEC. doi: 10.2118/230173-MS.

[3] Algerøy, J. (2018). *Through tubing conveyed ESP: Effective pump swap maximizing production and well uptime*. Retrieved from https://www.spe-aberdeen.org/wp-content/uploads/2018/06/AccessESP-2018-EuALF-Presentation-Final.pdf.

[4] AL-Hejjaj, M.A., Sadeq, D.J., & Al-Fatlawi, O. (2023). A review of the electrical submersible pump development chronology. *Iraqi Journal of Chemical and Petroleum Engineering*, 24(2), 123-135. doi: 10.31699/IJCPE.2023.2.14.

[5] Baker Hughes. (2021). *TransCoil™ ESP system testing and analysis report*. Retrieved from https://www.bakerhughes.com/sites/bakerhughes/files/2021-01/TransCoil-ESP-system-testing-analysis-report-whtp.pdf.

[6] Biletskyi, V.S., Orlovskyy, V.M., & Malikova, O.A. (2025). Modern classification of methods and trends in intensification of oil, gas, and condensate recovery. *Geotechnologies*, 8, 171-180.

[7] Chen, B., Ramos Barboza, B., Sun, Y., Bai, J., Thomas, H.R., Dutko, M., Cottrell, M., & Li, C. (2022). A review of hydraulic fracturing simulation. *Archives of Computational Methods in Engineering*, 29. doi: 10.1007/s11831-021-09653-z.

[8] Chu, T., Nguyen, T.C., Yoo, H., Wang, J., & Vuong, D. (2022). Predicting ESP motor's overheating due to high free gas fraction. In *SPE artificial lift conference and exhibition – Americas* (article number SPE-209738-MS). Galveston: SPE. doi: 10.2118/209738-MS.

[9] Jahn, F., Kotlyar, L., Fajardo, F., Gabdullin, A., Vatne, O., Froyland, T., Tomczak, D., Bårdsen, J., Ramah, K.M., & Nesheim, H. (2026). Real-time data-driven decision-making for reliable and more efficient coiled tubing cleanouts in depleted reservoirs. In *SPE/ICoTA Well intervention conference and exhibition* (article number SPE-231356-MS). The Woodlands: SPE. doi: 10.2118/231356-MS.

[10] Kuper, I., Mykhailyshyn, B., & Lartseva, I. (2025). Identification of hydraulic fracturing impact factors on the skin effect in the near-wellbore zone of the reservoir. *Technology Audit and Production Reserves*, 4(1(48)), 40-49. doi: 10.15587/2706-5448.2025.333613.

[11] Lartseva, I.I., Korovainyi, O.A., & Lobunets, K.M. (2025). Application of hydraulic fracturing for stabilization of gas production in Ukraine. In *77th scientific conference of professors, teachers, researchers, postgraduates and students of the university* (pp. 97-98). Poltava: National University "Yuri Kondratyuk Poltava Polytechnic".

[12] Lazebna, Yu.V., Zezekalo, I.G., & Dmitrenko, V.I. (2022). Prospects of searches and problems of gas development of sealed collectors of the Dnipro-Donetsk depression. *Bulletin of the National Technical University "KhPI". Series: Chemistry, Chemical Technology and Ecology*, 1(7), 59-61. doi: 10.20998/2079-0821.2022.09.

[13] Leon, F., Pancho, J., Franco, E., Balseca, D., Ruales, F., Quinzo, M.E., Perez, M., & Villalobos, J. (2022). A fit-for-purpose ESP technical solution enables 17% production increase in complex reservoirs in mature fields in Ecuador. In *ADIPEC* (article number SPE-211331-MS). Abu Dhabi: ADIPEC. doi: 10.2118/211331-MS.

[14] Matkivskyi, S.V., & Khaydarova, L.I. (2021). Study of the influence of operating parameters of electric submersible pumps on the productivity of watered gas wells. *Mineral Resources of Ukraine*, 4, 30-35. doi: 10.31996/mru.2021.4.30-35.

[15] Moroz, L., Hryhorash, B., & Zhekalo, A. (2023a). Study of problems and prospects for increasing hydrocarbon production using hydraulic fracturing. *Prospecting and Development of Oil and Gas Fields*, 23(3), 68-78. doi: 10.69628/pdogf/3.2023.68.

[16] Moroz, L.B., Uhrynovskyi, V., & Kogut, G.M. (2023b). Investigation of the effect of polymer concentration in fracturing fluid on crack size and permeability during hydraulic fracturing. *Archives of Materials Science and Engineering*, 122(2), 70-77. doi: 10.5604/01.3001.0053.9594.

[17] Mysliuk, M.A., & Kravets, V.P. (2024). Intensification of the development of wells at the Zahidnohrestyshchensky field. *Mineral Resources of Ukraine*, 4, 42-49. doi: 10.31996/mru.2024.4.42-49.

[18] Pashchenko, O.A., Khomenko, V.L., Ratov, B.T., Koroviaka, Ye.A., & Rastsvietaiev, V.O. (2024). Comprehensive approach to calculating operational parameters in hydraulic fracturing. *IOP Conference Series: Earth and Environmental Science*, 1415, article number 012080. doi: 10.1088/1755-1315/1415/1/012080.

[19] Salah, A., Sabaa, A., Mokhtar, M., Sorour, A., & Shams Eddien, M.A. (2025). Optimizing electrical submersible pump (ESP) design and operation for low-productivity gassy wells. In *GOTECH* (article number SPE-224811-MS). Dubai: GOTECH. doi: 10.2118/224811-MS.

[20] Schlumberger. (n.d.a). *A novel approach to retrofitting ESPs into existing subsea wells*. Retrieved from https://www.slb.com/resource-library/technical-paper/al/spe-esp-workshop-al-subsea-reda-coil.

[21] Schlumberger. (n.d.b). *Pipesim steady-state multiphase flow simulator*. Retrieved from https://www.slb.com/products-and-services/delivering-digital-at-scale/software/pipesim-steady-state-multiphase-flow-simulator.

[22] Shcherbyna, A.V. (2024). Study of the effectiveness of the application of complex geological and technological measures on the example of gas-condensate generation in the central part of the priaxial zone of the Dnipro-Donets Basin. *Integrated Technologies and Energy Saving*, 1, 73-79. doi: 10.20998/2078-5364.2024.1.07.
[23] Vechietti, M., Di Benedetto, B., Krasuk, R.M., Mirande, J.M., Franco Delgado, E., Trujillo, S., Palombizio, G., Jahn, F., & Carreno, N. (2022). The challenges to retrieve a stuck coiled-tubing pipe without downhole check valves in a high-pressure well: A case study from Argentina. In *SPE/ICoTA well intervention conference and exhibition* (article number SPE-209011-MS). The Woodlands: SPE. doi: 10.2118/209011-MS.
[24] Zhulaj, M., & Serbin, O. (2024). Modern technologies of intensification of oil and gas wells in Ukraine. In *BMC-2024 – international scientific-practical conference of young scientists "Build-master-class-2024"* (pp. 255-256). Kyiv: Kyiv National University of Construction and Architecture. doi: 10.59647/978-617-520-936-3/1.

Застосування електровідцентрових насосів для освоєння газових свердловин з пониженим пластовим тиском після гідравлічного розриву пласта

Леся Мороз
Кандидат технічних наук, доцент
Івано-Франківський національний технічний університет нафти і газу
76019, вул. Карпатська, 15, м. Івано-Франківськ, Україна
https://orcid.org/0000-0002-5183-4940

Єгор Селінний
Аспірант
Івано-Франківський національний технічний університет нафти і газу
76019, вул. Карпатська, 15, м. Івано-Франківськ, Україна
https://orcid.org/0009-0002-7376-6050

Анотація. З огляду на тривалу експлуатацію та виснаженість більшості українських родовищ, пошук ефективних методів відновлення їхньої продуктивності є пріоритетним завданням для енергетичної галузі України. Робота присвячена оптимізації процесу освоєння свердловин із аномально низьким пластовим тиском після інтенсифікації припливу методом гідравлічного розриву пласта. Метою дослідження було впровадження технології успішного вилучення рідини розриву, що дозволить значно розширити критерії підбору свердловин та успішно виконувати операції гідравлічного розриву на завершальній стадії розробки покладів газу. Проведено порівняльний техніко-економічний теоретичний аналіз трьох альтернативних технологій механізованого освоєння (електровідцентровий насос на гнучкій трубі, на кабелі та на збірних трубах) для вибору оптимального методу, враховуючи поточний стан газовидобувної галузі України. Дослідження базувалося на інженерних розрахунках, вузловому аналізі та аналізі гідростатичного дисбалансу на прикладі типової глибокої свердловини з пониженим пластовим тиском (4 150 метрів, 6,0 МПа). Розрахунок гідростатичного дисбалансу для умовної свердловини показав критичну надлишкову репресію на пласт, що унеможливлює освоєння без примусового механічного відкачування. Гідростатичний тиск стовпа рідини значно перевищує пластовий, що призводить до зворотного заштовхування рідини (fluid fallback) та в подальшому до пошкодження тріщини через кольматацію. При порівняльному аналізі вищезгаданих технологій, на основі теоретичних даних, встановлено, що технологія спуску насоса на кабелі («Rigless») є технічно непридатною для глибин понад 3 000 метрів, а технологія спуску насоса на гнучкій трубі є економічно недоцільною в умовах, коли верстат капітального ремонту вже змонтований на гирлі. Встановлення електровідцентрового насоса на збірних насосно-компресорних трубах є прагматичним та економічно обґрунтованим рішенням. Розраховано параметри необхідної компоновки та змодельовано повний цикл від етапу проведення гідравлічного розриву до запуску свердловини в роботу. Запропоновано прагматичний підхід, що дозволяє вилучити технологічну рідину розриву без репресії на пласт, використовуючи наявні ресурси з мінімальними додатковими витратами, що є критичним для рентабельності робіт по стимуляції виснажених покладів

Ключові слова: поклад; інтенсифікація; дебіт; тріщина; експлуатація; ремонт; колтюбінг

ISSN 1993-9973, e-ISSN 2415-332X

Vol. 26, No. 1
2026

PROSPECTING AND DEVELOPMENT OF OIL AND GAS FIELDS

https://pdogf.com.ua/en

Received: 19.01.2026. Revised: 24.04.2026. Accepted: 29.05.2026. Published: 29.06.2026.

UDC 622.276.5:004.85

DOI: 10.63341/pdogf/1.2026.65

A data-driven approach for minimising production deferrals in sand-prone oil wells

Zaur Mirzayev*

Postgraduate Student

Azerbaijan State Oil and Industry University

AZ1010, 16/21 Azadliq Ave., Baku, Azerbaijan

https://orcid.org/0009-0003-9066-3114

Abstract. The aim of the study was to develop an analytical approach to minimising lost production in sand-prone oil wells based on operational data from the Caspian region, including facilities in Azerbaijan. The research methodology was based on an empirical analysis of monthly production observations from 48 producing wells for the period 2024-2025 and included a comparison of stable and unstable production intervals, a quantitative assessment of the contribution of operational factors to the formation of lost production, predictive modelling of unstable states and production losses, as well as an engineering verification of the identified patterns under real operational constraints. It was established that the transition to an unstable operational state was accompanied by a 23.5% decrease in oil flow rate, a 47.9% increase in water cut, a 69.8% increase in pressure drop across the filter elements, a 3.8-fold increase in downtime duration, and a 154.5% increase in the frequency of operational interventions. A statistical comparison showed that the most pronounced differences between stable and unstable intervals were associated with the rate of decline in flow rate, an increase in water cut, the cumulative duration of downtime over a six-month window, and a reduction in the proportion of stable production without signs of sand production. Regression analysis revealed that the greatest contribution to the change in lost production was made by the pressure drop across the filter elements, the proportion of stable operation, cumulative downtime and the frequency of interventions, whilst in the predictive modelling block, the XGBoost model demonstrated the best results, with an average absolute error of 2.18 m^3 per month and a coefficient of determination of 0.79. The practical significance of the results lies in their potential application in production monitoring and operational management systems for sand-prone wells, enabling the early detection of unstable conditions, the justification of operational interventions, and the adjustment of production rates to minimise lost production

Keywords: operational instability; filtration resistance; accumulation of downtime; frequency of operational interventions; proportion of stable operation; predictive modelling; production losses

Introduction

Sand production in oil wells is regarded as one of the factors reducing operational stability and production efficiency, since the transport of solid particles is accompanied by a disruption of the operating conditions in the bottomhole zone, an increase in the load on well equipment, a rise in the number of operational interventions, and an increase in downtime duration. For weakly cemented reservoirs, this relationship is systemic in nature, as the transition to an unstable operating regime is caused by the combined action of geomechanical, hydrodynamic and operational factors. Consequently, the analytical focus has shifted from describing individual manifestations of sand washout to developing integrated solutions based on a combination of control methods, operational monitoring and predictive modelling. Scientific interest in the problem of sand blowouts has gradually shifted from describing individual mechanisms of sand blowouts to developing integrated approaches based on a combination of methods for preventing sand blowouts, operational monitoring and predictive analytics (Deryaev, 2024a).

Suggested Citation: Mirzayev, Z. (2026). A data-driven approach for minimising production deferrals in sand-prone oil wells. *Prospecting and Development of Oil and Gas Fields*, 26(1), 65-79. doi: 10.63341/pdogf/1.2026.65.

*Corresponding author (*z.mirzayev8785@gmail.com*)

In a review paper by D.T. Asfha *et al.* (2024), the mechanisms of sand migration, approaches to its prediction, and the potential applications of fibre-optic technologies and machine learning methods for monitoring well conditions are systematised. It is shown that the development of sand control risk management systems is linked not only to the improvement of technical monitoring tools, but also to the expanded use of real-time data and intelligent analysis methods. A similar aspect of sand control management in the context of selecting technological solutions is considered in the work by M. Muhammad and A.A. Rasol (2025). The authors' analysis showed that the management of sand production is complicated not by a lack of available technologies, but by the need to select them judiciously, taking into account operating conditions, well operating modes and economic constraints. The study by H. Wu *et al.* (2025) summarises current understanding of the mechanisms of sand production, risk factors, forecasting methods and directions for further development in this field. The authors concluded that sand production should be regarded as a dynamic, multi-factor process, the analysis of which requires a combination of mechanistic models and predictive methods.

The chemical approach to controlling sand migration is presented in the publication by I. Karimov (2026a), which examines the transition from polymer solutions to nanomaterials in chemical sand stabilisation technologies. It is shown that the stability of such treatment should be assessed taking into account the preservation of the collector's filtration properties, which allows it to be considered in the context of long-term operational efficiency, rather than merely a short-term reduction in sand washout. A separate area of research concerns the evaluation of the performance of filtration systems. In the work by S. Liu (2024), a method for analysing the efficiency of slotted filters is proposed, according to which their operational characteristics depend not only on design parameters but also on operating conditions that determine the pressure drop, the degree of clogging, and the stability of solid particle retention.

The diagnostic aspect is addressed in the field study by D.T. Asfha *et al.* (2026), which demonstrates the capabilities of vertical seismic profiling technology using distributed acoustic sensing for the real-time detection of sand migration in an offshore well. It is shown that sand flow signatures can be used for the rapid detection of adverse changes in operating conditions, confirming the importance of continuous monitoring in production management systems. In the work by M.H. Shabdirova *et al.* (2023), machine learning methods are applied to predict non-stationary sand intrusions using the Karazhanbas field as an example. It has been shown that non-linear relationships between operational parameters and the development of sand production can be identified analytically; however, their correct interpretation requires consideration of the specific production context and the structure of the source data. In a review paper by B.A. Suleimanov *et al.* (2024) systematise mechanical technologies for preventing sand production in oil and gas wells. The authors demonstrate that the performance of filters and gravel packs is determined not only by their design characteristics, but also by their suitability to the selection conditions, flow capacity requirements, and the actual operating regime of the well. Early signs of instability in the bottomhole zone were examined by I. Karimov (2026b) based on an analysis of wellhead pressure and throttling parameters. A conclusion was drawn regarding the diagnostic significance of standard field indicators, which expands the possibilities for analytical forecasting by identifying adverse changes in operating conditions without the mandatory use of specialised measurements. The relationship between sand control and production efficiency is examined in the study by S. Ismayilov and Z. Mirzayev (2025), where innovative approaches to the operation of wells with sand production are analysed through a system of operational indicators. It is shown that their effectiveness is determined not only by a reduction in sand carryover, but also by their impact on flow rate stability, well operating conditions and the overall set of operational parameters.

Thus, a review of the literature shows that studies of sand production in oil wells cover the mechanisms of sand carryover, risk factors for unstable operation, mechanical and chemical control methods, monitoring tools, as well as analytical and predictive approaches to identifying adverse operating conditions. At the same time, there is a limited number of studies in which well operational data are simultaneously used to quantitatively assess lost production, predict the transition to an unstable operating regime, and justify technological solutions for reducing production losses. In this regard, the aim of the study was to substantiate an analytical approach to reducing lost production in sand-prone oil wells in the Caspian region, including Azerbaijan. In accordance with the stated objective, the study was aimed at addressing the following tasks: identifying key operational predictors of an unstable operational state of a well, assessing factors influencing the volume of lost production, and determining analytically sound guidelines for the engineering interpretation of threshold states and the selection of possible technological solutions.

Materials and Methods

The study was carried out between 2024 and 2025 as an empirical analysis of operational data, involving the development of an analytical approach designed to reduce production losses in sand-prone oil wells. The methodological framework was developed taking into account the conditions for the development of weakly cemented reservoirs in the Caspian region, including sites in Azerbaijan. This research framework is consistent with published engineering literature on the Azeri, Chirag and Azeri-Chirag-Gunashli fields, where sand production is considered a significant factor in reducing production efficiency and the operational reliability of equipment (BP, 2002; Susilo *et al.*, 2013; SLB, 2024).

The empirical basis of the study was formed using production monitoring data from 48 production wells and comprised a dataset of 1,728 monthly observations. The sample included wells with a continuous or quasi-continuous series of observations spanning at least 36 months. To ensure comparability between sites, a single analytical horizon of 36 months was used. This approach enabled the data on flow rates, bottomhole and wellhead pressures, water cut, signs of sand production, operational interventions and downtime duration to be presented in a comparable format. An integrated analytical profile was formed based on the initial dataset, combining production, hydrodynamic and operational indicators, as well as information on the dates of interventions and the duration of downtime. Operational interventions were identified using retrospective production data containing information on the occurrence of shutdowns, the nature of the operations performed, the duration of downtime, and the subsequent resumption of well operations. The study considered unscheduled operations aimed at restoring or stabilising well performance as operational interventions, including the cleaning of filter elements, the removal of sand and mechanical deposits, the restoration of bottomhole zone permeability, and flushing operations. In engineering practice, such interventions are regarded as measures for the maintenance, repair and restoration of well performance, including in conditions where sand control systems are malfunctioning (Schlumberger, 2015; Tang *et al.*, 2022).

The frequency of operational interventions was defined as the number of relevant events per 12 months of observation for each well. Objects with significant data gaps, disrupted temporal consistency, and values lacking operationally interpretable content were excluded from further processing. Intervals within which changes in operating mode could not be reliably correlated with the actual condition of the well were also excluded. Data preparation involved cleaning the dataset, standardising time intervals, and converting the indicators into a uniform analytical format. Missing values were imputed only where this did not conflict with the operational logic of the process. For short gaps in the time series, local linear interpolation was applied, as with a short gap and no signs of technological intervention, this approach allowed the continuity of the series to be maintained without significantly distorting the overall dynamics of the operational indicators. This procedure was used only on locally stable sections of the observations. For parameters exhibiting step-like changes, the nearest valid value was carried over, provided that a physically permissible operating regime was maintained. Anomalous values were interpreted taking into account the operational context, as sharp deviations could be associated with both recording errors and actual manifestations of unstable well operation. Derivative indicators were calculated based on the initial operational parameters to characterise the well's transition to an unstable operational state. The rate of decline in flow rate was defined as the relative change in average flow rate between the current and previous three-month observation windows (1):

$$R_q = (\bar{Q}_t - \bar{Q}_{t-1})/\bar{Q}_{t-1}, \tag{1}$$

where $\bar{Q}_t$ – average flow rate in the current three-month period, m³/day; $\bar{Q}_{t-1}$ – average flow rate in the preceding three-month window, m³/day. In addition, the rate of change in water saturation (ΔWC), the absolute and relative changes in bottomhole and wellhead pressures ($\Delta P₦_h$ and ΔPw_h), the cumulative duration of downtime within a six-month window (DT_{6m}), and the frequency of operational interventions over a 12-month period were calculated. The choice of a three-month window for the flow rate and water cut indicators was determined by the need to smooth out short-term operational fluctuations whilst maintaining sensitivity to adverse changes in operating conditions. A six-month window was used to assess the cumulative effect of downtime and recurring interruptions to the well's continuous operation. Calculations were performed using a moving average method with a monthly step. The average flow rate in the current three-month window was defined as the arithmetic mean of the values for months t, $t-1$ and $t-2$, and the average flow rate in the preceding window as the arithmetic mean of the values for months $t-1$, $t-2$ and $t-3$. The cumulative duration of downtime was calculated as the sum of the duration of downtime over six consecutive months, including the current month of observation (2):

$$DT_{6m} = \Sigma DT_{t-1},\ i = 0 \ldots 5, \tag{2}$$

where DT_{t-1} is the duration of downtime in the relevant month, in days. This approach made it possible to identify a consistent trend of deterioration in operating conditions, rather than isolated technical deviations. An unstable operating condition was identified based on a combination of operational indicators, including signs of solid particle carryover, an increase in pressure drop across the filter elements of at least 15% compared with the preceding stable interval, a reduction in oil flow rate of at least 10% in the absence of external constraints on the production regime and unscheduled operational interventions (Abduljabbar *et al.*, 2024). Their selection was based on the field interpretability of the indicators, a preliminary comparison of stable and unstable observation intervals, and an engineering verification of the physical plausibility of the identified deviations within the framework of scenario analysis. For analytical processing, such states were coded in two ways: as a binary event of transition to an unstable operational state and as a quantitative indicator of the severity of production losses, expressed as the volume of lost production. The *SFR* indicator was calculated as the ratio of the duration of stable operation intervals without recorded signs of sanding to the total duration of the period under analysis (3):

$$SFR = T_{sta\beta le}/T_{total}, \tag{3}$$

where $T_{sta\beta le}$ – total duration of stable operation without signs of sand transport; T_{total} – total duration of the analysed period. This indicator was used as an integral measure of the well's operational stability. The main target variable was the volume of oil not produced, defined as the difference between the expected production, calculated based on the well's baseline steady-state flow rate, and the actual production over the analysed interval (4):

$$L_o = (Q_{base} - Q_{fact}) \times t, \quad (4)$$

where L_o – volume of oil not produced, m^3; Q_{base} – base oil production rate, determined by the average production rate during the preceding steady-state period of operation for a specific well, m^3/day; Q_{fact} – actual oil production rate in the interval under analysis, m^3/day; t – duration of the analysed interval, days.

In addition, the probability of a well entering an unstable operational state, accompanied by sand production, an increase in the number of interventions and a rise in downtime, was assessed. The analytical procedure comprised several stages. In the first stage, a descriptive analysis was performed to identify stable relationships between operational parameters, signs of sand production, reduced production, and downtime duration. In the second stage, regression models were applied to quantitatively assess the contribution of individual factors to production losses. To this end, multiple linear regression, ridge regression and models with selection of the most significant predictors were used. This made it possible to assess the influence of pressure, flow rate, water cut, frequency of interventions and sand production indicators on the amount of lost production. In the third stage, machine learning methods were used to solve three analytical problems: classification of unstable operational states, forecasting of lost production volume, and assessment of the significance of input variables. Logistic regression was applied for the binary classification of well conditions. Random forest and gradient boosting were used to identify non-linear relationships and rank factors by degree of influence. To improve the accuracy of the forecast of lost production, the XGBoost algorithm was additionally applied. The data were split into training and test sets in an 80:20 ratio, whilst preserving the group structure of observations by well and time interval. This prevented the transfer of information between samples and minimised the risk of data leakage. The robustness of the results was further verified using a five-fold cross-validation method with grouping by well.

Statistical analysis of the data was carried out on a case-by-case basis, taking into account the distribution type of the variables under analysis and the research objective. In the first stage, the normality of the distribution was tested using the Shapiro-Wilk test. Statistical comparison of operational indicators between groups of wells with stable and unstable operating modes was carried out taking into account the type of data distribution. For a normal distribution, Student's t-test was applied; for deviations from normality, the Mann-Whitney test was used. The Wilcoxon criterion was used to analyse related states of the same well, including periods before and after technological intervention or before and after the transition to a regime with signs of sand production. The level of statistical significance was set at $p < 0.05$. Classical statistical methods were used to test inter-group and intra-group differences, whilst the machine learning module was focused on solving predictive and ranking tasks. The quality of the predictive models was assessed by the mean absolute error, root mean square error and coefficient of determination in regression tasks, as well as by classification accuracy, completeness, positive prediction accuracy and F1-score in classification tasks. When interpreting the results, priority was given to the completeness of identifying unstable states, as missing such episodes was associated with higher production losses and a risk of equipment damage. Data processing and model building were performed in the Python environment using Jupyter Notebook (n.d.). The PIPESIM (n.d.) hydraulic simulator was additionally used for engineering verification of the results and scenario analysis. This was used to assess the relationship between production modes, well completion parameters and changes in key operational indicators, including additional filtration resistance, productivity coefficient, pressure drop and the stability of filtration systems. The practical applicability of the proposed approach was further assessed taking into account the regulatory constraints of American Petroleum Institute (1991) and ISO 17824:2009 (2009). The scenario analysis considered options for varying formation pressure, the use of sand control systems, and their combination with other operational interventions. The results of the PIPESIM simulation were used for engineering verification of the calculations, interpretation of the threshold values established by statistical and predictive models, and to confirm the physical plausibility of the identified predictors of an unstable operating state.

Results

Initial differences between stable and unstable operating intervals

A comparison of stable and unstable production intervals in a dataset comprising 48 production wells and 1,728 monthly observations showed that the transition to an unstable production state was accompanied not by an isolated deviation in a single operational parameter, but by a coordinated change in the key parameters of well performance. Even at the initial descriptive level, unstable intervals were characterised by a simultaneous decrease in oil production, an increase in water cut, a rise in pressure drop across the filter elements, longer downtime periods, and a higher frequency of operational interventions. This pattern of changes was accompanied by a simultaneous deterioration in production, hydrodynamic and operational characteristics and was consistent with the general engineering logic described for sand-prone development conditions at the Azeri-Chirag-Gunashli fields (BP, 2002; Susilo *et al.*, 2013; SLB, 2024).

The most pronounced differences between stable and unstable intervals were identified in terms of oil flow rate, pressure drop across the filter elements, duration of downtime and volume of lost production. In stable intervals, the flow rate remained at a higher level, whereas in unstable conditions it decreased against a background of increasing water cut and local flow resistance. At the same time, downtime duration and the frequency of operational interventions increased, accompanied by changes not only in filtration and hydrodynamic conditions but also in the overall operational load on the production system. Consequently, production losses in such intervals became recurrent and accumulated over time. The decline in productivity, the increase in internal resistance and the rise in the number of operational disruptions manifested themselves as interrelated processes (Deryaev, 2024b). To systematise the primary differences between stable and unstable operational intervals, Table 1 presents summary characteristics of the main technological indicators.

Table 1. Descriptive characteristics of stable and unstable operating intervals

Indicator	Stable intervals	Unstable intervals	Change
Oil flow rate, m^3/day	96.8 ± 10.9	74.1 ± 12.6	-23.5%
Bottomhole pressure, MPa	19.4 ± 2.3	17.2 ± 2.7	-11.3%
Wellhead pressure, MPa	6.3 ± 0.9	7.5 ± 1	+19%
Water saturation, %	26.9 ± 8.7	39.8 ± 10.6	+47.9%
Pressure drop across the filter elements ΔP_f, MPa	0.96 ± 0.21	1.63 ± 0.29	+69.8%
Downtime duration, days/month	1.4 ± 0.9	5.4 ± 1.7	+285.7%
Frequency of technical interventions, cases/year	1.1 ± 0.4	2.8 ± 0.7	+154.5%
Unrealised production, m^3/month	2.1 ± 1.3	14.7 ± 4.8	7 times higher

Source: compiled by the author based on the results of processing the operational dataset and computational procedures in the Python/Jupyter environment

As can be seen from Table 1, the differences between stable and unstable intervals were not localised but rather consistent in nature, and encompassed production, hydrodynamic and operational parameters simultaneously. In unstable intervals, the oil flow rate decreased from 96.8 to 74.1 m^3/day, i.e., by 23.5%, whilst water cut increased from 26.9 to 39.8%, indicating a deterioration in the inflow structure and a reduction in production recovery efficiency. At the same time, the pressure drop across the filter elements ΔP_f increased from 0.96 to 1.63 MPa, or by 69.8%, reflecting an increase in local flow resistance and a deterioration in filtration conditions in the bottomhole zone. The change in pressures throughout the system was also consistent: bottomhole pressure decreased by 11.3%, whilst wellhead pressure, conversely, increased by 19%, which further indicated a shift in the well's operating regime as operating conditions deteriorated. The most pronounced shifts were related to the operational component: downtime duration increased from 1.4 to 5.4 days/month, i.e., by more than 3.8 times, whilst the frequency of operational interventions rose from 1.1 to 2.8 instances per year, or by 154.5%. As a result, lost production in unstable intervals reached 14.7 m^3/month compared to 2.1 m^3/month in stable intervals, i.e., it was 7 times higher. This combination of changes indicated that the transition to an unstable operating state was accompanied not by a separate deterioration of a single indicator, but by a simultaneous decline in productivity, an increase in hydrodynamic resistance, a reduction in operational continuity, and an accumulation of production losses. This interpretation is consistent with the general engineering view of the degradation of a well's operating regime as a process accompanied by the need for more frequent restorative and stabilising measures, particularly when the functioning of sand-control systems deteriorates (Schlumberger, 2015; Tang *et al.*, 2022).

Thus, an initial comparison of stable and unstable operating intervals revealed that the development of an unstable state in sand-prone wells manifested itself as a complex of interrelated changes affecting flow rate, water cut, pressure parameters, downtime duration, intervention frequency and lost production. Even at a descriptive level, this indicated that operational instability manifested as a systemic deterioration in well performance, rather than as an isolated deviation in a single operational parameter. The differences identified formed the basis for further analysis of derived indicators, statistical signs of the transition to an unstable state, and a quantitative assessment of factors associated with an increase in production losses.

Derivative indicators and statistical signs of the transition to an unstable operational state

A comparison of the derived indicators revealed that the transition to an unstable operational state was accompanied not only by changes in the initial operational parameters, but also by changes in the indicators reflecting the dynamics of the operating regime, the accumulation of operational irregularities, and a reduction in the proportion of stable well operation. This approach to interpreting an unstable state as a set of operational markers corresponds to the accepted scheme for its identification (Abduljabbar *et al.*, 2024). Differences between stable and unstable intervals were identified based on the rate of decline in flow rate, the rate of increase in water cut, changes in bottomhole and wellhead pressure, the accumulated duration of downtime within a six-month window, the annual frequency of interventions, and the *SFR* indicator. This pattern of differences was accompanied by the accumulation of interrelated signs of operational deterioration, including a decline in productivity, changes in hydrodynamic conditions, and a reduction in the duration of stable operation. In unstable intervals, the negative flow rate trend was accompanied by increased water cut and simultaneous pressure changes throughout the production system. The increase in DT_{6m} and the annual intervention frequency indicated that the change in operating regime was accompanied not only by filtration and hydrodynamic deviations, but also by changes in operational parameters. The *SFR* indicator decreased during such intervals, reflecting a reduction in the proportion of time during which the well operated without signs of sand production and associated disruptions. Taken together, the derived indicators reflected not isolated deviations, but a transition process from a steady state to a regime in which production losses recurred over time. For a quantitative comparison of the indicators calculated on the basis of the initial operational data, including the derived indicators determined by formulas (1)-(4), the results of the statistical analysis are presented in Table 2.

Table 2. Results of the statistical comparison of derived indicators and associated signs of deterioration in operating conditions

Indicator	Stable Intervals	Non-Robust Intervals	p-value
R_q	-0.03±0.02	-0.11±0.04	<0.001
ΔWC, %	+1.8±1.1	+6.9±2.4	<0.001
$\Delta P_{\beta h}$, MPa	-0.4±0.3	-1.7±0.6	<0.001
ΔP_{wh}, MPa	+0.2±0.2	+0.9±0.4	<0.001
DT_{6m}, days	6.1±2.8	18.7±5.3	<0.001
Frequency of interventions, cases/year	1.1±0.4	2.8±0.7	<0.001
SFR	0.84±0.07	0.46±0.09	<0.001
Shortfall in production, m^3/month	2.1±1.3	14.7±4.8	<0.001

Note: to compare indicators between stable and unstable intervals, the Student's t-test or the Mann-Whitney test was used, depending on the nature of the data distribution as determined by the Shapiro-Wilk test
Source: compiled by the author based on the results of statistical analysis of operational data using Python/Jupyter

According to the data in Table 2, the transition to an unstable operational state was most clearly evident in the R_q, ΔWC, DT_{6m} and *SFR* indicators. In unstable intervals, the value of R_q varied from -0.03±0.02 to -0.11±0.04, reflecting a more pronounced decrease in discharge compared to stable states. At the same time, ΔWC increased from +1.8±1.1 to +6.9±2.4%, accompanied by a more pronounced adverse trend in water availability. The cumulative duration of downtime in the six-month DT_{6m} window increased from 6.1±2.8 to 18.7±5.3 days, i.e., more than threefold. Against this background, the *SFR* decreased from 0.84±0.07 to 0.46±0.09, reflecting a reduction in the proportion of operating time without signs of sanding and associated disruptions. All differences remained statistically significant at the $p < 0.001$ level. This combination of changes indicated that the transition to an unstable state was accompanied not by a single isolated shift, but by a simultaneous change in several interrelated characteristics of the operating regime. A more pronounced decrease in flow rate was accompanied by an increase in waterlogging, an accumulation of downtime, and a reduction in the duration of stable operation. Consequently, differences between stable and unstable intervals were recorded not only in terms of the absolute values of the parameters, but also in terms of the direction of their change over time. In this form, the derived indicators were used to identify that part of the operational dynamics which was accompanied by a further increase in lost production and characterised the development of an unstable operational state.

Regression analysis of factors influencing lost production

A regression analysis of the factors influencing lost production revealed that changes in production volume in sand-prone wells were accompanied by the combined effect of several operational parameters, reflecting changes in filtration conditions, an increase in hydrodynamic resistance, and changes in the stability of the operating regime. The strongest correlation with the magnitude of production losses was found for the pressure drop across the filter elements, the frequency of operational interventions, the cumulative duration of downtime, and the *SFR* index. The coefficients of the regression models showed that the volume of lost production varied both as hydrodynamic conditions deteriorated and as the proportion of time spent in stable operation decreased. This pattern of results indicated a link between production losses and the well's transition to a regime in which operational disruptions recurred over time. The direction of influence of individual factors remained consistent in both the multiple linear regression model and the regularised model. This indicated the stability of the identified relationships between operational indicators and the volume of lost production. A decrease in flow rate, an increase in ΔP_f, an increase in DT_{6m} and an increase in the frequency of interventions were considered, within the framework of regression analysis, as interrelated changes in the operating regime. With this combination of parameters, an increase in deviations was accompanied by an increase in accumulated production losses and a change in the well's operating conditions. For a visual comparison of the relative contribution of key predictors within the regression approach, their effects are presented in Figure 1. As shown in Figure 1, a graphical comparison of the coefficients revealed a similar pattern of how the predictors influenced the volume of lost production in both regression models. The coefficients with the largest absolute values were ΔP_f, *SFR*, DT_{6m} and the frequency of technical interventions, indicating a link between an increase in filtration resistance, a reduction in the proportion of stable operation, the accumulation of downtime and an increase in the number of operational disruptions, and the occurrence of production losses. In the multiple linear regression model, the coefficient for ΔP_f was 0.34, for *SFR* -0.32, for DT_{6m} 0.29, and for the frequency of interventions 0.25. In the ridge regression, the same direction of influence was maintained, along with coefficients of similar magnitude: 0.31 for ΔP_f, -0.29 for *SFR*, 0.27 for DT_{6m} and 0.23 for the frequency of interventions. This indicated that an increase in the pressure drop across the filter elements, the accumulated downtime and the number of operational interventions was accompanied by a rise in lost production, whereas an increase in the proportion of time spent in stable operation was accompanied by a decrease in lost production.

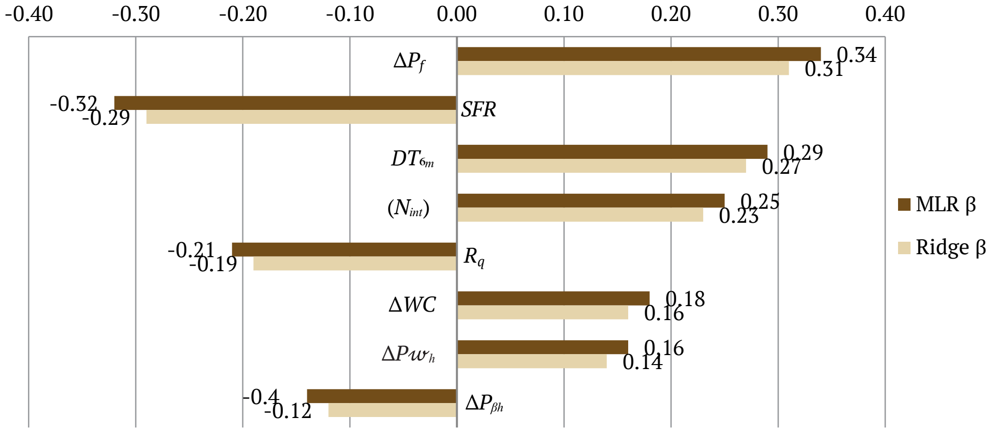

Figure 1. Comparison of β coefficients in regression models of lost production
Source: compiled by the author based on the results of visualising the β coefficients of regression models in the Python/Jupyter environment

The differences between the models did not alter the overall structure of the relationships, and the similar values of the coefficients indicated the comparability of the estimates across different regression analysis methods. Derived indicators of operational mode changes were also associated with production losses. The coefficient for R_q was -0.21 in the linear model and -0.19 in the peak model, reflecting the relationship between a decrease in flow rate and an increase in lost production. For ΔWC, the coefficients were 0.18 and 0.16 respectively, indicating a link between increased water cut and increased production losses. Pressure parameters also maintained a unidirectional relationship with the dependent variable: for $\Delta P_{\beta h}$, the coefficients were -0.14 and -0.12, and for ΔPw_h, 0.16 and 0.14. All the coefficients mentioned remained statistically significant, as the p-values ranged from <0.001 to 0.011. The explanatory power of the models was similar: R^2 was 0.71 for multiple linear regression and 0.69 for ridge regression. The results obtained indicated a link between shortfall in production and the combined change in several parameters characterising filtration, hydrodynamic and operational conditions. Thus, the regression analysis showed that the increase in lost production in sand-prone wells was associated not with a single operational deviation, but with a simultaneous change in several operating parameters. The coefficients with the largest absolute values were obtained for ΔP_f, *SFR*, DT_{6m} and the frequency of operational interventions, whilst the indicators of flow rate dynamics, water cut and pressure complemented the overall structure of the identified relationships. The consistency in the direction of the effects and the similar values of the coefficients in both models indicated the comparability of the regression analysis results. This allowed the findings to be used for subsequent comparison with machine learning results and for ranking features according to their predictive significance.

Machine learning results for the classification of unstable states, the prediction of lost production, and the ranking of features

The machine learning results showed that the transition to an unstable operational state and changes in the volume of lost production were reflected not only in statistical and regression relationships, but also in predictive patterns within the operational data. A comparison of algorithms revealed differences between models in terms of the completeness of unstable interval detection and the accuracy of production loss forecasting. Ensemble algorithms proved to be the most sensitive to combinations of features associated with a deterioration in operating conditions. Among these, the most significant were a decrease in flow rate, an increase in ΔP_f, a decrease in *SFR*, an accumulation of DT_{6m}, and an increase in the frequency of operational interventions. This configuration of features indicated that an unstable operational state was described not by a single variable, but by a system of interrelated parameters. The results of classification and regression modelling were consistent in terms of the general logic of feature selection. Models that more accurately identified unstable intervals simultaneously demonstrated greater sensitivity to the combination of parameters previously identified in statistical and regression analysis. This indicated the stability of the feature structure across different analytical levels and confirmed that key operational mode indicators retained their significance both for classifying well states and for predicting the magnitude of production losses. To compare the predictive performance of the algorithms used, the model quality metrics are presented in Table 3.

Table 3. Comparison of the quality of machine learning models for instability classification and production shortfall prediction

Model	Task	Accuracy	Recall	Precision	F1-score	MAE	RMSE	R^2
Logistic Regression	Classification	0.84	0.81	0.79	0.80	-	-	-
Random Forest	Classification	0.89	0.87	0.85	0.86	-	-	-
Gradient Boosting	Classification	0.91	0.89	0.88	0.88	-	-	-
XGBoost	Forecast of lost revenue	-	-	-	-	2.18	3.04	0.79
Random Forest Regressor	Forecast of lost production	-	-	-	-	2.54	3.41	0.74
Gradient Boosting Regressor	Forecast of lost revenue	-	-	-	-	2.31	3.17	0.77

Note: Accuracy, Recall, Precision and F1-score were used to evaluate models for classifying unstable operational states; MAE, RMSE and R^2 were used to evaluate models for predicting lost production. The symbol "-" indicates that the metric is not applicable to the corresponding model

Source: compiled by the author based on the results of operational data processing and machine learning in the Python/Jupyter environment

As can be seen from Table 3, in the task of classifying unstable operational states, higher metric values were obtained for ensemble algorithms. For Gradient Boosting, the accuracy was 0.91, recall 0.89, precision 0.88, and F1-score 0.88. For Random Forest, the corresponding values were 0.89, 0.87, 0.85 and 0.86, and for Logistic Regression – 0.84, 0.81, 0.79 and 0.80. These differences indicated that ensemble models distinguished between stable and unstable intervals more accurately. The higher Recall value for Gradient Boosting indicated a smaller number of undetected unstable intervals. The differences between logistic regression and ensemble algorithms also showed that the classification of operational states was related not only to a linear combination of features, but also to their more complex structure.

In the task of forecasting shortfall in production, the lowest error values and the highest coefficient of determination were obtained for XGBoost: MAE was 2.18 m^3/month, RMSE was 3.04 m^3/month, and R^2 was 0.79. For the Gradient Boosting Regressor, the corresponding values were 2.31 m^3/month, 3.17 m^3/month and 0.77, and for the Random Forest Regressor – 2.54 m^3/month, 3.41 m^3/month and 0.74. These results showed that XGBoost provided a lower prediction error and a higher proportion of explained variation in lost production within the dataset under consideration. The differences between the models indicated that the prediction of production losses was associated with a combination of several interrelated features. The machine learning results reproduced the same pattern of relationships that had been identified in the previous stages of the analysis. The features that demonstrated statistical significance and a regression relationship with lost production in this block also determined the quality of classification and prediction. This showed that the identified system of variables was used not only to distinguish operational states, but also to predict the transition to an unstable regime and changes in the volume of production losses. For a visual comparison of the significance of features in machine learning models, the results of their ranking are presented in Figure 2.

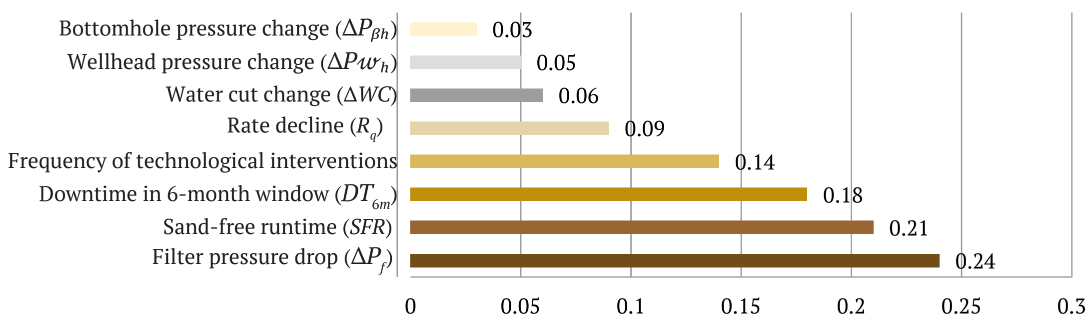

Figure 2. Ranking of feature importance in machine learning models

Source: compiled by the author based on the results of feature importance analysis and visualisation in the Python/Jupyter environment

As shown in Figure 2, the features with the highest significance in the machine learning models were ΔP_f, *SFR*, DT_{6m}, the frequency of process interventions and the rate of flow rate decline. Their relative significance values were 0.24 for ΔP_f, 0.21 for *SFR*, 0.18 for DT_{6m}, 0.14 for the frequency of operational interventions and 0.09 for R_q. These variables were associated with both the probability of a well transitioning to an unstable operational state and the magnitude of lost production. This distribution of significance indicated that the models primarily utilised features reflecting changes in local resistance, a reduction in the proportion of time spent in stable operation, and the accumulation of operational disruptions. In this respect, machine learning reproduced the same feature structure that had been identified in the statistical and regression analyses.

The significance of *SFR* and DT_{6m} was comparable to that of ΔP_f and flow rate dynamics. This showed that not only hydrodynamic deviations but also temporal characteristics of well operation, including changes in the proportion of stable operation, the accumulation of downtime, and the frequency of operational interventions, were used to identify unstable modes. Thus, production losses in sand-prone wells were associated not only with changes in the filtration state, but also with a restructuring of the operational regime. Machine learning results showed that unstable operational states and the associated increase in lost production were identified based on a combination of operational parameters. The greatest contribution to the quality of classification and forecasting was made by features reflecting changes in resistance, a decline in productivity, the accumulation of downtime, and a reduction in the duration of stable operation. This indicated that the transition to an unstable regime was determined not by a single indicator, but by a system of interrelated variables.

Engineering verification of the identified patterns and applied interpretation of threshold states

An engineering review of the identified statistical and predictive relationships showed that they remain physically and operationally interpretable within the constraints typical of sand-prone wells. Scenario analysis in PIPESIM confirmed that combinations of characteristics previously associated with an increase in lost production and a transition to an unstable operational state correspond to an engineering-based deterioration in well operating conditions. This was most clearly evident when changes occurred in formation pressure, the condition of the filter zone, and the sand control configuration. Under such conditions, an increase in the pressure drop across the filter elements, an accumulation of downtime, a reduction in *SFR*, and an increase in the frequency of interventions indicated the system's transition to a regime of heightened hydrodynamic stress and an increasing likelihood of production losses. From an engineering perspective, the results showed that the unstable operating condition developed as a sequential change in operating mode. The increase in formation pressure drop at the initial stage was accompanied by an intensification of inflow; however, upon reaching the threshold range, it was combined with the mobilisation of mechanical impurities, an increase in local resistance in the near-wellbore zone, and an increase in the load on the filter elements. This, in turn, was accompanied by an increase in ΔP_f, a reduction in periods of stable operation without signs of sand production, and a transition to a regime in which operational interventions became recurrent. Under such conditions, a short-term improvement in productivity did not compensate for the accumulation of subsequent losses, as the system more frequently deviated from steady-state operation and required additional operations to restore flow or stabilise performance. Engineering verification confirmed that the previously identified statistical, regression and predictive relationships reflected the pattern of operational deterioration. Scenario analysis also made it possible to distinguish between a high-production regime and an unstable operational state, during which losses began to accumulate. With a moderate change in wellbore pressure and the maintenance of a controlled state of the filter zone, the system sustained a relatively stable level of production without a marked increase in downtime or the frequency of interventions. However, with a further intensification of the production regime and a simultaneous deterioration in sand control conditions, a change in the operational pattern was observed: an increase in short-term flow rate was followed by a rise in resistance, instability in inflow, and a subsequent decline in overall operational efficiency. Threshold conditions manifested in this zone, which were recorded in the statistical module through an increase in ΔP_f, DT_{6m}, a rise in the frequency of interventions, and a reduction in *SFR*. In engineering terms, this corresponded to a transition from an acceptable intensification regime to a regime in which continued operation without corrective measures was accompanied by higher losses than potential additional production. For the engineering interpretation of the identified threshold states and the assessment of technological response options, the results of the scenario modelling are presented in Figure 3.

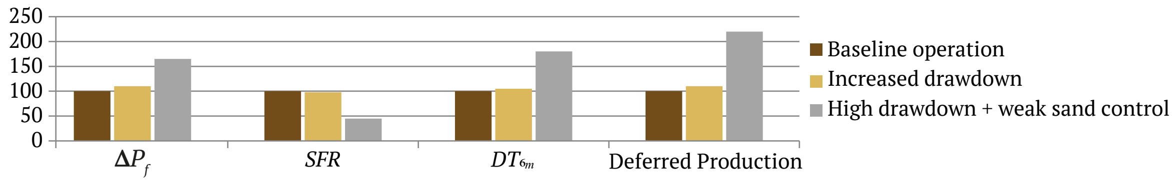

Figure 3. Engineering interpretation of scenarios for transition to an unstable regime under changing drawdown and sand control conditions

Note: values are normalised to the base scenario, set at 100, which allows for the comparison of relative changes in indicators across different units of measurement. The operational significance of a deviation from the 100 level depends on the nature of the indicator: for ΔPf, DT6m and Deferred Production, an increase relative to 100 indicates a deterioration in operating conditions, whereas for SFR, a decrease below 100 is unfavourable, as it reflects a reduction in the proportion of stable operation

Source: compiled by the author based on the results of simulation scenarios in Python/Jupyter and PIPESIM

As shown in Figure 3, the greatest deterioration in operating conditions was observed in scenarios combining increased reservoir depression with reduced sand control efficiency. Under these conditions, the ΔP_f index rose to 165, the DT_{6m} indicator to 180, and Deferred Production to 220 from a baseline of 100, whilst the *SFR*, conversely, fell to 45. This combination of changes indicated a concerted increase in hydrodynamic resistance, an accumulation of downtime and a rise in production losses, accompanied by a reduction in the proportion of stable operation. Under such conditions, the increase in pressure drop across the filter elements was accompanied by a reduction in stable operating intervals, an accumulation of downtime, and a shift in the operating regime towards a higher probability of lost production. Conversely, scenarios in which a change in production regime was combined with the maintenance or strengthening of sand control demonstrated a less pronounced change in regime: resistance increased more slowly, periods of stable operation remained longer, and the transition to an unstable operating state was shifted to a later stage. This indicated that the engineering interpretation of the identified thresholds was linked not only to the identification of a specific state but also to the distinction between regimes where intervention was already required and those where the possibility of adjustment still remained. The scenario analysis also confirmed the significance of temporal and operational indicators alongside hydrodynamic parameters. In previous stages of the analysis, *SFR*, DT_{6m} and the frequency of interventions had already demonstrated statistical and predictive significance. This was further confirmed in the engineering verification: a reduction in stable operation time and an accumulation of downtime reflected the moment when the system ceased to compensate for internal disturbances using its own margin of stability. Even with acceptable values for individual pressure or flow rate parameters, the well could already be entering a regime of deteriorating performance if the intervals of stable operation were shortening and the number of unscheduled interventions was increasing.

The engineering interpretation confirmed that monitoring only instantaneous operational indicators was insufficient; the approach to an unstable regime was more accurately identified through coordinated monitoring of the dynamics of operational stability. From a practical standpoint, this meant that threshold conditions were interpreted not as strictly isolated failure points, but as ranges of operational risk within which the system rapidly lost stability. The increase in ΔP_f, the decrease in *SFR*, the increase in DT_{6m} and the frequency of interventions collectively signalled that the current production regime was no longer economically or technologically viable. In the absence of corrective measures, this was accompanied not only by an increase in lost production, but also by an increased load on filtration systems, a higher probability of abrasive wear on equipment, and more frequent shutdowns. In this form, the results obtained could be interpreted taking into account the permissible operational limits and reliability requirements set out in API RP 14E (American Petroleum Institute, 1991) and ISO 17824:2009 (2009). To summarise the practical significance of the identified predictors and their link to potential operational measures, a practical interpretation is presented in Table 4.

Table 4. Practical interpretation of key predictors and recommended operational measures

Predictor	Operational significance	Associated risk	Recommended operational decision
Increase in ΔP_f	Increase in local resistance and deterioration of filtration conditions	Transition to an unstable inflow, accelerated accumulation of losses	Adjustment of the extraction regime, inspection of the filter zone, assessment of the need for cleaning or enhanced sand control
Reduction in *SFR*	Reduction in the proportion of stable operation without signs of sanding	Loss of operational stability, increased frequency of adverse incidents	Enhanced monitoring, early adjustment of operating parameters, reduction of drawdown at signs of accelerated degradation
Increase in DT_{6m}	Accumulation of downtime within a six-month window	Loss of operational continuity, increase in lost production	Revision of intervention tactics, transition from reactive to preventive maintenance
Increase in intervention frequency	Increase in operational instability and recurrence of faults	Increased costs, shorter intervals between overhauls	Optimisation of intervention strategy, investigation of causes of recurring faults, adjustment of operating regime
Deterioration in R_q and increase in ΔWC	Decrease in productivity and deterioration of inflow structure	Accelerated decline in production efficiency	Early assessment of production regime, comparison with the condition of the filtration zone and permissible operating conditions

Source: compiled by the author based on the results of a synthesis of computational, statistical and scenario-based results in Python/Jupyter and PIPESIM

As shown in Table 4, operational deterioration was associated with an increase in ΔP_f, a decrease in *SFR*, an increase in DT_{6m} and a rise in the frequency of interventions. The increase in ΔP_f reflected an increase in local resistance and a change in filtration conditions. The decrease in *SFR* indicated a reduction in the proportion of time spent in stable operation without signs of sanding. The increase in DT_{6m} indicated an accumulation of downtime within a six-month window, whilst the increase in the frequency of interventions indicated an increase in the number of instances of operational mode correction. The combined change in these indicators showed that the transition to an unstable operating state was accompanied by a simultaneous change in the hydrodynamic and operational characteristics of the system. Practical interpretation also showed that operational measures corresponded to the type of deviation identified. An increase in ΔP_f was associated with monitoring the condition of the filtration zone and sand control parameters. A decrease in *SFR* and an increase in DT_{6m} indicated a reduction in the duration of stable operating intervals and an accumulation of interruptions in production continuity. An increase in the frequency of interventions reflected a transition to a regime in which maintaining operational status required more frequent process adjustments. In this form, the identified predictors were used to identify conditions accompanied by a further increase in lost production.

Discussion

The results obtained showed that the shortfall in production from sand-prone wells was not caused by a single isolated anomaly, but rather by the combined effect of changes in several operational parameters. These included an increase in the pressure drop across the filter elements, a reduction in the proportion of stable operation, an accumulation of downtime, and an increase in the frequency of operational interventions. A similar approach is presented by A. Safaei *et al*. (2023), where chemical methods for controlling sand production were considered as one element of a sand control system, the effectiveness of which was determined by the properties of the formation, the conditions of application, and the well operating regime. This comparison showed that the transition to an unstable operating state was determined by the interaction of several factors and could not be reduced to a single indicator of deterioration in operating conditions. The most pronounced differences between stable and unstable intervals were associated with the rate of decline in flow rate, an increase in water cut, the accumulated duration of downtime, and a reduction in the proportion of time spent in stable operation without signs of sand production (Iskandarov *et al*., 2024; Kerimkhulle *et al*., 2025). These findings are consistent with the data of Z. Xu *et al*. (2024), where it was shown that the effectiveness of sand control was determined by a combination of material, technological and operational characteristics, rather than solely by the choice of a single reagent or treatment method. A comparison with the results obtained showed that the parameters reflecting the dynamics of the operating regime over time were of comparable significance to instantaneous hydrodynamic indicators, as they recorded the system's transition from an acceptable regime to the accumulation of production losses. The greatest contribution to the change in the volume of lost production was made by ΔP_f, *SFR*, DT_{6m} and the frequency of interventions, whilst R_q and ΔWC complemented this configuration as derivative indicators of mode deterioration. In the work by X. He *et al*. (2024), technologies for the prevention and control of sand ingress were also examined through a combination of rock failure causes, production mode and the limitations of the technical solutions employed. This comparison showed that the identified predictors formed an interconnected system of operational characteristics, through which operational deterioration was accompanied by an increase in the volume of lost production. Within this system, the increase in local resistance in the sand control zone occupied a distinct position.

The increase in pressure drop across the filter elements was associated with a rise in the volume of lost production and simultaneously reflected a change in filtration conditions within the sand control zone. A similar relationship was presented by C. Ma *et al*. (2023), where numerical modelling of a prepacked gravel screen demonstrated that sand retention and changes in hydrodynamic resistance should be considered jointly, as an increase in the resistance of the filtration system affected the operational condition of the well. In this context, ΔP_f was considered in statistical, regression and predictive analyses as an indicator linked to the engineering logic of the sand control system's operation. A similar result was presented by N.A. Ahad *et al*. (2020), where the selection of the filtration screen took into account the need for simultaneous assessment of retention capacity and hydraulic losses. A similar relationship was demonstrated by N.I. Ismail *et al*. (2021), where modelling of particle motion in the flow and their retention showed a link between changes in these conditions and the redistribution of resistance in the filtration screen zone. A comparison showed that ΔP_f could be regarded not only as a current hydrodynamic parameter, but also as an indication of a transition to a regime in which the deterioration of filtration conditions limited operational stability. In this regard, local resistance was considered not only as a diagnostic parameter, but also as a parameter related to the overall stability of well operation.

The reduction in the proportion of stable operation without signs of sand production and the accumulation of downtime were no less significant than instantaneous pressure and flow rate indicators (De Padova *et al*., 2018). These conclusions were consistent with the findings of H.B. Mahmud *et al*. (2020), where an intelligent sand control system was designed to enable the timely identification of risk and the selection of a response strategy before the situation escalated into more costly operational disruptions. A comparison with the results of the study showed that *SFR*, DT_{6m} and the frequency of interventions could be interpreted as indicators of changes in operational stability, rather than merely as secondary consequences of disruptions that had already occurred. From this perspective, minimising lost production was linked not to a single corrective action, but to the choice between a sand control strategy and a sand management strategy, depending on the combination of risks and operational constraints. These findings were consistent with the data presented by E. Araujo-Guerrero *et al*. (2021), where the choice between the two approaches was based on an assessment of the probability of sand production, production constraints and the operating conditions of a specific well. This comparison showed that the identified predictors were used not only to identify an already established deterioration in operating conditions, but also to justify the operational response. In this regard, the frequency of interventions and the accumulation of operational disruptions were interpreted as signs of a transition to a less stable operating regime.

The results of scenario-based and applied interpretation showed that an increase in the frequency of interventions and the accumulation of downtime accompanied the transition from an acceptable operating regime to a state in which losses began to rise faster than the potential additional production. These findings were consistent with the data presented by N. Kerya *et al*. (2022), where the strategy for managing sand production at an offshore field was viewed as a system for the early detection of signs of regime deterioration and timely intervention before the transition to more costly operational disruptions. In the context of the results obtained, the frequency of interventions was considered not only as an operational indicator but also as a sign of a change in the stability of the regime. This allowed the mechanisms of deterioration to be analysed not only through operational parameters but also through the dynamics of sand transport within the production system. In this context, changes in flow rate, an increase in local resistance and the subsequent deterioration of the operating regime were associated with more complex dynamics of sand transport than could be explained solely by the current state of the bottomhole zone. These findings were consistent with the data of Z. Wang *et al*. (2025), where the migration of sand particles in the wellbore system was analysed based on experiments and numerical modelling and linked to changes in their movement trajectories, accumulation conditions, and the formation of local flow disruption zones. A similar relationship was observed in the field study by Y. Xiao *et al*. (2024), where sand production in wells with sliding couplings without a sand control system was linked to a combination of the reservoir's geomechanical properties, well completion design and operating conditions. In this context, signs of sand production translated into practical production constraints, indicating that the deterioration in production regime arose not only as a local filtration problem but also as a consequence of the interaction between formation conditions, wellbore configuration and the nature of the production flow. A similar approach was presented by S.K. Subbiah *et al*. (2021), where the causes of sand production and methods for predicting it were examined through a combination of matrix failure, flow characteristics and operating conditions. This comparison showed that an increase in ΔP_f, a deterioration in R_q and an increase in the probability of lost production could reflect not only a general deterioration in operating conditions, but also a redistribution of sand transport processes within the production system. In this regard, the system of predictors was considered as an integrated operational configuration rather than as a set of isolated variables.

The engineering interpretation of the identified relationships was further correlated with scenario modelling in PIPESIM: a combination of increased formation pressure and deteriorating sand control conditions was accompanied by an increase in ΔP_f, a decrease in *SFR*, an increase in DT_{6m}, and a higher probability of production shortfall. These findings were consistent with the results of M. Adil Issa *et al*. (2022), where a reduction in the risk of sand production was linked to the consideration of geomechanical and operational constraints, including allowable depression and changes in formation stability as it is depleted. A similar relationship between sand retention conditions and the filtration system regime was observed by C. Ma *et al*. (2021), where the properties of pre-packed sand control screens were examined in terms of the ratio of sand retention to flow capacity. This comparison showed that the statistical and predictive relationships were confirmed by engineering data within scenarios reflecting the operational constraints of sand-prone wells. Comparison with the results of the study showed that a data-driven approach to minimising lost production gained practical significance whilst maintaining the engineering interpretability of the model's indicators. Unlike studies focused primarily on describing individual control methods or specific technical solutions, this analytical framework combined statistical comparison, regression analysis of factor contributions, predictive modelling and engineering verification within a unified analytical scheme. This made it possible to consider the identified system of predictors as a basis for the earlier detection of unstable operational states and for adjusting the production regime before the transition to a sustained accumulation of production losses.

Conclusions

The results of the study indicate that the lost production in sand-prone oil wells in the Caspian region, including those in Azerbaijan, was not caused by a single localised failure, but rather by a combination of interrelated operational changes affecting the production, hydrodynamic and operational characteristics of the well. A comparison of stable and unstable production intervals across a dataset of 48 wells and 1,728 monthly observations revealed that the transition to an unstable production state was accompanied by a decline in oil production, increased water cut, a rise in the pressure drop across the filter elements, an accumulation of downtime, and an increase in the frequency of operational interventions. Derivative indicators, including R_q, ΔWC, ΔPw_h, DT_{6m} and *SFR*, confirmed that the deterioration in operating conditions was evident not only in the absolute values of the parameters but also in the directional dynamics of their change over time.

Regression analysis established that the greatest contribution to the change in the volume of lost yield was made by ΔP_f, *SFR*, DT_{6m} and the frequency of interventions. In the multiple linear regression model, the coefficients for these variables were 0.34, -0.32, 0.29 and 0.25 respectively, whilst the model's explanatory power reached $R^2 = 0.71$. In the peak regression, the same directions of influence and coefficients of similar magnitude were retained, confirming the stability of the identified relationships. It was thus established that an increase in local resistance, a reduction in the proportion of stable operation and an accumulation of downtime are directly linked to an increase in production losses and can be regarded as key predictors of operational deterioration. The machine learning module complemented the results of the statistical and regression analysis. In the task of classifying unstable operational states, the Gradient Boosting model demonstrated the best performance, with an Accuracy of 0.91, Recall of 0.89, Precision of 0.88, and an F1-score of 0.88. In the task of forecasting lost production, the XGBoost model provided the highest accuracy, with an MAE of 2.18 m^3/month, an RMSE of 3.04 m^3/month, and an R^2 of 0.79. Feature ranking showed that ΔP_f, *SFR*, DT_{6m}, intervention frequency and rate of decline in flow rate retained the greatest significance in the models. This confirmed that the unstable operational state was described by a system of interrelated parameters, rather than a single isolated indicator. Engineering verification in PIPESIM confirmed the physical interpretability of the identified patterns. Scenario analysis showed that a combination of increased formation pressure and deteriorating sand control conditions was accompanied by an increase in ΔP_f, a reduction in stable operating intervals, an accumulation of downtime, and a shift in the operating regime towards a higher probability of lost production. This allowed the threshold states to be interpreted not as isolated failure points, but as ranges of operational risk, upon reaching which continued operation without corrective measures was accompanied by increasing losses.

Thus, the reduction of production losses in sand-prone wells is linked to a shift from reactive responses to disruptions that have already occurred to analytically grounded management of the operating regime based on operational data, statistical models, machine learning algorithms and engineering verification of scenarios. Prospects for further research involve expanding the empirical database, verifying the robustness of the proposed approach under various sand-related conditions, and comparing its predictive results with other modern models for the analysis and predictive management of lost production.

Acknowledgements
None.

Funding
None.

Conflict of Interest
None.

References

[1] Abduljabbar, A., Amadi, A., Mohyaldinn, M.E., Ridha, S., Younis, O., & Alakbari, F.S. (2024). The application and performance of sand screens for sand control: A review of selection criteria, screen materials, and causes of failure. *Heliyon*, 10(10), article number e30731. doi: 10.1016/j.heliyon.2024.e30731.

[2] Adil Issa, M., Ali Hadi, F., & Nygaard, R. (2022). Coupled reservoir geomechanics with sand production to minimise the sanding risks in unconsolidated reservoirs. *Petroleum Science and Technology*, 40(9), 1065-1083. doi: 10.1080/10916466.2021.2014522.

[3] Ahad, N.A., Jami, M., & Tyson, S. (2020). A review of experimental studies on sand screen selection for unconsolidated sandstone reservoirs. *Journal of Petroleum Exploration and Production Technology*, 10, 1675-1688. doi: 10.1007/s13202-019-00826-y.

[4] American Petroleum Institute. (1991). *API Recommended Practice 14E: Design and installation of offshore production platform piping systems (RP 14E)*. Retrieved from https://m.saigaogroup.com/uploads/file/api-14e-standard.pdf.

[5] Araujo-Guerrero, E., Alzate-Espinosa, G., Cross-Arroyave, Y., Vega-Niño, Y.P., Cartagena-Pérez, D.F., & Naranjo-Agudelo, A.J. (2021). A new methodology for selecting sand control or sand management as a strategy in wells with sand production potential. In *ISRM 9th international symposium on geomechanics* (article number ISRM-ISG-2021-01). Virtual.

[6] Asfha, D.T., Abdul Latiff, A.H., Otchere, D.A., Tackie-Otoo, B.N., Babikir, I., Rafi, M., Riyadi, Z.A., Putra, A.D., & Adeniyi, B.A. (2024). Mechanisms of sand production, prediction – a review and the potential for fibre optic technology and machine learning in monitoring. *Journal of Petroleum Exploration and Production Technology*, 14, 2577-2616. doi: 10.1007/s13202-024-01860-1.

[7] Asfha, D.T., Latiff, A.H.A., Soleimani, H., Arshad, A.R.M., Rashid, A., Yogi, I.B.S., Otchere, D.A., Mousa, A., & Dhiaulhaq, R.R. (2026). Real-time sand transport detection in an offshore hydrocarbon well using distributed acoustic sensing-based VSP technology: Field data analysis and operational insights. *Technologies*, 14(3), article number 175. doi: 10.3390/technologies14030175.

[8] BP. (2002). *ACG phase 1 environmental and social impact assessment*. Retrieved from https://www.bp.com/content/dam/bp/country-sites/en_az/azerbaijan/home/pdfs/esias/acg/acg-phase1-esia-eng.pdf.

[9] De Padova, D., Mossa, M., & Sibilla, S. (2018). SPH numerical investigation of characteristics of hydraulic jumps. *Environmental Fluid Mechanics*, 18, 849-870. doi: 10.1007/s10652-017-9566-4.

[10] Deryaev, A. (2024a). Drilling of a directional exploration well in Turkmenistan in the waters of the Caspian Sea. *Journal of Mines, Metals and Fuels*, 72(3), 199-209. doi: 10.18311/jmmf/2024/36590.

[11] Deryaev, A.R. (2024b). Regulation of rheological properties of weighted grouting solutions during cementing of deep wells under conditions of abnormally high reservoir pressure. *Neftyanoe Khozyaystvo Oil Industry*, 2024(5), 86-90. doi: 10.24887/0028-2448-2024-5-86-90.

[12] He, X., Pang, Z., Ren, L., Zhao, L., Lu, X., Wang, Y., & Liu, P. (2024). A critical review of sand production and sand control technologies for oil wells in oilfields. *Frontiers in Energy Research*, 12, article number 1399033. doi: 10.3389/fenrg.2024.1399033.

[13] Iskandarov, E.K., Baghirov, A.N., Shikhiyeva, L.M., & Aliyev, I. (2024). Method for assessing the hydrate formation from a mixture of natural gas flows of varying degrees of moisture content. *Nafta – Gaz*, 80(1), 39-44. doi: 10.18668/NG.2024.01.05.

[14] Ismail, N.I., Kuang, S., & Yu, A. (2021). CFD-DEM study of particle-fluid flow and retention performance of sand screen. *Powder Technology*, 378, 410-420. doi: 10.1016/j.powtec.2020.10.012.

[15] Ismayilov, S., & Mirzayev, Z. (2025). Innovative methods for improving production efficiency at wells with sand production: Technological metrics and their role. *Mining Journal of Kryvyi Rih National University*, 59(2), 32-45. doi: 10.31721/2306-5435-2025-2-32-45.

[16] ISO 17824:2009. (2009). *Petroleum and natural gas industries – downhole equipment – sand screens*. Retrieved from https://www.iso.org/obp/ui/en/#iso:std:iso:17824:ed-1:v1:en.

[17] Jupyter Notebook. (n.d.). Retrieved from https://jupyter.org/try-jupyter/notebooks/?path=notebooks/Intro.ipynb.

[18] Karimov, I. (2026a). Study of chemical sand consolidation transition from polymers to nanoparticles. *Herald of Azerbaijan Engineering Academy*, 17(4). doi: 10.52171/herald.393.

[19] Karimov, I. (2026b). Wellhead pressure and choke signatures as early indicators of near-wellbore instability. *Scientific Work: International Scientific Journal*, 20(1), 162-168. doi: 10.36719/2663-4619/126/162-168.

[20] Kerimkhulle, S., Kuttykozhayeva, S., Turtkarayeva, G., Seitova, T., Ospanova, N., & Toleubay, D. (2025). Using the fuzzy logic models for analysis of time phases of crude oil prices: Brent-Europe. *Lecture Notes in Networks and Systems*, 1489, 9-17. doi: 10.1007/978-3-031-96798-6_2.

[21] Kerya, N., Leong, D.G., & Apiwathanasorn, S. (2022). Sand management strategy in offshore gas field in the gulf of Thailand. In *Offshore technology conference Asia* (article number OTC-31499-MS). Kuala Lumpur: OTC. doi: 10.4043/31499-MS.

[22] Liu, S. (2024). A new evaluation method for sand control performance of slotted screen. *Geoenergy Science and Engineering*, 243, article number 213368. doi: 10.1016/j.geoen.2024.213368.

[23] Ma, C., Deng, J., Dong, X., Sun, D., Feng, Z., Yan, X., & Luo, C. (2021). Comprehensive experimental study on the sand retention media of pre-filled sand control screens. *Particulate Science and Technology*, 39(3), 261-270. doi: 10.1080/02726351.2019.1687628.

[24] Ma, C., Dou, Y., Deng, J., Hui, C., Zhao, K., Feng, Y., & Dou, L. (2023). Numerical simulations of sand-screen performance in unconsolidated prepacked gravel screen. *Energy Science & Engineering*, 12(1), 685-698. doi: 10.1002/ese3.1635.

[25] Mahmud, H.B., Leong, V.H., & Lestariono, Y. (2020). Sand production: A smart control framework for risk mitigation. *Petroleum*, 6(1). doi: 10.1016/j.petlm.2019.04.002.

[26] Muhammad, M., & Rasol, A.A. (2025). Advances and challenges of sand production and control in oilfields: A review. *Results in Engineering*, 25, article number 104596. doi: 10.1016/j.rineng.2025.104596.

[27] PIPESIM. (n.d.). Retrieved from https://www.software.slb.com/software-news/software-top-news/pipesim/pipesim-2024-1.

[28] Safaei, A., Asefi, M., Ahmadi, M., Pourshamsi, T., Baloochestanzadeh, S., Khalilnezhad, A., & Riazi, M. (2023). Chemical treatment for sand production control: A review of materials, methods, and field operations. *Petroleum Science*, 20(3), 1640-1658. doi: 10.1016/j.petsci.2023.02.013.

[29] Schlumberger. (2015). *The defining series: Well intervention – maintenance and repair*. Retrieved from https://www.slb.com/resource-library/oilfield-review/defining-series/defining-intervention.

[30] Shabdirova, A., Kozhagulova, A., Minh, N.H., & Zhao, Y. (2023). Application of machine learning to predict transient sand production in the Karazhanbas Oil Field, Ustyurt-Buzachi Basin (West Kazakhstan). *Natural Resources Research*, 32, 1975-1986. doi: 10.1007/s11053-023-10234-z.

[31] SLB. (2024). *Flow scanner*. Retrieved from https://www.slb.com/products-and-services/innovating-in-oil-and-gas/reservoir-characterization/surface-and-downhole-logging/wireline-cased-hole-logging/flow-scanner.

[32] Subbiah, S.K., Samsuri, A., Mohamad-Hussein, A., Jaafar, M.Z., Chen, Y.R., & Kumar, R.R. (2021). Root causes of sand production and methodologies for prediction. *Petroleum*, 7(3), 263-271. doi: 10.1016/j.petlm.2020.09.007.

[33] Suleimanov, B.A., Abbasov, H.F., & Ismailov, S.Z. (2024). A comprehensive review on sand control in oil and gas wells. Part I. Mechanical techniques. *SOCAR Proceedings*, 3, 9-23. doi: 10.5510/OGP20240300988.

[34] Susilo, Y., Whaley, K., Loboguerrero, S., Jackson, P., Kerimov, N., Anderson, R., Keatinge, P., & Edment, B. (2013). Significant increase in sand control reliability of open-hole gravel pack completions in the ACG field – Azerbaijan. In *SPE European formation damage conference & exhibition* (article number SPE-165206-MS). Noordwijk: SPE. doi: 10.2118/165206-MS.

[35] Tang, C.Y., *et al*. (2022). Holistic performance review of through-tubing sand screens as a remedial sand control measure: Best practices and lessons learnt from past installations in offshore East Malaysian oil fields. In *ADIPEC* (article number SPE-211317-MS). Abu Dhabi: ADIPEC. doi: 10.2118/211317-MS.

[36] Wang, Z., Zhang, S., Zhou, H., Huang, K., Sun, J., Zhang, M., & Liao, R. (2025). Analysis of the migration patterns of sand particles below the screw pump in wells based on experiments and numerical simulations. *Scientific Reports*, 15, article number 22161. doi: 10.1038/s41598-025-03470-1.

[37] Wu, H., Shen, S.-L., & Zhou, A. (2025). Sand production during hydrocarbon exploitation: Mechanisms, factors, prediction, and perspectives. *Geoenergy Science and Engineering*, 252, article number 213954. doi: 10.1016/j.geoen.2025.213954.

[38] Xiao, Y., Agrawal, M., Vaziri, H., & Anthony, R. (2024). Sanding in sliding sleeve completed wells without sand control in moderately competent sand-prone reservoir formations: A field case. *Rock Mechanics and Rock Engineering*, 59, 5639-5647. doi: 10.1007/s00603-024-03984-6.

[39] Xu, Z., Shen, K., Zhou, J., Huang, Q., Liu, P., Du, J., & Wu, J. (2024). Chemical sand production control: A review of materials, methods and characterisation. *Frontiers in Energy Research*, 12, article number 1424059. doi: 10.3389/fenrg.2024.1424059.

Підхід на основі аналізу даних для мінімізації перерв у видобутку на нафтових свердловинах, схильних до запіскування

Заур Мірзаєв

Аспірант

Азербайджанський державний університет нафти та промисловості

AZ1010, просп. Азадлік, 16/21, м. Баку, Азербайджан

https://orcid.org/0009-0003-9066-3114

Анотація. Метою дослідження було розроблення аналітичного підходу до мінімізації втрат видобутку в нафтових свердловинах, схильних до запіскування, на основі експлуатаційних даних з Каспійського регіону, включаючи об'єкти в Азербайджані. Методологія дослідження базувалася на емпіричному аналізі щомісячних даних про видобуток із 48 діючих свердловин за період 2024-2025 рр. і включала порівняння стабільних та нестабільних інтервалів видобутку, кількісну оцінку впливу експлуатаційних факторів на втрати видобутку, прогнозне моделювання нестабільних станів та втрат видобутку, а також інженерну верифікацію виявлених закономірностей за реальних експлуатаційних обмежень. Було встановлено, що перехід до нестабільного експлуатаційного стану супроводжувався зниженням нафтовидобутку на 23,5 %, збільшенням водної фракції на 47,9 %, зростанням перепаду тиску на фільтрувальних елементах на 69,8 %, збільшенням тривалості простоїв у 3,8 рази та зростанням частоти експлуатаційних втручань на 154,5 %. Статистичне порівняння показало, що найвиразніші відмінності між стабільними та нестабільними інтервалами були пов'язані з темпами зниження дебіту, зростанням вмісту води, сумарною тривалістю простоїв протягом шестимісячного періоду та зменшенням частки стабільної видобутку без ознак виходу піску. Регресійний аналіз показав, що найбільший внесок у зміну втрат видобутку зробили перепад тиску на фільтруючих елементах, частка стабільної роботи, сумарний час простою та частота втручань, тоді як у блоці прогнозного моделювання найкращі результати продемонструвала модель XGBoost із середньою абсолютною похибкою 2,18 м³ на місяць та коефіцієнтом детермінації 0,79. Практичне значення отриманих результатів полягає в можливості їх застосування в системах моніторингу видобутку та управління експлуатацією свердловин, схильних до пісковиділення, що дозволяє здійснювати раннє виявлення нестабільних умов, обґрунтовувати експлуатаційні втручання та коригувати інтенсивності видобутку з метою мінімізації втрат видобутку

Ключові слова: експлуатаційна нестабільність; опір фільтрації; сукупний час простою; частота експлуатаційних втручань; частка стабільної роботи; прогнозне моделювання; втрати видобутку

ISSN 1993-9973, e-ISSN 2415-332X

Vol. 26, No. 1
2026

PROSPECTING AND DEVELOPMENT OF OIL AND GAS FIELDS ***https://pdogf.com.ua/en***

Received: 21.11.2025. Revised: 27.04.2026. Accepted: 29.05.2026. Published: 29.06.2026.

UDC 622.276.054

DOI: 10.63341/pdogf/1.2026.80

Research into the characteristics of the hydrate formation process in water-logged gas wells

Roman Kondrat

Doctor of Technical Sciences, Professor
Ivano-Frankivsk National Technical University of Oil and Gas
76019, 15 Karpatska Str., Ivano-Frankivsk, Ukraine
https://orcid.org/0009-0002-0928-2748

Oleksandr Kondrat

Doctor of Technical Sciences, Professor
Ivano-Frankivsk National Technical University of Oil and Gas
76019, 15 Karpatska Str., Ivano-Frankivsk, Ukraine
https://orcid.org/0000-0003-4406-3890

Liliia Matiishyn*

PhD in Technical Sciences, Associate Professor
Ivano-Frankivsk National Technical University of Oil and Gas
76019, 15 Karpatska Str., Ivano-Frankivsk, Ukraine
https://orcid.org/0000-0002-8529-4807

Natalia Dremliukh

PhD in Technical Sciences, Associate Professor
Ivano-Frankivsk National Technical University of Oil and Gas
76019, 15 Karpatska Str., Ivano-Frankivsk, Ukraine
https://orcid.org/0000-0002-6991-0227

Abstract. The relevance of this research is driven by the transition of most natural gas fields to the late stage of development, which is accompanied by a significant increase in water production and creates thermodynamic conditions conducive to the emergency blockage of wellbores by gas hydrates. The aim of the study was to determine the influence of water cut and reservoir drawdown on the characteristics of the hydrate formation process in watered gas wells in order to optimise their operating conditions. To achieve this objective, a comprehensive mathematical model of the thermodynamic state of a multiphase fluid was developed and applied to a series of simulations on a model well under different reservoir drawdown values (2.5%, 5.0%, 7.5%, 10.0%, and 15.0% of the initial reservoir pressure) and water cut values (0-1,000 L/thousand m^3). The results showed that, at low reservoir drawdown (2.5% of the initial pressure) and limited water inflow, the hydrate formation risk zone is most critical and extends to depths exceeding 1,000 m. The temperature distribution along the wellbore was analysed, demonstrating that when the water cut exceeds 500 L/thousand m^3, the gas-liquid flow becomes sufficiently "hot" due to the high heat capacity of water, enabling the well to leave the hydrate formation zone without external intervention. Critical water cut values corresponding to the cessation of natural flowing conditions were determined, at which the actual wellhead temperature decreased to a minimum of 0.28°C. A graph-analytical method for constructing hydrate formation boundaries was developed, making it possible to clearly distinguish between the thermodynamic states associated with active hydrate formation and those corresponding to stable well operation. It was demonstrated that increasing reservoir drawdown leads to an increase in the critical water cut value at which hydrate formation in the production tubing ceases without external intervention.

Suggested Citation: Kondrat, K., Kondrat, O., Matiishyn, L., & Dremliukh, N. (2026). Research into the characteristics of the hydrate formation process in water-logged gas wells. *Prospecting and Development of Oil and Gas Fields*, 26(1), 80-91. doi: 10.63341/pdogf/1.2026.80.

*Corresponding author (*liliia.matiishyn@nung.edu.ua*)

The practical significance of the results lies in the possibility of using the developed model by petroleum engineers and field specialists for the justified selection of hydrate-free operating modes for watered gas wells

Keywords: water cut; well operation; reservoir drawdown; hydrate formation temperature; natural gas

Introduction

Hydrate formation in water-flooded gas wells is a critically important task for ensuring uninterrupted operation of gas fields at the late stage of development. The appearance of formation or condensation water in the wellbore significantly changes the thermodynamic equilibrium of the system, creating a favourable environment for the formation of technogenic hydrate deposits. Hydrate formation in the wellbore leads to partial or complete overlap of the cross-section of the tubing (tubing) and flow rate reduction. Studying the kinetics of this process allows not only to better understand the physicochemical features of phase transitions, but also to develop effective methods for preventing hydrate deposits.

The problem of water-flooded gas wells, which is accompanied by a natural decrease in reservoir pressure and intensive waterlogging of products, which critically changes the operating conditions of gas wells, is being studied by prominent scientists. In particular, the authors R. Kondrat & L. Matiishyn (2025) noted in their work that most of the fields of Ukraine are at the final stage of development and require the implementation of new approaches to modelling well drives in conditions of significant waterlogging. Scientists draw attention to the fact that it is necessary to take into account the dynamics of reservoir energy when predicting complications in the operation of gas wells. Researchers O.A. Lukin & O.R. Kondrat (2025) in their studies concluded that uncertainty in predicting production from compacted reservoirs affects the accuracy of determining zones of possible moisture condensation. This suggests that even minor errors in predicting hydrocarbon production rates lead to critical errors in determining the actual locations of hydrate formation. Scientists F. Yin *et al*. (2026) in their studies focused on the fact that the transition of the liquid-gas system to the hydrate state significantly changes the physicochemical properties along the wellbore. The authors noted that the location of hydrate formation is critical in the drilling and exploitation of deep-water horizons.

Scientists M. Gudala *et al*. (2025) in the process of studying the Joule-Thomson effect found that when gas is injected into depleted reservoirs, the sharp expansion of the gas provokes local freezing of the formation water. The authors developed a model that confirms that even at high initial temperatures, the risk zone for hydrate formation remains in high-permeability zones due to nonlinear pressure gradients. Authors A. Qu *et al*. (2023) using the example of North Sea fields found that the most dangerous intervals of hydrate formation are localised closer to the wellhead, where the lowest ambient temperatures are observed. Scientists suggested the use of special simulators to accurately calculate the time until the pipe cross-section is completely blocked by a hydrate plug.

In the work of J. Pei *et al*. (2024) reviewed the current state of CO_2 capture technologies using the gas hydrate method as one of the promising areas of decarbonisation. The authors summarised the main mechanisms of CO_2 hydrate formation, analysed the influence of thermodynamic and kinetic promoters, as well as design and process factors that increase the efficiency of hydrate formation. They concluded that gas hydrate technology is an energy-efficient and environmentally attractive alternative to traditional CO_2 capture methods, but its industrial implementation is still limited by the problems of slow kinetics, the need for high pressure, and the complexity of scaling up processes. In the study by J. Gauteplass *et al*. (2020) focuses on the processes of gas hydrate formation during CO_2 injection into porous media and their impact on the permeability and hydrodynamics of formations. The authors analysed the conditions for the occurrence of hydrate blocking, and also proposed approaches to its prevention and restoration of filtration characteristics by controlling thermobaric conditions and flow drives. As a result, they showed that the formation of hydrates can significantly reduce the efficiency of CO_2 injection, however, with proper process control, this phenomenon can be partially controlled and taken into account in CO_2 storage and transportation technologies in geological formations.

Analysis of the above-mentioned scientific works showed that despite the in-depth study of the hydrate formation process, in the analysed works, scientists did not pay enough attention to the complex relationship between different values of the water factor and the magnitude of the depression on the formation directly for water-flooded gas wells. Most of the research results take into account static conditions of phase equilibrium, or pure “gas-water” systems without taking into account the real influence of the nature of the multiphase flow, which is typical for the late stage of development. The lack of clear patterns of how the value of the water factor and depression on the formation on the process of hydrate formation served as the basis for conducting this study. The aim of the work was to study the influence of the water factor and depression on the formation on the characteristics of the hydrate formation process in water-flooded gas wells.

Materials and Methods

Research of the characteristics of the hydrate formation process in water-flooded gas wells were performed for the conditions of a hypothetical (model) gas well with the following data: well depth – 3,400 m, gas-saturated layer thickness – 18 m, current layer pressure – 32 MPa, layer temperature – 341 K, relative gas density – 0.6, tubing lowered to the middle of the perforation interval to a depth of 3,391 m; internal tubing diameter – 0.062 m; filtration resistance coefficients of the bottomhole zone of the layer: $A = 0.12$ MPa^2·day/thousand m^3; $B = 0.0027$ (MPa·day/thousand m^3)^2. The specified parameters (coefficients *A* and *B*) of the model well were used as a base scenario for conducting a series of calculations. These indicators remained unchanged throughout the study.

The studies studied the effect of different values of depression on the formation (2.5; 5.0; 7.5; 10.0; 15.0% of the initial pressure) and water factor values (0; 5; 10; 21; 25; 46; 50; 83; 100; 157; 188; 250; 350; 500; 800; 1,000 l/thousand m^3) on the hydrate formation temperature and wellhead temperature, as well as the depth of hydrate formation in the wellbore. To perform the calculations, the values of the bottomhole pressure were specified, which was determined through a given percentage of depression per reservoir from the initial reservoir pressure. From the equation of gas flow to the wellhead, the gas flow rate was determined for each value of bottomhole pressure using the formula R.M. Kondrat *et al*. (2023):

$$q_g = -\frac{A}{2B} + \sqrt{\left(\frac{A}{2B}\right)^2 + \frac{P_f^2 - P_{bh}^2}{B}}, \quad (1)$$

where P_f, P_{bh} – reservoir and bottomhole pressures, MPa, respectively; q_g – reservoir gas flow rate under standard conditions, thousand m^3/day; *A*, *B* – filtration resistance coefficients of the bottomhole zone of the reservoir; $A = 0.12$ MPa^2·day/thousand m^3; $B = 0.0027$ (MPa·day/thousand m^3)^2.

For each value of bottomhole pressure and gas flow rate, the pressure distribution along the working wellbore was calculated using the formula for gas movement in vertical wellbore pipes, corrected for the movement of the gas-liquid mixture in the tubing according to the method given in the work of R.M. Kondrat *et al*. (2023):

$$P(x) = \sqrt{\frac{P_{bh}^2 - \Theta \cdot q_{mix}{}^2}{e^{2S_0}}}, \quad (2)$$

where each component is calculated using the formulas:

$$S_0 = \frac{0.03415\overline{\rho}_g \rho \cdot x}{Z_{aver} T_{aver}}; \quad (3)$$

$$\theta = 0.0133\lambda \frac{Z_{aver}^2 T_{aver}^2}{d_{in}{}^5}\left(e^{2S_0} - 1\right); \quad (4)$$

$$q_{mix} = \frac{G_g + G_l}{\rho_g} = \frac{q_g \rho_g + q_w \rho_w}{\rho_g}; \quad (5)$$

$$\rho = \varphi + (1 - \varphi)\frac{\rho_w}{\rho_g(P)}; \quad (6)$$

$$\rho_g(P) = \frac{\rho_g P_{aver} T_{st}}{P_{at} T_{aver} Z_{aver}}; \quad (7)$$

$$\varphi \le \beta = \frac{q_g(P)}{q_g(P) + q_w}; \quad (8)$$

$$q_g(P) = \frac{q_g P_{at} T_{aver} Z_{aver}}{P_{aver} T_{st}}; \quad (9)$$

$$P_{aver} = \frac{2}{3}\left(P_{bh} + \frac{P_{(x)}^2}{P_{bh} + P_{(x)}}\right); \quad (10)$$

$$T_{aver} = \frac{T_{bh} - T_{(x)}}{ln\frac{T_{bh}}{T_{(x)}}}, \quad (11)$$

where *x* – the distance from the middle of the well perforation interval, m; Z_{aver} – the gas compressibility coefficient for P_{aver} and T_{aver}; T_{aver} – the average temperature in the wellbore, K; P_{bh}, $P_{(x)}$ – the pressure at the bottom and at a distance *x* from the wellbore, MPa; P_{aver} – the average pressure in the wellbore, MPa; G_g, G_w – the mass flow rate of gas and water, t/day; q_g, q_w, q_{mix} – the volumetric flow rate (flow rate) of gas, water and water-gas mixture, thousand m^3/day; T_{aver}, $T_{(x)}$ – the temperature at the bottom and at a distance *x* from the wellbore, K; d_{in} – the internal diameter of the tubing, cm; ρ_g, ρ_w – the density of gas and water under standard conditions, kg/m^3; $\rho_g(P)$ – gas density at average pressure and average temperature in the wellbore, kg/m^3; $\overline{\rho}_g$ – relative gas density; λ – coefficient of hydraulic resistance of the tubing; φ – actual (true) volumetric gas content (shows the actual amount of gas in the pipe at a certain moment); β – flow gas content (shows what part gas occupies in the production).

Dependence (8) describes the phenomenon of phase slippage. The water flow rate q_w can be expressed in terms of the gas flow rate q_g and the water factor F_w:

$$q_w = 10^{-6} F_w q_g, \quad (12)$$

where F_w – water factor, l/thousand m^3.

To determine the minimum required gas flow rate for removing water from the face to the surface, the dependence of the minimum required gas flow rate $q_{min,}$ obtained by R.M. Kondrat and V.S. Petryshak based on the results of statistical processing of industrial data on the operation of watered wells of one of the fields that stopped working due to water-flooded wells, which are shown in the works of R.M. Kondrat *et al*. (2023):

$$q_{min.} = 2{,}213 d_{in}^{1.94} q_l^{0.22} \sqrt{\frac{P_{bh}\rho_w}{\overline{\rho}_g Z_{bh} T_{bh}}}, \quad (13)$$

where q_w – water flow rate, m^3/day; Z_{bh} – gas compressibility coefficient for P_{bh} and T_{bh}; d_{in}, m; P_{bh}, MPa, ρ_w, kg/m^3.

Shukhov's formula, which are given in the scientific works of R.M. Kondrat *et al*. (2023) the temperature distribution along the wellbore at each segment *x* is determined:

$$t(x) = t_f - G_{gr}\, x - \Delta t_i\, e^{-ax} + \frac{1 - e^{-ax}}{a}\left(G_{gr} - D_j \frac{P_{bh} - P_x}{x} - \frac{A}{C_{l.mix}}\right), \quad (14)$$

where

$$t_j = D_j\left(P_f - P_{bh}\right)\frac{lg\left(1 + \frac{G \cdot C_{l.mix} \cdot \tau}{\pi \cdot h \cdot c_V \cdot r_W^2}\right)}{lg\frac{R_c}{r_w}}; \quad (15)$$

$$a = \frac{2\pi\lambda_c}{G C_{l.mix} \cdot f(t)}; \quad (16)$$

$$f(t) = ln\left(1 + \sqrt{\frac{\pi\lambda_c \tau}{c_V r_W^2}}\right), \quad (17)$$

where $t(x)$ – gas temperature at a distance *x* from the middle of the perforation interval,°C; G_{gr} – geothermal gradient,°C/m; D_j – differential Joule-Thomson coefficient,°C/MPa; A – thermal equivalent of work, equal to 1/427 kcal/kg·m; Δt_j – decrease in gas temperature in the bottomhole zone of the well due to the Joule-Thomson effect, taking into account heat exchange with the environment,°C; $C_{l.mix}$ – isobaric heat capacity of the mixture at average pressure, J/kg·°C; *G* – mass flow rate of gas, kg/h; τ – total well operation time, h; C_v – volumetric heat capacity of rocks, J/m^3·°C (kcal/m^3·°C); r_w, R_c – radius of the well and supply circuit, m; λ_c – thermal conductivity of rocks, J/m·h·°C; $f(t)$ – dimensionless function of time.

By pressure values $P(x)$ determine the temperature of hydrate formation in the wellbore according to the formula given in the works of R.M. Kondrat *et al*. (2023):

$$t_p(x) = 18.47 \cdot lg(10P(x)) - B, \quad (18)$$

where P_{wh} – the pressure at the wellhead, MPa; B – coefficient, which is determined depending on the conventional density of the gas according to the known component composition of the gas (methane CH_4 = 90.0148%; ethane C_2H_6 – 5.487%; propane C_3H_8 – 1.0091%; iso-butane C_4H_{10} – 0.0925%; n-butane C_4H_{10} – 0.1712%; neo-pentane C_5H_{12} – 0.0004%; iso-pentane C_5H_{12} – 0.0406%; n-pentane C_5H_{12} – 0.0235%; Hexane C_6H_{14} + higher – 0.0499%; Nitrogen N_2 – 1.1799%; Carbon dioxide CO_2 – 1.9318%; Oxygen O_2 – 0.0001%), B = 16.835.

Results and Discussion

Table 1 shows the values of pressure and temperature distribution along the borehole of an operating gas well in the absence of water inflow into the well and at a water factor of 100 l/thousand m³ at a depression in the formation of 15.0% of the initial pressure.

Table 1. The value of the pressure and temperature distribution along the shaft of an operating gas well in the absence of water inflow into the well and at a water factor of 100 l/thousand m³ at a depression on the formation of 15.0% of the initial pressure

Depth, m	In the absence of the water factor			At a water factor of 100 l/thousand m³		
	P, MPa	*t*,°C	$T_{hydr.}$,°C	*P*, MPa	*t*,°C	$T_{hydr.}$,°C
0	18.55	17.20	25.06	17.908	22.93	24.78
-141	19.15	22.36	25.32	18.548	27.59	25.06
-391	19.76	27.35	25.57	19.193	32.07	25.34
-641	20.37	32.15	25.81	19.844	36.35	25.60
-891	20.99	36.74	26.05	20.501	40.4	25.86
-1,141	21.61	41.07	26.29	21.164	44.19	26.12
-1,391	22.24	45.12	26.52	21.835	47.71	26.37
-1,641	22.87	48.83	26.74	22.515	50.92	26.62
-1,891	23.51	52.16	26.96	23.202	53.77	26.86
-2,141	24.15	55.05	27.18	23.898	56.24	27.09
-2,391	24.81	57.43	27.39	24.604	58.28	27.33
-2,641	25.47	59.23	27.60	25.319	59.83	27.56
-2,891	26.14	60.35	27.81	26.044	60.84	27.78
-3,141	26.81	60.70	28.02	26.78	61.26	28.01

Source: developed by the authors

Figure 1 shows the distribution of the actual temperature and the temperature of hydrate formation along the wellbore in the absence of water inflow into the well and at a water factor of 100 l/thousand m³ at a depression in the formation of 15.0% of the initial pressure. Analysis of the graphical dependence allows to determine the conditions of stable operation of the well and the place of hydrate formation.

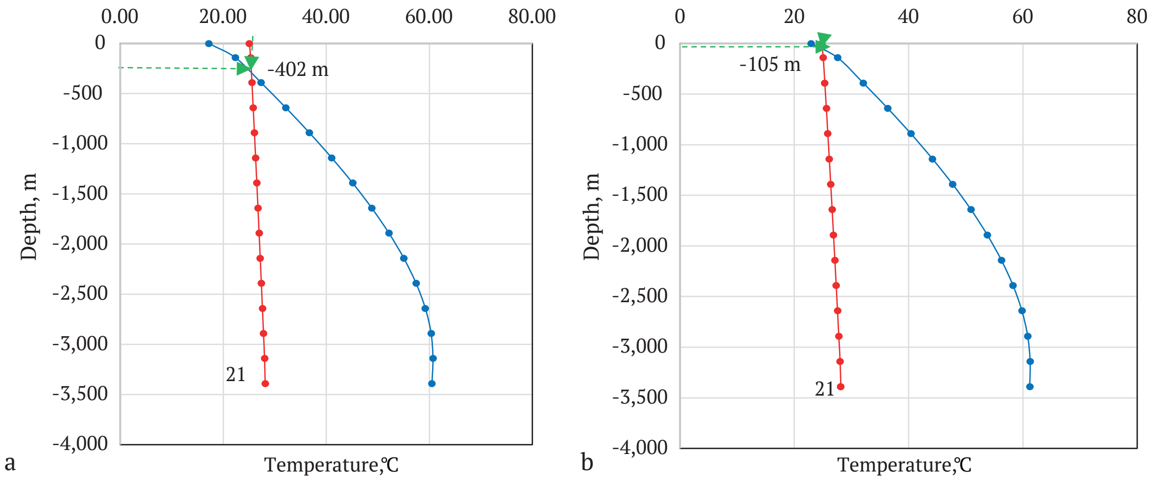

Figure 1. Distribution of actual temperature (a) and hydrate formation temperature along the wellbore (b) in the absence of water inflow into the well and at a water factor of 100 l/thousand m³ at a depression in the formation of 15.0% of the initial pressure

Note: a – actual temperature; b – hydrate formation temperature
Source: created by the authors

Analysis of the dependences of Figure 1 indicates intensive cooling of the gas during the ascent from the bottom to the wellhead (curve 1), which is due to the Joule-Thomson effect and heat exchange with colder surrounding rocks. Comparative analysis of Figure 1a and Figure 1b shows that the change in thermobaric conditions significantly affects the position of the zone of possible hydrate formation, shifting it from a depth of 402 m (Fig. 1a) to 105 m (Fig. 1b). Such a temperature distribution indicates the need to use inhibitors or thermal insulation of tubing to prevent hydrate deposition in the upper part of the wellbore. Figure 2 shows the distribution of the actual temperature at the wellhead and the equilibrium temperature of hydrate formation from the water factor at different depressions in the reservoir.

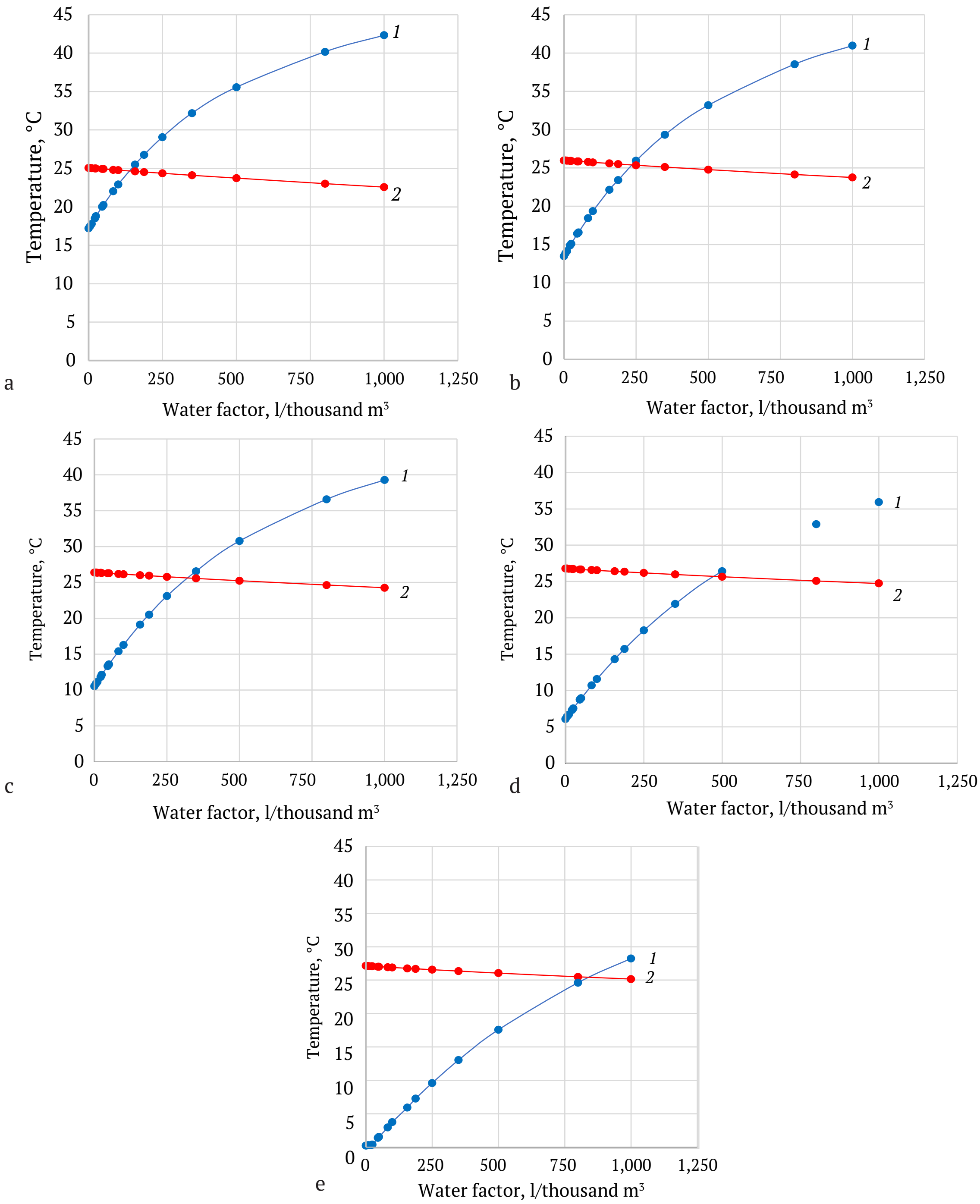

Figure 2. Distribution of the actual temperature at the wellhead and the equilibrium temperature of hydrate formation from the water factor at depression on the reservoir from the initial pressure

Note: depression on the layer 15% (a); 10% (b); 7.5% (c); 5.0% (d); 2.5% (e)

Source: created by the authors

The point of intersection (Fig. 2) between the actual temperature and the hydrate formation temperature lines is a critical technological indicator. To the left of the point, thermodynamic conditions favour the formation of hydrates, since the flow temperature is lower than the hydrate formation temperature. An increase in the water factor leads to an increase in the actual temperature, which gradually brings the system into a safe zone (to the right of the intersection point). With an increase in the water factor, the actual flow temperature increases rapidly, which is explained by the high heat capacity of water compared to gas. The hydrate formation temperature (curve 2) tends to decrease slightly with an increase in the amount of water in the flow. Analysis of the dependencies of Figure 2 shows that with a decrease in depression from 15 to 2.5 % of the initial pressure, the actual gas temperature at the mouth decreases significantly. With a decrease in depression, the zone of the hydrate-free drive shifts towards higher values of the water factor. This means that at low depressions, the well requires a significantly larger amount of formation water to "self-heat" the flow above the hydrate formation point. Table 2 shows the values of the depth of hydrate formation in tubing depending on the water factor at different values of depression in the reservoir.

Table 2. The value of the depth of hydrate formation in tubing depending on the water factor at different values of depression per reservoir

No. n/n	Water factor, l/thousand m³	Hydrate depth, m				
		15% P_{in}	10% P_{in}	7.5% P_{in}	5.0% P_{in}	2.5% P_{in}
1	0	402	593	718	900	1,158
2	5	382	564	705	881	1,142
3	10	363	555	670	869	1,129
4	21	334	525	651	841	1,110
5	25	306	497	645	832	1,102
6	46	258	453	612	794	1,071
7	50	239	440	593	784	1,066
8	83	133	382	507	727	995
9	100	105	325	469	689	965
10	157	15-20	191	354	545	899
11	188		105	249	506	842
12	250		15-20	143	392	755
13	350			15-20	191	611
14	500				15-20	392
15	800					15-20
16	1,000					

Source: created by the authors

The results of the studies (Table 2) reflect the general dynamics of the depth of hydrate formation in the tubing depending on the water factor. However, the analysis of the studies showed that when a certain critical value of the water factor is reached, stable operation of the well is stopped ($q_g < q_{min}$). At low depressions in the formation (for example, 2.5 % of the initial pressure), such a state occurs already at minimum values of the water factor, which predicts a rapid cessation of natural gushing due to self-extinguishing of the well. Taking this into account, further studies of the pressure and temperature distribution in the wellbore were carried out taking into account the prospective transition to mechanised methods of well operation (gas lift, plunger lift). Thus, the obtained results of studies on the depth of hydrate formation depending on water factors are the basis for designing hydrate formation prevention systems (for example, determining the location / points of injection of hydrate formation inhibitors) already at the stage of well operation using mechanised methods. Figure 3 shows the dependence of the depth of hydrate formation in tubing on the water factor at different values of depression on the reservoir, which make it possible to assess the hydrate formation zones in which well operation becomes impossible without constant supply of hydrate formation inhibitors.

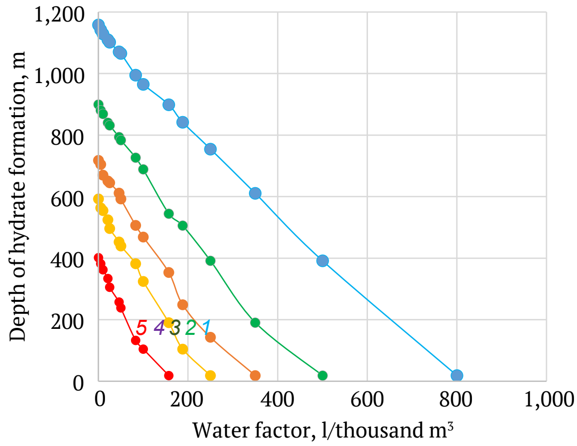

Figure 3. Dependences of the depth of hydrate formation in tubing on the water factor at different values of depression on the reservoir

Note: 1 – 2.5% 2 – 5.0%; 3 – 7.5%; 4 – 10.0%; 5 – 15%

Source: created by the authors

According to the results of the conducted studies, it was established that at low values of the water factor (F_w < 25 l/thousand m³) the zone of potential hydrate formation is the deepest and reaches over 1,000 m. All this is explained by the low heat capacity of pure gas: during the lifting of well products, the flow is intensively cooled through Joule-Thomson, therefore the curve of the actual temperature intersects the curve of the hydrate formation temperature at significant depths. With an increase in the water factor (over 100 l/thousand m^3) the reverse process is observed. The high heat capacity of water stabilises the flow temperature, "pushing" the hydrate formation zone to the wellhead. Analysis of the dependencies of Figure 3 shows that with an increase in the water factor, the depth of hydrate formation decreases. That is, with a large amount of water, hydrates begin to form much higher in the wellbore (closer to the wellhead). For example, with a depression of 5.0% of the initial pressure and the absence of water inflow into the well, an increase in the water factor to 500 l/thousand m^3 "raises" the hydrate formation zone from 900 to 15-20 m. An increase in the depression per reservoir leads to a significant decrease in the depth of the hydrate formation zone. This is explained by a change in the temperature mode and thermodynamic equilibrium in the tubing string. At minimum depression (2.5% of the initial pressure), the risk zone of hydrate formation is the deepest (reaches 1,158 m). At maximum depression (15% of the initial pressure), hydrates are formed only in the upper part of the well, and at high water factors (more than 188 l/thousand m^3) the conditions for their formation in the tubing are completely absent. For most operating modes, the upper part of the wellbore is critical (depths up to 400-600 m). At high water content (more than 800 l/thousand m^3), the risk of hydrate formation is shifted directly to the surface (depth about 15-20 m), which creates a threat of hydrate formation in wellhead equipment and plumes.

The results of the research allow to predict the intervals of possible hydrate deposition for specific well operating modes. This is the basis for choosing an effective technology for preventing hydrate formation, in particular, determining the required dose of inhibitors or establishing the optimal thermal mode of well operation by choosing the appropriate depression in the formation. Figure 4 shows the dependence of the maximum water factor on the depression in the formation at the moment of cessation of hydrate formation in the tubing.

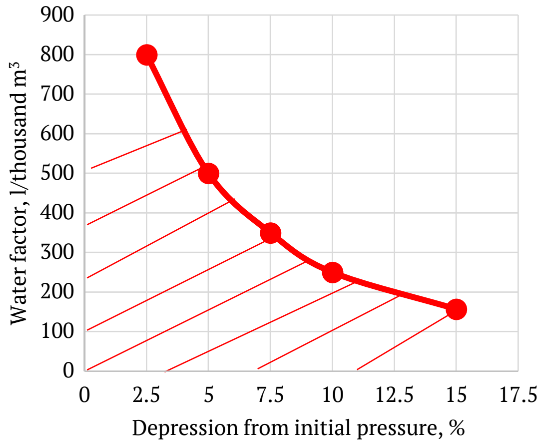

Figure 4. Dependence of the maximum water factor on the depression in the reservoir at the moment of cessation of hydrate formation in the tubing

Source: created by the authors

The analysis of the research results (Fig. 4) was based on finding the intersection points of the curves of the distribution of the actual temperature and the equilibrium temperature of hydrate formation along the wellbore for different values of depression per reservoir. With an increase in depression per reservoir, the critical value of the water factor, at which the formation of hydrates in the tubing stops, decreases rapidly. The area located to the left and below the red line in Figure 4 corresponds to the thermodynamic conditions under which active formation of hydrates occurs. This is a zone that combines high water content and low values of depression per reservoir, which leads to the rapid accumulation of hydrate deposits, which can cause complete overlap of the cross-section of the tubing. The area located to the right and above the red line determines the well operating conditions under which hydrates do not form. For a specific assessment of the well operating conditions at the time of cessation of natural gushing, the calculation of key technological indicators was carried out depending on the values of depression per reservoir. The results of the studies are presented in Table 3.

Table 3. Values of water factor, gas flow rate, minimum required gas flow rate, wellhead pressure, wellhead temperature and hydrate formation temperature for different values of depression in the formation at the time of cessation of natural well flow

Depression from initial pressure, %	Water factor, l/thousand m^3	Gas flow rate, thousand m^3/day	Minimum required gas flow rate, thousand m^3/day	Throat pressure, MPa	Temperature of wellhead,°C	Hydration temperature,°C
2.5	5	116.4	116.4	24.01	0.28	27,131
5	21	171.4	171.4	22,827	7.31	26,725
7.5	46	212.8	212.8	21,587	13.34	26,277
10	83	247.1	247.1	20.26	18.44	25,769
15	188	302.9	302.9	17,373	26.78	24,535

Source: created by the authors

Figure 5 shows the dependence of the water factor, wellhead pressure, wellhead temperature, and hydrate formation temperature on the depression in the reservoir at the moment of cessation of natural well flow.

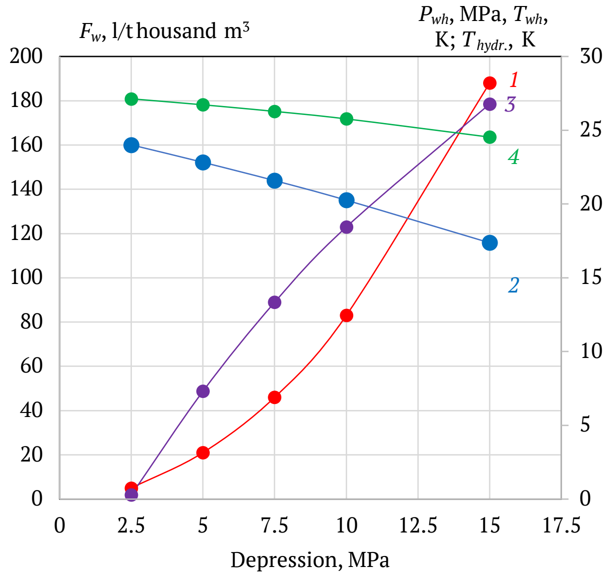

Figure 5. Dependence of water factor (1), wellhead pressure (2), wellhead temperature (3) and hydrate formation temperature (4) on the depression in the reservoir at the time of cessation of natural well flow

Source: created by the authors

Analysis of the research results at the time of cessation of natural well gushing shows that with a decrease in depression from 15% to 2.5% of the initial pressure, a sharp decrease in the actual wellhead temperature is observed (from 26.78 to 0.28°C). At the same time, the hydrate formation temperature increases from 24.535 to 27.131°C. This indicates that at low depressions, the actual gas-liquid flow temperature becomes significantly lower than the hydrate formation temperature and the hydrate formation process is inevitable without external intervention. A decrease in depression leads to an increase in wellhead pressure (from 17.373 to 24.01 MPa), which additionally contributes to the stability of hydrates at higher temperatures. The water factor, at which natural well gushing is still possible, significantly decreases with a decrease in depression. Thus, with a depression of 15% of the initial pressure, the well can deliver up to 188 l/thousand m^3 of liquid, and with a depression of 2.5% of the initial pressure, this figure is only 5 l/thousand m^3.

With increasing depression on the formation, the maximum value of the water factor increases at the moment of cessation of natural well gushing. Thus, the obtained results confirm that the transition to modes with low depression on the formation is accompanied not only by a deterioration in the conditions for liquid removal to the surface, but also by a rapid entry into the zone of active hydrate formation due to significant cooling of the gas flow in the well. This requires comprehensive measures for thermal insulation of the tubing or constant supply of hydrate formation inhibitors to the annulus. To prevent hydrate formation, the most effective is to maintain a high depression. If the well is forced to operate at low depressions, it is necessary to ensure the supply of hydrate formation inhibitors to the gas-liquid flow. The obtained results of modelling the formation of hydrates in the wellbore of watered gas wells confirm the complex relationship between depression on the formation and the water factor. Scientific research by J.G. Delgado-Linares *et al.* (2022) are devoted to systems containing carbon dioxide CO_2. The authors' conclusions regarding the mechanisms of particle aggregation are of fundamental importance for explaining the obtained dependencies. Scientists prove that the risk of hydrate formation depends on the viscosity of the extracted product, which increases significantly with an increase in the water factor. The results obtained indicate that at high water factors the hydrate formation zone shifts to the wellhead not only due to the thermodynamics of the processes, but also due to an increase in the viscosity of the extracted mixture.

The results of the obtained studies are also confirmed in the studies of M.O. Kehinde (2018). The authors focus their attention on the implementation of thermal intensification methods, which lead to the saturation of the production fluid with aggressive components (CO_2, H_2, oxygen). These fluids, under condensation conditions, cause intensive liquid corrosion and erosive wear of equipment due to the formation of iron sulfides. The obtained studies on the analysis of depression on the reservoir complement this theory. Phase instability and moisture condensation are determining factors of complications both in the wellbore and in the places of collection of production products. However, if in the studies the author considers the presence of hot water vapor as a negative factor, then in the results obtained for watered gas wells, the high heat capacity of formation water and the rational depression mode for the formation are used as a useful tool for preventing hydrate formation.

The results of the obtained studies are also confirmed in the studies of L.F. Dalla *et al.* (2026). The authors focus their attention on predicting hydrates during well shutdown or start-up using transient multiphase flow simulators. Taking into account such factors as the viscosity of the hydrate suspension and hydrate washout processes allows for highly accurate reproduction of the system behaviour in complex dynamic scenarios. The obtained studies on the depth of hydrate formation complement this theory, as they focus on the method of choosing the optimal depression in the reservoir, which ensures stable fluid removal and eliminates the conditions for hydrate formation. Static calculations based on reservoir parameters are insufficient, since the real risk of hydrate formation is determined by the hydraulic parameters in transient modes.

The results of the obtained studies, which are related to thermodynamic processes in water-filled wells, demonstrate the critical role of heat balance in preventing phase transitions. A similar approach to thermal mode control is noted in the work of researchers K. Ito *et al.* (2024). Although the object of their analysis is the extraction of methane from natural hydrate deposits of the sea shelf, the physical laws of the processes have deep parallels with the obtained studies. The results of the obtained studies on the temperature modes of watered wells are also confirmed in the studies of V. Indina *et al*. (2024). The authors focus their attention on the fact that the Joule-Thomson effect directly depends on the reservoir permeability k and the initial pressure P_{in}, which leads to the formation of hydrates when the working fluid temperature is higher than the equilibrium temperature of hydrate formation. The results of the obtained studies are compared with the scientific results of J. Ye *et al*. (2023), where the authors investigated the Joule-Thomson effect during CO_2 injection. Although the object of the research itself is different in the authors' scientific achievements, the physics of the process is identical – that is, a sharp expansion of the gas leads to intense cooling. The obtained studies confirm the authors' conclusions that at low reservoir pressures (in conditions of depleted reservoirs) this effect becomes dominant.

Researcher Z. Zhang *et al*. (2021) in their studies argued that the detection of the place of hydrate formation should be based on the transition from static thermodynamic regions to dynamic hydraulic indicators. The results obtained indicate that the static calculation according to reservoir conditions is not entirely sufficient. The results obtained for a depression in the reservoir of 2.5% of the initial pressure (Fig. 3) demonstrate that it is the dynamics of pressure reduction and gas cooling in the tubing that determines the real depth of hydrate formation, which can reach more than 1,000 m, which significantly exceeds the predictions based on average statistical indicators. Research by L. Wang & A.Y. Sun (2020) on the adhesion of hydrates on the walls of pipes indicates that the roughness of the tubing accelerates the growth of deposits. The obtained studies on the analysis of the depth of hydrate formation complement this theory, that at low values of the water factor, when the risk zone of hydrate formation covers more than 1,000 m of the wellbore, the surface area for potential crystal adhesion is maximum. All this contributes to the creation of prerequisites, which creates prerequisites for the gradual narrowing of the passage cross-section of the pipes.

The results of the research are closely intertwined with the scientific developments of D. Biberg *et al*. (2025). The authors focus their attention on the formation of significant liquid plugs that occur at low gas flow rates. These complications disrupt the operation of production collection systems. The results obtained indicate that the implementation of an integral wave instability indicator allows for fairly rapid prediction of the moments of occurrence and cessation of fluid flow pulsations. The results of studies on the analysis of depression per reservoir complement this theory. The transition to a mode with low depression per reservoir creates prerequisites for the accumulation of fluid in the upper part of the wellbore. The authors' scientific studies focus on assessing the risks of pulsations in pipelines. The results of the above studies show the dynamics of pressure reduction and gas cooling in tubing to determine the real depth of hydrate formation. Research by X. Sui *et al*. (2023) are directed to the fact that the supply of a significant amount of ethylene glycol to combat hydrates significantly reduces the solubility of salts and contributes to the formation of salt deposits. The methodology for selecting the optimal depression in the formation, which was obtained in the studies, is more rational in this context, since it allows using the so-called natural "self-heating" of the fluid flow due to the heat capacity of the formation water, which minimises the need for chemical reagents.

The results of the obtained studies are also confirmed in the studies of A. Abdullah *et al*. (2026). The authors in their scientific works focus their attention on low temperatures in combination with high pressure, which creates conditions for the formation of hydrates in anisotropic conditions of the annulus. The obtained research results indicate that the injection of diesel fuel through flexible pipes instead of expensive chemical reagents provides effective destruction of hydrate-paraffin formations without the risk of damage to the formation. The obtained studies on the analysis of depression in the formation and determination of the real depth of hydrate formation confirm these statements. Temperature modes in the wellbore are of crucial importance. The authors propose to solve the problem of hydrate formation by periodic artificial thermal exposure and injection of heated petroleum products from the surface, and the results obtained for water-filled wells focus on optimising the hydrodynamics of fluid production.

In their research A.G. Aregbe & A.I. Fadeyi (2021) provide important context on methods for increasing hydrate dissociation and stabilising gas production. Scientists note that one of the main methods for producing gas from hydrates is depression, thermodynamic influence and the supply of hydrate formation inhibitors. All this is fully correlated with the methodology, where depression on the formation is considered as one of the key factors determining the depth of hydrate formation in the wellbore (Fig. 3). However, if the authors analyse depression on the formation as a method for destroying hydrates in the formation, then the results of the research substantiate its optimal values to prevent their formation during the lifting of production. In their research, scientists also point out the risk of hydrate reformation during cooling of the produced gas, which requires more precise control of temperature and pressure. The obtained research results (Table 3) quantitatively confirm this statement that at low depressions in the reservoir, the actual temperature at the wellhead decreases, which makes the process of repeated hydrate formation inevitable without external intervention. Thus, the research results indicate the need for comprehensive monitoring of thermobaric parameters along the entire path of fluid movement. Summing up, the results of the research performed, it can be concluded that they are not only consistent with global trends in the oil and gas industry, but also offer specific solutions for depleted fields.

Conclusions

The results of the performed studies indicate that the process of hydrate formation in water-flooded gas wells clearly depends on the value of the depression on the formation and the water factor. Studies performed for different values of the depression on the formation (2.5; 5.0; 7.5; 10.0;

15.0% of the initial pressure) and the water factor (0; 5; 10; 21; 25; 46; 50; 83; 100; 157; 188; 250; 350; 500; 800; 1,000 l/thousand m^3), made it possible to estimate the thermal effect of the liquid phase on the total energy of the flow of production products in the tubing. The key aspect of the methodology was the determination of the depths of hydrate formation for different values of the depression on the formation and the water factor. For practical identification of well operation modes, a graphical analytical construction of hydrate formation boundaries was used, which allowed dividing the thermodynamic states of the system into a stable zone and a zone at risk of hydrate formation.

It was established that at a depression on the formation of 2.5% of the initial pressure, the most critical is the operation of the well at low values of the water factor (up to 26 l/thousand m^3), where the risk zone of hydrate formation covers more than 1,000 m of the wellbore. As a result of the performed studies, it was established that when the water factor reaches a value of more than 500 l/thousand m^3, the gas-liquid flow of the produced products becomes "hot" enough to independently exit the zone of hydrate formation even at low depressions on the formation. It was quantitatively estimated that an increase in the depression on the formation contributes to an increase in the critical value of the water factor, at which the formation of hydrates in the tubing stops. The dependence of the maximum water factor on the depression on the formation at the moment of the cessation of the formation of hydrates in the tubing allows to clearly delimit the thermodynamic conditions into the zone of active hydrate formation and the zone of stable operation of the wells.

The proposed method allows predicting the intervals of hydrate formation and justifying the operating modes of wells that ensure their hydrate-free operation. The prospects for further scientific research lie in the detailing of the developed model by taking into account the influence of formation water mineralisation on the thermobaric parameters of hydrate formation. A separate direction is the study of the kinetics of adhesion of hydrate particles to the inner wall of the tubing in the presence of salt deposits, which will allow specifying the time until the pipe cross-section is completely blocked. Also relevant is the modelling of the influence of thermally insulated lift columns on the expansion of the limits of hydrate-free operation of wells with low formation pressures.

Acknowledgements

None.

Funding

None.

Conflict of Interest

None.

References

[1] Abdullah, A., Selamat, K., Raman, I., Perng, C., & Thulus, S.A.M. (2026). Application of heated diesel in hydrate removal across the annulus of production riser and coiled tubing gas lift system in deepwater wells – a journey to success in unlocking the production recovery. In *SPE/ICoTA well intervention conference and exhibition* (article number SPE-231341-MS). Woodlands: SPE. doi: 10.2118/231341-MS.

[2] Aregbe, A.G., & Fadeyi, A.I. (2021). A comprehensive review on CO2/N2 mixture injection for methane gas recovery in hydrate reservoirs. In *SPE Nigeria annual international conference and exhibition* (article number SPE-207092-MS). Lagos: SPE. doi: 10.2118/207092-MS.

[3] Biberg, D., Sinkov, K., Kirkedelen, M.B., Johansson, P.S., Nordsveen, M., & Kjeldby, T.K. (2025). Predicting surge waves in gas-condensate pipelines using long-wave stability analysis. In *ISAVFT 21st international conference on multiphase production technology* (article number ISAVFT-2025-371). Lisbon: ISAVFT.

[4] Dalla, L.F., Zerpa, L.E., & Koh, C.A. (2026). Offshore field gas hydrate plug events evaluation using a unified gas hydrate transient model. In *Offshore technology conference* (article number OTC-36967-MS). Houston: OTC. doi: 10.4043/36967-MS.

[5] Delgado-Linares, J.G., Pohl, M., Majid, A.A A., Yoda, C., Tanaka, N., Zerpa, L.E., Prasad, M., & Koh, C.A. (2022). Early detection and assessment of asphaltene precipitation and gas hydrate formation at field conditions. In *Offshore technology conference* (article number OTC-31712-MS). Houston: OTC. doi: 10.4043/31712-MS.

[6] Gauteplass, J., Almenningen, S., Barth, T., & Ersland, G. (2020). Hydrate plugging and flow remediation during CO_2 injection in sediments. *Energies*, 13(17), article number 4511. doi: 10.3390/en13174511.

[7] Gudala, M., Alanazi, A., Fahs, M., & Hoteit, H. (2025). Comprehensive investigation of transient Joule-Thomson cooling and CO2 hydrate formation in depleted gas reservoirs. In *Middle East oil, gas and geosciences show (MEOS GEO)* (article number SPE-227472-MS). Bahrain: SPE. doi: 10.2118/227472-MS.

[8] Indina, V., Fernandes, B.R.B., Delshad, M., Farajzadeh, R., & Sepehrnoori, K. (2024). On the significance of hydrate formation/dissociation during CO_2 injection in depleted gas reservoirs. In *SPE conference at Oman petroleum & energy show* (article number SPE-218550-MS). Muscat: SPE. doi: 10.2118/218550-MS.

[9] Ito, K., Sawano, Y., Tada, K., & Sato, T. (2024). Numerical simulation of enhanced gas recovery from methane hydrate using the heat of CO2 hydrate formation. In *Offshore technology conference Asia* (article number OTC-34780-MS). Kuala Lumpur: OTC. doi: 10.4043/34780-MS.

[10] Kehinde, M.O. (2018). Corrosion of casing vapor recovery piping in steam flooding operation. In *CORROSION 2018* (article number 1-12). Phoenix: NACE International. doi: 10.5006/C2018-11541.

[11] Kondrat, R., & Matiishyn, L. (2025). Influence of the relative opening of the gas-bearing formation on the process of watering wells in reservoirs with bottom water. *Mining of Mineral Deposits*, 19(3), 14-21. doi: 10.33271/mining19.03.014.
[12] Kondrat, R.M., Kondrat, O.R., & Matiishyn, L.I. (2023). *Development and operation of gas and gas condensate fields*. Ivano-Frankivsk: Foliant.
[13] Lukin, O.A., & Kondrat, O.R. (2025). Probabilistic uncertainty of production forecasting from tight gas-saturated reservoirs. *Mineral Resources of Ukraine*, 4, 26-34. doi: 10.31996/mru.2025.4.26-34.
[14] Pei, J., Chen, J., Wang, J., Li, Z., & Kan, J. (2024). CO_2 capture technology based on gas hydrate method: A review. *Frontiers in Chemistry*, 12, article number 1448881. doi: 10.3389/fchem.2024.1448881.
[15] Qu, A., Ravichandran, S., Hatscher, S., Ugueto, L., Torsvik, M., Zerpa, L.E., & Koh, C. (2023). Predicting hydrate formation and plugging in a gas condensate subsea tieback using a transient hydrate simulation tool. In *SPE annual technical conference and exhibition* (article number SPE-215013-MS). San Antonio: SPE. doi: 10.2118/215013-MS.
[16] Sui, X., Wang, Z., Tong, S., Guo, Y., & Zhang, J. (2023). Experimental study on the compatibility of hydrate inhibitor and anti-scale agent. In *Abu Dhabi international petroleum exhibition & conference (ADIPEC)* (article number SPE-216989-MS). Abu Dhabi: ADIPEC. doi: 10.2118/216989-MS.
[17] Wang, L., & Sun, A.Y. (2020). Well spacing optimization for Permian Basin based on integrated hydraulic fracturing, reservoir simulation and machine learning study. In *SPE/AAPG/SEG unconventional resources technology conference* (article number 3104). Austin: URTeC. doi: 10.15530/urtec-2020-3104.
[18] Ye, J., *et al*. (2023). Evaluation of geological CO2 storage potential in Saudi Arabian sedimentary basins. *Earth-Science Reviews*, 244, article number 104539. doi: 10.1016/j.earscirev.2023.104539.
[19] Yin, F., Gao, Y., Di, J., Sun, B., Yao, H., Zhang, L., & Zhao, X. (2026). Effect of annulus phase transition on equivalent circulating density in deepwater hydrate formation drilling: Analysis of hydrate trial production well drilling in the South China Sea. *SPE Journal*, 31(3), 1563-1585. doi: 10.2118/231831-PA.
[20] Zhang, Z., Gao, Y., Li, Y., Wang, W., Liu, C., Hu, Q., & Gong, P. (2021). Identification of hydrate risk region for deepwater gas field flow assurance: Transition from static thermodynamic region to dynamic hydraulic region. In *31st international ocean and polar engineering conference* (article number ISOPE-I-21-2114). Rhodes: ISOPE.

Дослідження характеристик процесу гідратоутворення в обводнених газових свердловинах

Роман Кондрат

Доктор технічних наук, професор
Івано-Франківський національний технічний університет нафти і газу
76019, вул. Карпатська, 15, м. Івано-Франківськ, Україна
https://orcid.org/0009-0002-0928-2748

Олександр Кондрат

Доктор технічних наук, професор
Івано-Франківський національний технічний університет нафти і газу
76019, вул. Карпатська, 15, м. Івано-Франківськ, Україна
https://orcid.org/0009-0002-0928-2748

Лілія Матіїшин

Кандидат технічних наук, доцент
Івано-Франківський національний технічний університет нафти і газу
76019, вул. Карпатська, 15, м. Івано-Франківськ, Україна
https://orcid.org/0000-0002-8529-4807

Наталія Дремлюх

Кандидат технічних наук, доцент
Івано-Франківський національний технічний університет нафти і газу
76019, вул. Карпатська, 15, м. Івано-Франківськ, Україна
https://orcid.org/0000-0002-6991-0227

Анотація. Актуальність наукових досліджень зумовлена переходом більшості родовищ природних газів на пізню стадію розробки, що супроводжується значним обводненням видобувної продукції та створює термодинамічні передумови для аварійного перекриття стовбурів свердловин газовими гідратами. Метою роботи було встановлення впливу значень водного фактора та депресії на пласт на характеристики процесу гідратоутворення в обводнених газових свердловинах для оптимізації їхніх технологічних режимів. Для вирішення поставлених завдань розроблено комплексну математичну модель термодинамічного стану багатофазного флюїду, за допомогою якої виконано серію досліджень на модельній свердловині за різних значень депресії на пласт (2,5; 5,0; 7,5; 10,0; 15,0 % від початкового тиску) та водного фактора (0-1 000 л/тис.м^3). Встановлено, що за низьких значень депресії на пласт (2,5 % від початкового тиску) та незначного припливу води зона ризику утворення гідратів є найбільш критичною і сягає глибини понад 1 000 м. Виконано температурний розподіл по стовбуру свердловини та доведено, що при досягненні водного фактора більше 500 л/тис.м^3 газорідинний потік стає достатньо «гарячим» завдяки високій теплоємності води, що дозволяє свердловині самостійно вийти із зони гідратоутворення. Визначено критичні значення водного фактора на момент припинення природного фонтанування, за яких фактична гирлова температура знижується до мінімальних значень 0,28 °С. Розроблено графоаналітичну методику побудови меж гідратоутворення, яка дозволяє чітко розмежувати термодинамічні стани системи на зону активного гідратоутворення та зону стабільної роботи свердловини. Продемонстровано, що збільшення депресії на пласт сприяє зростанню критичного значення водного фактора, за якого припиняється утворення гідратів у насосно-компресорних трубах без зовнішнього втручання. Практична цінність результатів полягала у можливості використання розробленої моделі інженерно-технічними фахівцями нафтогазової галузі для обґрунтованого вибору безгідратних режимів експлуатації обводнених свердловин

Ключові слова: водний фактор; експлуатація; депресія на пласт; температура гідратоутворення; газ

Розвідка та розробка нафтових і газових родовищ

Науково-технічний журнал

Том 26, № 1, 2026

Відповідальний редактор:
О. Трубенко

Підписано до друку 29.05.2026 р. Формат 60*84/8
Умовн. друк. арк. 10,9
Тираж: 100 прим.

Адреса видавництва:
Івано-Франківський національний технічний університет нафти і газу
76019, вул. Карпатська, 15, м. Івано-Франківськ, Україна
Тел.: +380 (342) 54-72-66
Факс: +380 (342) 54-71-39
E-mail: info@pdogf.com.ua
https://pdogf.com.ua/uk

Prospecting and Development of Oil and Gas Fields

Scientific and Technical Journal

Vol. 26, No. 1, 2026

Managing Editor:
O. Trubenko

Signed for print 29.05.2026. Format 60*84/8
Conventional printed pages 10.9
Circulation 100 copies

Publishing Address:
Ivano-Frankivsk National Technical University of Oil and Gas
76019, 15 Karpatska Str., Ivano-Frankivsk, Ukraine
Tel.: +380 (342) 54-72-66
Fax: +380 (342) 54-71-39
E-mail: info@pdogf.com.ua
https://pdogf.com.ua/en